

MOLECULAR DYNAMICS SIMULATIONS OF
BARRIER CROSSINGS
IN THE CONDENSED PHASE

CONFORMATIONAL TRANSITIONS IN SUPRAMOLECULES

PROEFSCHRIFT

ter verkrijging van
de graad van doctor aan de Universiteit Twente,
op gezag van de rector magnificus,
prof. dr. F. A. van Vught,
volgens besluit van het College van Promoties
in het openbaar te verdedigen
op vrijdag 16 januari 1998 te 16.45 uur

door

Wouter Koenraad den Otter

geboren op 20 mei 1969
te Eindhoven

Dit proefschrift is goedgekeurd door:

Promotor : Prof. dr. D. Feil

Ass. promotor : Dr. W. J. Briels

Voor mijn ouders

ISBN 90 365 10848

Contents

1	Introduction	1
1.1	Reaction rates.....	1
1.2	Supramolecules.....	2
1.3	Survey.....	3
1.4	References.....	4
2	Theory	5
2.1	Statistical mechanics.....	5
2.1.1	Static properties.....	5
2.1.2	Dynamic properties.....	6
2.2	Reaction rate theory.....	7
2.2.1	Macroscopic reaction rate.....	8
2.2.2	Microscopic reaction rate.....	9
2.2.3	Transition state theory.....	10
2.2.4	Transmission coefficient.....	11
2.3	Molecular dynamics simulations.....	13
2.4	References.....	17
3	The reactive flux method applied to complex isomerisation reactions: using the unstable normal mode as a reaction coordinate	19
3.1	Introduction.....	19
3.2	The reaction coordinate.....	22
3.3	Sampling the transition state.....	25
3.3.1	Constrained dynamics.....	25
3.3.2	The conditional average at the transition state.....	27
3.4	Implementation.....	31
3.5	Results.....	32
3.5.1	Flexible <i>n</i> -butane in carbon tetrachloride.....	32
3.5.2	Liquid rigidified <i>n</i> -butane.....	38
3.5.3	Calix[4]arene.....	40
3.6	Conclusions.....	46
3.7	Appendix: calculation of Z_{ξ}	47
3.8	References.....	47

4	Free energy and conformational transition rates of calix[4]arene in chloroform	49
4.1	Introduction	49
4.2	Theory.....	51
4.2.1	Reaction coordinate.....	51
4.2.2	Theory of small vibrations.....	53
4.2.3	Umbrella sampling	56
4.2.4	Transition state crossing velocity	57
4.3	Results	58
4.3.1	Small vibrations.....	59
4.3.2	Umbrella sampling	60
4.3.3	Rate constants.....	63
4.4	Conclusions	67
4.5	Appendix: Normal mode analysis and $Q(\xi)$	67
4.6	References	70
5	Solvent effect on the isomerisation rate of calix[4]arene studied by molecular dynamics simulations	71
5.1	Introduction	71
5.2	Theory.....	72
5.2.1	Reaction rate.....	72
5.2.2	Reaction coordinate.....	74
5.2.3	Free energy	77
5.3	Results	78
5.3.1	Free energy	79
5.3.2	Transmission coefficient	82
5.4	Conclusions	84
5.5	References	84
6	The calculation of free energy differences by constrained molecular dynamics simulations	87
6.1	Introduction	87
6.2	Constraints and probability distributions.....	88
6.2.1	Generalised coordinates	88
6.2.2	Simulation in Cartesian coordinates.....	91
6.3	Thermodynamic integration and perturbation	92
6.3.1	Reaction coordinate ξ	92
6.3.2	Coupling parameter λ	95
6.4	Relation between the thermodynamic force and the constraint force.....	97
6.5	Numerical examples	98

6.6	Comments on the literature.....	102
6.6.1	Use and misuse of Z_ξ , $ \mathbf{Z}_\sigma $ and $ \mathbf{Z}_{\xi\sigma} $	102
6.6.2	Equivalence of thermodynamic force and constraint force	103
6.6.3	Potential force method.....	104
6.6.4	Mean force independent of complementary coordinates	105
6.6.5	Generalised Alteration of Structure and Parameters (GASP).....	106
6.6.6	Monte Carlo.....	107
6.7	Conclusions.....	108
6.8	References.....	108
7	Summary and outlook	111
7.1	Summary.....	111
7.2	Outlook	112
7.3	References.....	114
	Samenvatting	115
	Dankwoord	117
	Curriculum Vitae	118

1a

Chapter 1

Introduction

1.1 Reaction rates

Reaction rates have been the subject of experimental and theoretical research in chemistry and physics for well over a century.¹ Examples of reaction rates include chemical reactions, isomerisations, adatoms hopping over surfaces, nucleation in undercooled liquids, diffusion of molecules through polymers and ceramics, protein folding, and decay of uranium-235 nuclei. The common characteristic of all these processes is that they are rare compared to the normal dynamics of the system. For instance, in the reaction on which we shall focus in this thesis a molecule reacts about once every 10^{-2} second, while the typical time of normal mode oscillations is of the order of 10^{-13} second: a difference of eleven orders of magnitude. The reason why reactions are infrequent is well understood: the stable states of the system, i.e. the minima of the potential energy surface, are separated by barriers of higher energy, which have to be surmounted in order to go from one stable state to the next.² If these barriers are high compared with the thermal energy of the system, $E_{therm} = k_B T$ where k_B is Boltzmann's constant and T is the absolute temperature, there is only a very small chance of the system to arrive at the top of the energy barrier, the activated state. This notion is reflected in the well-known expression for the rate as a function of the temperature,³

$$k_f = A e^{-E_{act}/k_B T}, \quad (1.1)$$

as formulated by Van 't Hoff and Arrhenius in the 1880's. Here A is the frequency factor, and E_{act} is the energy of activation. The Boltzmann factor, i.e. the exponential factor, is proportional to the probability of a molecule to be at the activated state. A molecule acquires the energy needed to reach the activated state by collisions with the molecules by which it is surrounded. An interesting aspect of Eq. (1.1) is that one and the same reaction, when studied in different solvents, may give different values for A and E_{act} . This indicates that the solvent can stabilise or destabilise the activated state with respect to the stable states,⁴ just like the solvent can stabilise or destabilise one stable state with respect to another stable state.

The aim of the research presented in this thesis is to calculate the rate of a reaction in a condensed phase, and to study the influence of the particular solvent. In order to realistically

account for the influence of the solvent on the reaction, we simulate the dynamics of the molecule and the surrounding solvent on a computer. In molecular dynamics simulations (MD) the atoms are modelled as interacting particles moving according to the laws of classical mechanics. Typical MD simulations cover the motion of several thousands of atoms over a period of a few nanoseconds; on current computers such a run would take of the order of a week to complete. Comparing this time scale with the aforementioned rate constant of circa 100 s^{-1} , it is obvious that MD simulations are much too slow to study reactions. Yet, by combining simulations with statistical mechanics, in particular the transition state theory and the reactive flux method, it proves possible to calculate even the slowest reaction rates. The basic idea is to reformulate the rate as the product of the probability for a molecule to reach the activated state, and the probability for this activated state to proceed to the next stable state; the second factor is called transmission coefficient. These ideas have previously been applied successfully to a wide variety of reactions.⁵⁻⁷ We shall apply them to an isomerisation reaction of a calix[4]arene, one of the building blocks in supramolecular chemistry.

1.2 Supramolecules

Chemical processes in living organisms often depend on the weak but very specific non-covalent interactions between molecules.⁸ Supramolecular chemistry, the field founded by the 1987 Nobel laureates Pedersen, Cram and Lehn, is devoted to the design of host-guest systems that are stabilised by the same interactions. These synthetic hosts offer convenient model systems to get a better understanding of the recognition processes that occur in nature. A variety of hosts exists: crown-ethers, spherands, cyclodextrins, carcerands and calixarenes, to mention but a few.

The name calix[n]arene was coined by Gutsche for a class of cavity-shaped cyclic compounds build from 4 to 8 phenol rings linked by methylene groups.^{9,10} Several of these molecules are shaped like a Greek vase, *calix crater*, which gives them their name, see Fig. 1.1. The explicit hydrogens in Fig. 1.1 can be replaced by sidegroups to give the calixarene the desired property, a procedure called functionalisation. For instance, the

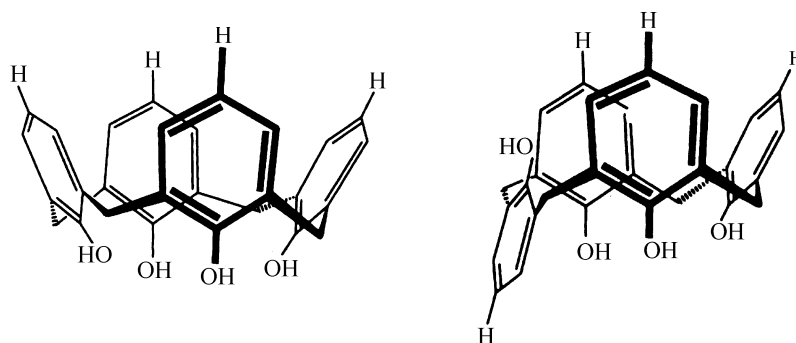


Figure 1.1. Cone (left) and partial cone (right) conformation of a calix[4]arene.

calixarene can be made to bind selectively with sodium or potassium ions, or to bind organic molecules in aqueous solution, or even to catalyse a hydrolysis reaction.

The calix[4]arene in Fig. 1.1 can take on four discrete forms. The most abundant conformation is the ‘cone’ conformation in which all phenol rings are orientated in the same direction. The four hydroxyl groups at the lower rim then form a circular array of four internal hydrogen bonds which stabilise the molecule. In the ‘partial cone’ conformation one of the phenol rings is rotated with respect to the other three, see Fig. 1.1. Since this conformation allows for only two internal hydrogen bonds it is energetically less favourable. There are two conformations in which two phenols are orientated in one direction and the other two phenols in the other direction, namely the 1,2-alternate with two internal hydrogen bonds, and the 1,3-alternate devoid of internal hydrogen bonds. In this thesis we shall focus on the cone to partial cone isomerisation. In order to apply Eq. (1.1) we introduce the concept of a reaction coordinate. This coordinate discriminates reactants from products. In the present case, for example, it may be the angle ξ between the central annulus and the phenol ring making the transition. In Fig. 1.2 the minimum potential energy, Φ , is plotted as a function of ξ . The activated state, also called transition state, is seen to be located at $\xi \approx -20^\circ$. The activation energy E_{act} of this reaction has been measured by $^1\text{H-NMR}$ to vary between 12 and 15 kcal/mol, depending on the solvent.

1.3 Survey

In chapter 2 we give a concise introduction to statistical mechanics, followed by a derivation of the reaction rate expressions that will be used in latter chapters. The basic

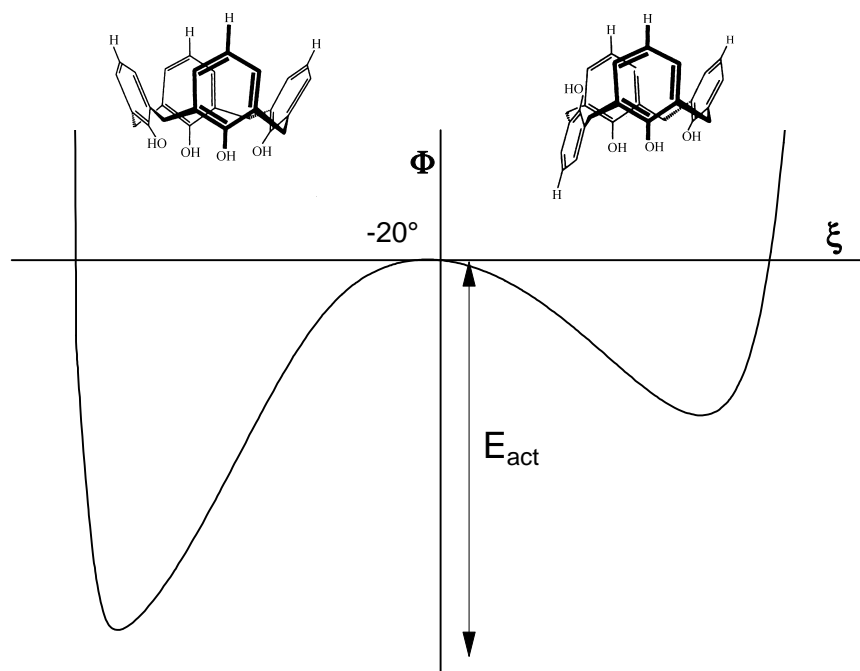


Figure 1.2. Energy, Φ , as a function of the angle, ξ , between the central annulus and the reacting phenol ring.

concepts of molecular dynamics simulations are discussed. In these simulations the use of an angle ξ , as introduced above, would be very inconvenient. In chapter 3 a new reaction coordinate is introduced, with suitable properties for use in molecular dynamics simulations. Also in this chapter the transmission coefficient of the isomerisation of a calix[4]arene *in vacuo* and in chloroform is calculated. In the next chapter it will be shown that it is not the energy but the free energy as a function of the reaction coordinate which determines the probability factor of the exact reaction rate. Therefore, in chapter 4 the free energy of the calix[4]arene in chloroform is calculated. The reaction rate calculated with these two results is in excellent agreement with experimental data. In chapter 5 we study the effect of two different solvents, namely chloroform and benzene, on the reaction. The reader who wants to get familiar with the applied methods and its results without going through the mathematical rigor will find this chapter most rewarding. In chapter 6 we discuss the calculation of free energies by means of constrained molecular dynamics simulations. The relation between the free energy and the constraint force is shown to be less trivial than what was assumed by many authors. We end with a summary and a brief look at the future in chapter 7.

1.4 References

- ¹ P. Hanggi, P. Talkner and M. Borkovec, *Rev. Mod. Phys.* **62**, 251 (1990).
- ² We shall not consider the quantum mechanical process of tunneling through the barrier, since it is highly improbable for the reaction studied here.
- ³ S. Glasstone, K. J. Laidler and H. Eyring, *The Theory of Rate Processes* (McGraw-Hill Book Company, New York, 1941).
- ⁴ Note that a distinctive explanation may hold for diffusion controlled reactions.
- ⁵ D. L. Beveridge and F. M. DiCapua, *Annu. Rev. Biophys. Biophys. Chem.* **18**, 431-92, (1989).
- ⁶ R. M. Whitnell and K. R. Wilson, *Rev. Comp. Chem.* **IV**, 67 (1993).
- ⁷ J. B. Anderson, *Adv. Chem. Phys.* **XCI**, 381 (1995).
- ⁸ L. Stryer, *Biochemistry* (W. H. Freeman and Company, New York, 1995).
- ⁹ C. D. Gutsche, *Calixarenes* (Royal Society of Chemistry, Cambridge, UK, 1989).
- ¹⁰ J. Vicens and V. Böhmer, Eds., *Calixarenes: A Versatile class of macrocyclic compounds* (Kluwer Academic Publishers, Dordrecht, The Netherlands, 1991).

Chapter 2

Theory

2.1 Statistical mechanics

Thermodynamics studies the mathematical relations between the experimental properties of a macroscopic system in equilibrium, but it does not predict the magnitude of these properties, nor does it provide a link between these properties and the atomic constitution of the system. In statistical mechanics the microscopic or atomic point of view is used to study the properties of the macroscopic system. As will be discussed below, statistical mechanics offers alternative interpretations for macroscopic properties and thermodynamical relations, as well as providing numerical values.

2.1.1 Static properties

At the heart of statistical mechanics lies the notion that a macroscopic system has an incredible large number of microscopic realisations.¹ The probability for each of these realisations to occur can be calculated, and a macroscopic property can be calculated as the average of the corresponding microscopic property over all realisations. Consider for example the canonical ensemble, the collection of all realisations of a system of N identical atoms in a volume V at an absolute temperature T . From the classical point of view any realisation can be characterised by the coordinates, \mathbf{r}_i , and the momenta, \mathbf{p}_i , of the atoms. In the canonical ensemble the probability to find a system in the volume element $d\Gamma^N$ centred at the point $\Gamma^N = (\mathbf{r}_1, \dots, \mathbf{r}_N, \mathbf{p}_1, \dots, \mathbf{p}_N)$ in phase space is given by the Boltzmann distribution,

$$\rho(\Gamma^N)d\Gamma^N = \frac{1}{Q} \frac{1}{h^{3N} N!} \exp[-\beta H(\Gamma^N)]d\Gamma^N, \quad (2.1)$$

where $\beta = 1/k_B T$, k_B is Boltzmann's constant and H is the Hamiltonian, i.e. the energy of the realisation. The second factor on the right hand side, containing Planck's constant h , arises to make the classical mechanical distribution agree with the quantum mechanical distribution. The first term on the right hand side is used to normalise the distribution, where

$$Q = \frac{1}{h^{3N} N!} \int \exp[-\beta H(\Gamma^N)]d\Gamma^N \quad (2.2)$$

is known as the partition function. The partition function is related to the Helmholtz free energy, $A = U - TS$, the macroscopic potential of a closed system of constant volume in contact with a heat bath, by

$$A = -k_B T \ln Q. \quad (2.3)$$

Combining this result with the usual thermodynamical expressions, one may relate the (derivatives of the) microscopic partition function to macroscopic properties, such as the pressure and the entropy.

If a macroscopic property, F , has a microscopic analogue, f , the measured value of F is equal to the expectation value of f over the microscopic realisations:

$$F = \frac{1}{Q} \frac{1}{h^{3N} N!} \int f(\Gamma^N) \exp[-\beta H(\Gamma^N)] d\Gamma^N, \quad (2.4)$$

henceforth to be written as

$$F = \langle f \rangle. \quad (2.5)$$

The analytic solution of the integral is terribly complicated, so one normally resorts to numerical methods to approximate the result. In Monte Carlo simulations a random number generator is used to sample points in phase space according to the Boltzmann distribution. Another way of calculating F is based on the notion that the microscopic realisations of a system by evolving according to classical or quantum mechanics, in the long term constitute a representation of the distribution $\rho(\Gamma^N)$. The average obtained by following a realisation over a time interval T is

$$\bar{f} = \frac{1}{T} \int_0^T f[\Gamma^N(t)] dt. \quad (2.6)$$

The ergodic hypothesis¹ states that this average equals the phase space average, provided the interval T is long enough:

$$\langle f \rangle = \lim_{T \rightarrow \infty} \bar{f}. \quad (2.7)$$

The average of Eq. (2.6) is obtained by molecular dynamics simulations, as described in section 2.3. We will now switch from static to dynamic properties.

2.1.2 Dynamic properties

Suppose we have a macroscopic system prepared in a non-equilibrium condition by an external perturbation. The property F then differs from its equilibrium value by $\Delta F(t) \equiv F(t) - F_{eq}$. At time $t = 0$ the perturbation is removed, and the system relaxes to equilibrium. If the perturbation is small enough to lie in the linear regime of the system, the deviation ΔF gradually vanishes according to the macroscopic law

$$\Delta F(t) = \Delta F(0) \phi(t), \quad (2.8)$$

where ϕ is the response function. We shall assume that this ‘phenomenological’ function is known, either from experiments or from intuitive reasoning.

At the microscopic level the situation is more involved. Even without an external perturbation, the parameter f will differ from its equilibrium value for nearly all realisations at time $t = 0$, simply because of the Boltzmann distribution. If we concentrate on a single realisation, we will see that as time progresses the value of f behaves very erratic because of the complex motion of the atoms in the system. All one knows is that for short times $\Delta f(t) \equiv f(t) - \langle f \rangle$ is correlated to $\Delta f(0)$, while for long times the correlation will vanish, $\langle \Delta f(\infty) \rangle = 0$. To reduce the noise, we now average over all realisations with the same initial value $\Delta f(0)$. Onsager’s regression hypothesis^{2,3} states that this average behaves as the macroscopic system,

$$\langle \Delta f(t) \rangle_{\Delta f(0)} = \Delta f(0) \phi(t), \quad (2.9)$$

where ϕ is the macroscopic response function of Eq. (2.8). Multiplying by $\Delta f(0)$ and integrating over all values of $\Delta f(0)$, we arrive at the more common notation,

$$\langle \Delta f(t) \Delta f(0) \rangle = \langle \Delta f^2(0) \rangle \phi(t). \quad (2.10)$$

Note that an external perturbation is not required; spontaneous fluctuations of the system will, on average, relax according to the macroscopic law too. We must, however, make the exception that the hypothesis does not hold for very short times, since the macroscopic law of Eq. (2.8) only holds on a macroscopic time scale.

On the left hand side of Eq. (2.10) we encountered a correlation function,

$$\langle f(t)g(0) \rangle = \int \rho(\Gamma^N, 0) f(\Gamma^N, t) g(\Gamma^N, 0) d\Gamma^N, \quad (2.11)$$

where $f(\Gamma^N, t)$ is to be interpreted as the value of f at time t for a realisation that was at Γ^N at time $t = 0$. For a system in equilibrium the correlation function depends on the time interval only, so

$$\langle f(t + \tau)g(\tau) \rangle = \langle f(t)g(0) \rangle. \quad (2.12)$$

After differentiating with respect to τ the right hand side equals zero, and upon substituting $\tau = 0$ in the left hand side we arrive at

$$\langle \dot{f}(t)g(0) \rangle = -\langle f(t)\dot{g}(0) \rangle, \quad (2.13)$$

where a dot indicates the derivative of a function with respect to time.

2.2 Reaction rate theory

As an application of the above described Onsager regression hypothesis, we will consider the reversible unimolecular reaction between reactants, R , and products, P , dissolved in a liquid:



We shall first consider the macroscopic system, then the microscopic system.

2.2.1 Macroscopic reaction rate

The phenomenological equations for the population dynamics read as

$$\begin{aligned} \dot{R} &= -k_f R + k_r P, \\ \dot{P} &= k_f R - k_r P, \end{aligned} \quad (2.15)$$

where k_f and k_r are the rate constants of the forward and the reverse reaction respectively. In the above master equations it is assumed that a certain fraction of the reactants is turned into products per unit of time, and likewise for the products. The sum of reactants and products is seen to be constant. The equilibrium constant of the reaction is defined as the ratio of the equilibrium fractions,

$$K = \frac{R_{eq}}{P_{eq}} = \frac{k_r}{k_f}, \quad (2.16)$$

where the right hand side follows from the fact that both expressions of Eq. (2.15) are zero at equilibrium. By combining the last two equations, any deviation from equilibrium, $\Delta P(t) \equiv P(t) - P_{eq}$, is seen to relax as

$$\Delta P(t) = \Delta P(0)e^{-\lambda t}, \quad (2.17)$$

with the relaxation rate

$$\lambda = k_f + k_r. \quad (2.18)$$

The forward rate constant is related to the overall relaxation rate by

$$k_f = \lambda \frac{P_{eq}}{R_{eq} + P_{eq}}, \quad (2.19)$$

as follows from combining Eqs. (2.16) and (2.18).

We want to calculate the forward rate constant of a reaction in a solvent. Molecular dynamics simulations, see sec. 2.3, provides the tools to calculate the motion of a solvated molecule, but unfortunately these simulations are fairly slow. On current computers the simulation time span is limited to a dozen nanoseconds, so the obvious route of using molecular dynamics simulations to follow a non-equilibrium system as it evolves to equilibrium is not feasible for most reactions. For slow reactions we need the machinery of statistical mechanics, as described below, to calculate a rate constant.

2.2.2 Microscopic reaction rate

For a microscopic discussion of the reaction we first of all need to introduce a more stringent definition of reactants and products than the above tacitly used definition. The reaction coordinate, $\xi(\mathbf{r}^N)$, is a function of the coordinates of the reacting system, defined in such a way that it is positive for products and negative for reactants. A concrete example, apart from a shift by 20 degrees of the horizontal axis, is given in Fig. 1.2. Another example is the dihedral angle of an isomerising *n*-butane molecule. A more general reaction coordinate, based on the normal modes of the saddle point on top of the energy barrier, is introduced in chapter 3. The dividing plane $\xi = 0$ will henceforth be called the transition state. We shall consider a system with a low solute concentration, in which case the reacting molecules do not interact. Each molecule then behaves identically, hence it suffices to concentrate on a single molecule. The probability for a molecule to be in the product state is obtained by summing over all realisations that classify as a product,

$$\langle p \rangle = \int \theta[\xi(\Gamma^N)] \exp[-\beta H(\Gamma^N)] d\Gamma^N = \langle \theta(\xi) \rangle, \quad (2.20)$$

where θ is the Heaviside step function,

$$\theta(\xi) = \begin{cases} 0 & \text{if } \xi < 0 \\ 1 & \text{if } \xi > 0. \end{cases} \quad (2.21)$$

An expression similar to Eq. (2.20), but with ξ replaced by $-\xi$, gives the expectation value of the fraction of reactants. Note that the expectation value of the number of product molecules, and hence its time derivative, will hardly depend on the chosen reaction coordinate, since the Boltzmann factor is very small near the top of the energy barrier. The deviation from equilibrium for any realisation reads as

$$\Delta p = \Delta \theta[\xi(\Gamma^N)] = \theta[\xi(\Gamma^N)] - \langle \theta(\xi) \rangle. \quad (2.22)$$

Inserting this result in Eq. (2.10), and using the macroscopic law of Eq. (2.17), we find

$$\frac{\langle \Delta \theta[\xi(t)] \Delta \theta[\xi(0)] \rangle}{\langle \Delta \theta^2[\xi(0)] \rangle} = e^{-\lambda t}. \quad (2.23)$$

We now face the problem of extracting the rate constant λ from the averages on the left hand side. Obviously, performing a long simulation to observe the exponential decay of the left hand side, as in the Einstein equation for the self diffusion, is out of the question. A common alternative, a Green-Kubo-type equation does not work either as the autocorrelation of the derivative \dot{p} also decays too slow.⁴ Differentiating Eq. (2.23) with respect to time gives

$$\frac{\langle \dot{\theta}[\xi(t)] \Delta \theta[\xi(0)] \rangle}{\langle \Delta \theta^2[\xi(0)] \rangle} = -\lambda e^{-\lambda t}. \quad (2.24)$$

Suppose, now, that we evaluate this expression at a time t in the interval

$$\tau_v \ll t \ll \frac{1}{\lambda}. \quad (2.25)$$

As was remarked earlier, Onsager's regression hypothesis does not hold on the very short time scale of molecular vibrations, τ_v . Under the second condition of Eq. (2.25) the exponential of Eq. (2.24) will be nearly unity, hence

$$\lambda = \frac{\langle \theta[\xi(t)] \dot{\xi}(0) \delta[\xi(0)] \rangle}{\langle \Delta\theta^2[\xi(0)] \rangle}, \quad (2.26)$$

where we have used Eq. (2.13). The Dirac delta function, $\delta(\xi)$, arises as the derivative of the Heaviside function; its defining properties are:

$$\delta(\xi) = 0 \quad \text{if} \quad \xi \neq 0, \quad (2.27)$$

and

$$\int_a^b \delta(\xi) d\xi = 1 \quad \text{if} \quad a < 0 < b. \quad (2.28)$$

From Eq. (2.20) one infers

$$\langle \Delta\theta^2 \rangle = \langle \theta^2 \rangle - \langle \theta \rangle^2 = \langle r \rangle \langle p \rangle, \quad (2.29)$$

using $\langle \theta^2 \rangle = \langle \theta \rangle$ and $\langle r \rangle + \langle p \rangle = 1$. Combining Eqs. (2.19), (2.26) and (2.29) gives the final result, first proposed by Yamamoto in 1960:^{5,6}

$$k_f^{RF}(t) = \frac{\langle \delta[\xi(0)] \dot{\xi}(0) \theta[\xi(t)] \rangle}{\langle \theta[-\xi(0)] \rangle}. \quad (2.30)$$

This theory is known as the reactive flux method (RF). In the numerator we have the average velocity of molecules that cross the transition state at $t = 0$ and end up in the product well a time t later, i.e. the 'flux' through the transition state of molecules going from the reactant well to the product well. This flux is called the reactive flux to distinguish it from the more common definition of the flux as the number of molecules that cross a plane per unit of time. In the denominator we recognise the equilibrium reactant fraction. The ratio of the reactive flux and the population of the reactant well equals the fraction of reactants turned into products per unit of time, which by Eq. (2.15) is seen to be the rate constant of the forward reaction.

2.2.3 Transition state theory

In the limit of time t going to zero Eq. (2.30) reduces to

$$k_f^{TST} = \frac{\langle \delta[\xi(0)] \dot{\xi}(0) \theta[\dot{\xi}(0)] \rangle}{\langle \theta[-\xi(0)] \rangle}. \quad (2.31)$$

(from Eq. (2.13), with $f = g$, it follows that the right hand side of Eq. (2.30) is zero at time $t = 0$). This is the renowned transition state theory (TST) expression for the rate, as proposed by Eyring⁷ in 1935. Unlike in Eq. (2.30), where the flux is calculated by averaging over all molecules that end up in the product well after they cross the transition state in whatever direction, the flux is now calculated by averaging over the molecules that cross the transition state in the positive direction. Wigner⁸ summarised the assumptions underlying transition state theory in 1937:

- The Born-Oppenheimer approximation, i.e. the electron wavefunction is at all times adapted to the nuclear configuration. The system always remains in the ground level. As a result, the potential energy of the system is a well defined function of the coordinates of the nuclei (adiabatic condition).
- The motion of the nuclei on the potential energy surface can be described by classical mechanics.
- Every reactant crossing the transition state will end up as a product.

The first two assumptions are also the fundamentals of the reactive flux method and of molecular dynamics.

For actual calculations Eq. (2.31) is conveniently rewritten as

$$k_f^{TST} = \frac{\langle \delta[\xi(0)] \dot{\xi}(0) \theta[\dot{\xi}(0)] \rangle \langle \delta[\xi(0)] \rangle}{\langle \delta[\xi(0)] \rangle \langle \theta[-\xi(0)] \rangle}. \quad (2.32)$$

The first factor on the right hand side is the average velocity of reactants as they cross the transition state, and the second factor is the probability for a molecule to be at the transition state relative to the probability to be in the reactant well. For a simple reaction coordinate such as the distance between two atoms, $\xi = |\mathbf{x}_A - \mathbf{x}_B| - l_{AB}$, the first factor turns out to be independent⁹ of l_{AB} . The second factor, however, strongly depends on l_{AB} because of the numerator; as we noted earlier, the denominator hardly depends on l_{AB} provided the transition state lies near the top of the free energy barrier. Thus we see that the TST rate depends on the location of the transition state, while the true rate does not depend on this definition.

2.2.4 Transmission coefficient

We shall now concentrate on Wigner's third assumption. Eyring⁷ already noted that 'For some reactions it will happen that the same activated complex may cross the barrier and return without decomposing. This fact reduces the actual reaction rate.' In order to compensate for these recrossings, see trajectory 3 in Fig. 2.1, he wrote

$$k_f^{exact} = \kappa k_f^{TST}, \quad (2.33)$$

where the transmission coefficient, κ , is a jet unknown factor between zero and unity. Eyring and Wigner considered reactions, like $A + BC \rightarrow AB + C$, in which there is no reverse reaction because the products drift apart. In reactions with a reverse reaction, such as

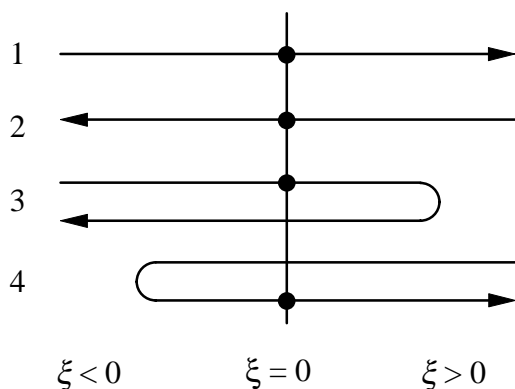


Figure 2.1. Four schematic trajectories of molecules crossing the transition state at time zero (dot).

isomerisations, the product bound flux through the transition state may also contain a contribution of products that recross the transition state after a short excursion to the reactant state, see trajectory 4 in Fig. 2.1. The transmission function must also correct for this contribution. An alternative way to look at κ is by realising, as already noted below Eq. (2.32), that the TST value strongly depends on the precise location of the transition state. Obviously, the experimental rate does not depend on this location, as long as it is in the neighbourhood of the top of the free energy barrier. The transmission coefficient, therefore, must depend on the chosen transition state to counteract the dependence of k_f^{TST} on this location.

By substituting Eqs. (2.30) and (2.31) in Eq. (2.33) we find that the transmission function is given by

$$\kappa(t) = \frac{\langle \delta[\xi(0)] \dot{\xi}(0) \theta[\xi(t)] \rangle}{\langle \delta[\xi(0)] \dot{\xi}(0) \theta[\dot{\xi}(0)] \rangle}. \quad (2.34)$$

In the denominator we average over all molecules that cross the transition state at time 0 in the positive direction. In the numerator we average over all molecules that cross the transition state at time zero and are in the product state a time t later, regardless of the direction in which they crossed the transition state. For very short times this ratio equals unity, but at longer times the ratio decreases because of recrossings, see Fig. 2.2. Gradually the numerator evolves from the instantaneous product bound flux at time $t = 0$ into the reactive flux: the flux of molecules that were in the reactant well at some time $t \ll -\tau_v$ and are in the product well at some time $t \gg \tau_v$. After a fairly short time all molecules that were at the transition state at time 0 will have arrived in the reactant or the product well. If the molecule has lost part of its excess energy to non-reactive motions or to the solvent, the chances for a spontaneous recrossing are virtually zero. The transmission function then has arrived at a plateau, which will be constant on the time scale of Eq. (2.25). The reactive flux rate of Eq. (2.30) is obtained by combining this plateau value with the TST rate:

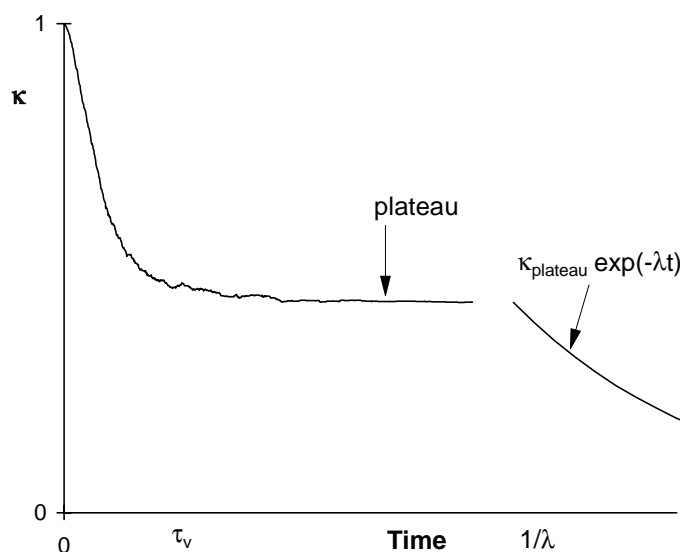


Figure 2.2. Typical plot of the transmission coefficient as a function of time.

$$k_f^{RF} = \kappa_{\text{plateau}} k_f^{TST}. \quad (2.35)$$

One may show, using Liouville's theorem and the separation of time scales, Eq. (2.25), that this rate constant is indeed independent of the location of the transition state.¹⁰ At time scales of the order of $1/\lambda$ the transmission function shows exponential decay.

The set of Eqs. (2.32) through (2.35), sometimes referred to as the Chandler-Bennett^{6,11} method, has all the characteristics we were looking for, as mentioned below Eq. (2.19), although this is not directly evident. The transmission coefficient is typically calculated by performing a thousand relaxation runs in which a molecule starts at the transition state and ends up in either of the local minima. The duration of these runs is of the order of several picoseconds, as determined by Eq. (2.25). It is less obvious why Eq. (2.32) should meet our demands, since calculating the probability for a molecule to reach the transition state still requires a simulation time much longer than $1/\lambda$. The simulation can be reduced to the order of several nanoseconds by using umbrella sampling, as explained in chapter 4. The basic idea is to bias the potential energy surface by a term, the umbrella, which makes the barrier between reactants and products effectively vanish; the effect of the umbrella on the sampled distribution is later corrected for. Alternatively, the probability for a molecule to reach the transition state can be calculated using thermodynamic integration or thermodynamic perturbation, as discussed in chapter 6.

2.3 Molecular dynamics simulations

In molecular dynamics simulations (MD) the motion of a collection of interacting atoms is calculated by means of classical mechanics.¹² Strictly speaking one would have to use quantum mechanics, but in many cases the approximation of classical mechanics will do.

With Wigner's first assumption, see section 2.2.3, the potential energy of the system becomes a unique function of the atomic coordinates only, $\Phi(\mathbf{r}^N)$. The motion of atom i with mass m_i at time t follows from Newton's equations of motion in Cartesian coordinates,

$$\dot{\mathbf{r}}_i(t) = \mathbf{v}_i(t), \quad (2.36)$$

$$\dot{\mathbf{v}}_i(t) = -\frac{1}{m_i} \nabla_i \Phi[\mathbf{r}^N(t)]. \quad (2.37)$$

The combination of the equations of motion for the N atoms of a system leads to a complicated set of coupled differential equations, which in general can not be solved analytically. Consequently, we will use a numerical scheme to approximate the solution on a computer. Rather than integrating Eqs. (2.36) and (2.37) directly, we rewrite the equations of motion in a form that is less subjected to numerical errors. From the Taylor expansion of the velocity at time $t_n = t_0 + n\Delta t$ it follows that the velocity an interval $\Delta t/2$ earlier or later is given by

$$\mathbf{v}_i(t_n \pm \frac{1}{2} \Delta t) = \mathbf{v}_i(t_n) \pm \dot{\mathbf{v}}_i(t_n) (\frac{1}{2} \Delta t) + \frac{1}{2} \ddot{\mathbf{v}}_i(t_n) (\frac{1}{2} \Delta t)^2 + O(\Delta t^3), \quad (2.38)$$

where the last term on the right hand side indicates that the truncation error is of the order of the cube of the time step. The difference between the former and the new velocity reads as,

$$\mathbf{v}_i(t_n + \frac{1}{2} \Delta t) = \mathbf{v}_i(t_n - \frac{1}{2} \Delta t) - \frac{\Delta t}{m_i} \nabla_i \Phi[\mathbf{r}^N(t_n)] + O(\Delta t^3), \quad (2.39)$$

where use was made of Eq. (2.37). A similar Taylor expansion of the coordinates, centred at time $t_n + \Delta t/2$, gives

$$\mathbf{r}_i(t_{n+1}) = \mathbf{r}_i(t_n) + \mathbf{v}_i(t_n + \frac{1}{2} \Delta t) \Delta t + O(\Delta t^3). \quad (2.40)$$

The set of Eqs. (2.39) and (2.40) is known as the leap-frog version of the Verlet algorithm. The simulations presented in this thesis were done with the GROMOS87 package,¹³ which employs this integration scheme. The time step of the integration scheme, Δt , is established by a trade-off between accuracy and speed.

The interactions between atoms, be they in the same molecule or in a different molecule, are of quantum mechanical origin. The calculation of these interactions from the appropriate equations is a rather time consuming process. In MD programs, therefore, it is assumed that the potential energy of a system can be described by the following expression:

$$\begin{aligned} \Phi(\mathbf{r}^N) = & \frac{1}{2} \sum_{i=1}^{bonds} k_{b,i} (b_i - b_{i,0})^2 + \frac{1}{2} \sum_{i=1}^{angles} k_{\phi,i} (\phi_i - \phi_{i,0})^2 \\ & + \frac{1}{2} \sum_{i=1}^{UB} k_{u,i} (u_i - u_{i,0})^2 + \frac{1}{2} \sum_{i=1}^{impropers} k_{\omega,i} (\omega_i - \omega_{i,0})^2 \\ & + \sum_{i=1}^{dihedrals} k_{\theta,i} [1 + \cos(n_i \theta_i - \theta_{i,0})] \end{aligned}$$

$$+ \sum_{j>i}^N \left[4\epsilon_{ij} \left\{ \left(\frac{\sigma_{ij}}{r_{ij}} \right)^{12} - \left(\frac{\sigma_{ij}}{r_{ij}} \right)^6 \right\} + \frac{q_i q_j}{4\pi\epsilon_0 r_{ij}} \right]. \quad (2.41)$$

The successive terms on the right hand side represent the energies of covalent bond stretching, angle bending, Urey-Bradley potential, improper dihedrals for out of plane bending, dihedrals for trans to gauche rotations around a covalent bond and finally the non-bonded interactions. The parameters of the force field are obtained by fitting the force field to experimental data and to quantum mechanical calculations. Various force fields are available; they depend on the class of molecules for which they are designed and on the choices made in the fitting process.

The non-bonded interactions are again subdivided into three parts, namely a repulsive term to represent the non-bonded overlap between electron clouds, an attractive term to represent the Van der Waals or London dispersion interaction, and a Coulomb interaction between charged atoms. The Lennard-Jones parameters for interactions between unlike atoms are given by the usual Lorentz-Berthelodt combination rules, $\sigma_{ij} = (\sigma_{ii} + \sigma_{jj})/2$ and $\epsilon_{ij} = (\epsilon_{ii}\epsilon_{jj})^{1/2}$. In the summation over all atom pairs it is to be understood that 1-2 neighbours and 1-3 neighbours are to be excluded, and that the interactions are cut-off beyond a certain distance. The interactions between 1-4 neighbours are not scaled. Covalently bonded charged atoms are grouped into charge groups of zero net charge. The Coulomb interactions in Eq. (2.41) are calculated as a double sum over the atoms in these groups. In this way the effect of the cut-off distance on the Coulomb interaction is smoothed in a better way than by using a switch function.

We end this section with sundry topics of MD simulations; the interested reader is referred to textbooks¹² for a more thorough coverage.

The time step of the integration algorithm is determined by the oscillation with the highest frequency. In organic molecules that is the stretching of the C-H and O-H bonds. These bonds hardly influence the motion of the slow degrees of freedom in which we are interested. By constraining these bond lengths, i.e. keeping them at a constant value throughout the simulation, the highest frequency in the system goes down by a factor of two, hence the time step can be increased by a factor of two. In GROMOS87 the constrained bond lengths are reset to their reference value after each simulation step using the SHAKE algorithm, as will be explained in chapters 3 and 6. A relatively short time is spent in this procedure, so effectively the simulation becomes almost twice as fast. In some situations it is useful to constrain other internal coordinates of the system as well. For instance, the transition state configurations needed in Eq. (2.34) can be sampled by a simulation in which the reaction coordinate is constrained, see chapter 3. In chapters 3 and 6 we discuss the not so obvious consequences of constraints on the sampled phase space distribution, and the counter-measures that have to be taken to get the correct averages.

In simulations the molecules are confined within a box. Since the simulated systems usually are of the order of several thousands of atoms, a relative large fraction of the atoms

will be in contact with the walls of the box. To minimise these effects, it is common practice to apply periodic boundary conditions. For a rectangular box this means that a molecule near the wall on the right interacts with the molecules near the wall on the left, and likewise a molecule near the front or near the top interacts with the molecules near the back or near the bottom respectively. The simulation box can be envisioned as being surrounded by 26 identical images. When calculating the interaction between atoms i and j , out of the 27 images of j the one closest to i must be used (minimum image convention). The box size and the cut-off radius of the non-bonded interactions must be chosen such that in the interaction between two molecules only one image of the second molecule is used, if possible. In our simulations we will frequently use a box shaped like a truncated octahedron; the minimum image convention is adapted accordingly.

The Newtonian equations of motion imply energy conservation, so the average over a simulation, Eq. (2.6), corresponds to a microcanonical ensemble. For a canonical average one may perform a series of runs at different energies and calculate the weighted average. Alternatively, one may imitate a coupling to an external heat bath by changing the energy of the system during the simulation. Generalised equipartition gives the following relation between the microscopic velocities and the macroscopic temperature:

$$\left\langle \frac{1}{2} \sum_{i=1}^N m_i \mathbf{v}_i^2 \right\rangle = \frac{3}{2} N k_B T, \quad (2.42)$$

where the left hand side is the average kinetic energy. This result is generalised by stating that the ‘instantaneous’ temperature θ of a realisation is given by

$$\theta = \frac{1}{3Nk_B} \sum_{i=1}^N m_i \mathbf{v}_i^2. \quad (2.43)$$

In the weak coupling method¹⁴ implemented in GROMOS87 the velocities after the integration step, Eq. (2.39), are multiplied by

$$\lambda = \sqrt{1 + \frac{\Delta t}{\tau_T} \left(\frac{T}{\theta} - 1 \right)}, \quad (2.44)$$

where T is the desired temperature and τ_T is the time constant of the coupling.

Since the volume occupied by a calix[4]arene in a solvent most likely depends on the conformation, it seems to be more appropriate to simulate at a constant pressure than at a constant volume. Generalised equipartition yields the virial theorem,

$$-\left\langle \sum_{i=1}^N \mathbf{r}_i \cdot \mathbf{F}_i^{tot} \right\rangle = 3Nk_B T, \quad (2.45)$$

where the total force acting on atom i , \mathbf{F}_i^{tot} , is due to the internal interactions and the external pressure exerted by the walls of the enclosing vessel. In a system with periodic boundary conditions the external pressure stems from the interactions of the central box with the surrounding images. The ‘instantaneous’ pressure then reads as¹⁵

$$\pi = \frac{2}{3V} \left(\frac{1}{2} \sum_{i=1}^N m_i \mathbf{v}_i^2 + \frac{1}{2} \sum_{i<j}^N \mathbf{R}_{ij} \cdot \mathbf{F}_{ij} \right), \quad (2.46)$$

where \mathbf{r}_{ij} and \mathbf{F}_{ij} are calculated by the minimum image convention. It is also possible to replace the sum over all atoms by a sum over all molecules, as is done in GROMOS87, by adapting the quantities on the right hand side of Eq. (2.46) accordingly.¹⁶ In the weak coupling method¹⁴ the coordinates after the integration step, Eq. (2.40), are multiplied by

$$\mu = \sqrt[3]{1 - \beta \frac{\Delta t}{\tau_p} (P - \pi)}, \quad (2.47)$$

where P is the desired pressure, τ_p is the time constant of the coupling, and β is the isothermal compressibility.

2.4 References

- ¹ D. A. McQuarrie, *Statistical mechanics* (Harper and Row, New York, 1976).
- ² L. Onsager, Phys. Rev. **37**, 405 (1931), *ibid* **38**, 2265 (1931).
- ³ D. Chandler, *Introduction to Modern Statistical Mechanics* (Oxford University Press, Oxford, U.K., 1987).
- ⁴ D. Brown and J. H. R. Clarke, J. Chem. Phys. **92**, 3062 (1990).
- ⁵ T. Yamamoto, J. Chem. Phys. **33**, 281 (1960).
- ⁶ D. Chandler, J. Chem. Phys. **68**, 2959 (1978).
- ⁷ H. Eyring, J. Chem. Phys. **3**, 107 (1935).
- ⁸ E. Wigner, Trans. Faraday Soc. **34**, 29 (1938).
- ⁹ This follows from Eq. (4.29).
- ¹⁰ W. H. Miller, Acc. Chem. Res. **9**, 306 (1976).
- ¹¹ C. H. Bennet in *Diffusion in Solids*, edited by J. J. Burton and A. S. Nowick, (Academic Press, NY, 1975), p. 73.
- ¹² M. P. Allen and D. J. Tildesley, *Computer Simulations of Liquids* (Clarendon Press, Oxford, U. K., 1987); J. M. Haile, *Molecular Dynamics Simulation: Elementary Methods* (John Wiley and Sons, New York, NY, 1992); D. Frenkel and B. Smit, *Understanding Molecular Simulations* (Academic Press, San Diego, CA, 1996).
- ¹³ H. J. C. Berendsen and W. F. van Gunsteren, *GROMOS Reference Manual* (University of Groningen, Groningen, The Netherlands, 1987).
- ¹⁴ H. J. C. Berendsen, J. P. M. Postma, W. F. van Gunsteren, A. DiNola and J. R. Haak, J. Chem. Phys. **81**, 3684 (1984).
- ¹⁵ A. J. C. Ladd in *Computer Modelling of Fluids Polymers and Solids*, edited by C. R. A. Catlow, S. C. Parker and M. P. Allen (Kluwer Academic Publishers, Dordrecht, The Netherlands, 1990), p. 55; R. T. W. Koperdraad, graduation report (University of Twente, Enschede, The Netherlands, 1991).
- ¹⁶ G. Ciccotti and J.-P. Ryckaert, Comput. Phys. Rep. **4**, 347 (1986).

Chapter 3

The reactive flux method applied to complex isomerisation reactions: using the unstable normal mode as a reaction coordinate^{*}

Abstract

A basic problem when calculating reaction rates using the reactive flux method is the introduction of a reaction coordinate. In this paper we show that it is advantageous to define a reaction coordinate by means of the unstable normal mode of the saddle point of the potential energy surface. This particular choice is made since it yields a high transmission function. Moreover, the reaction coordinate is calculated via a rapidly converging algorithm, and its derivative, which is needed in constrained runs, is calculated analytically. Calculations on the transmission coefficient of the isomerisation of *n*-butane are in good agreement with results published by others. Runs with an isomerising calix[4]arene *in vacuo* produce a very high transmission coefficient, as is the purpose of the reaction coordinate. The same molecule is also studied in chloroform.

3.1 Introduction

Conversion in condensed phases of reactants into products usually is a slow process compared with all other molecular processes. The conversion rate is expressed in terms of a rate coefficient, k_f , giving the fraction of reactants turned into products per unit of time. This article focuses on isomerisation reactions, but most of the ideas to be described are equally well applicable to other reaction types as well. In isomerisation reactions the reactants and products are different conformations of the same molecule, and

^{*} W. K. den Otter and W. J. Briels, J. Chem. Phys. **106** 5494 (1997).

interconversions are possible without forming or breaking chemical bonds. A well known and thoroughly studied example is the trans-gauche isomerisation of *n*-butane. This particular reaction is fast enough to be studied using regular equilibrium¹ or non-equilibrium² molecular dynamics simulations (MD), in spite of the simulation time being limited to a few nanoseconds. Most other reactions, however, are much too slow for this kind of simulations to be possible. To calculate their rate coefficients one needs to develop models providing the link between macroscopic long time quantities like k_f , and the microscopic short time behaviour of a single molecule in a solvent.³

Reactant and product conformations correspond to local minima of the potential energy surface (PES), separated by a barrier of elevated energy. The conformation space at the top of the barrier is called the transition state. Most of the time a molecule will be trapped in either one of the minima. By intramolecular energy redistribution and by interactions with the solvent a molecule may incidentally gain enough energy along its reactive coordinate to hop over the barrier from one well into the other. If the barrier is high compared with the thermal energy of the reactive coordinate then the transition state is sparsely populated and crossing events will be rare.

Eyring's transition state theory⁴ (TST) expresses the forward rate constant as the instantaneous flux through the transition state from reactants to products, divided by the number of reactants:

$$k_f^{TST} = \frac{\langle \delta[\xi(0)] \dot{\xi}(0) \theta[\dot{\xi}(0)] \rangle}{\langle \theta[-\xi(0)] \rangle}. \quad (3.1)$$

Here θ is the Heaviside function and the angular brackets denote a canonical average over phase space. The reaction coordinate $\xi(\{\mathbf{x}_i\})$ is a function of all molecular coordinates, defined in such a way that it is positive for products, negative for reactants and zero at the transition state. The time indication (0) is added to stress that all quantities are calculated at the same point in time. Assuming thermal equilibrium prevails throughout the reactants part of phase space, the rate constant may be shown to be given by Arrhenius' law,

$$k_f^{TST} = \frac{k_B T}{h} e^{-\Delta A^\ddagger / k_B T}, \quad (3.2)$$

where ΔA^\ddagger is the free energy difference between reactants and the transition state. This simple expression and the widespread techniques of calculating free energy differences make TST a popular technique for calculating rate constants.

At this point an important deficiency of TST needs to be addressed. The TST rate expression very much depends on ΔA^\ddagger , i.e. on the precise choice of the transition state. In principle, of course, the rate expression should indeed depend on this choice, since it implies the definition of reactants and products. In practice, however, provided the reaction is slow, the rate constant should hardly depend on the details of this definition as long as the surface dividing reactants from products lies somewhere near the top of the free energy barrier. A natural choice for this dividing surface is such that it carries the least flux,⁵ i.e. such that

ΔA^\ddagger is as large as possible. Even then, however, the result will in general be an overestimate of the true reaction rate. The reason for this is that in transition state theory it is assumed that every molecule in the reactant well that reaches the transition state will end up in the product region. Consequently, molecules which recross the transition state, e.g. after interaction with the solvent, and eventually stay in the reactant well will be treated incorrectly.

In this article the reactive flux method^{6,7} (RF) will be used to calculate the transition rate. Instead of counting all crossing events, attention shifts towards those crossing trajectories that actually reach the product well some time t after having crossed the transition state:

$$k_f^{RF}(t) = \frac{\langle \delta[\xi(0)] \dot{\xi}(0) \theta[\xi(t)] \rangle}{\langle \theta[-\xi(0)] \rangle}. \quad (3.3)$$

One easily realises that the process of averaging in combination with the time delay turns the numerator into the net flux from reactants to products.

Equation (3.3) is conveniently expressed as

$$k_f^{RF}(t) = \kappa(t) k_f^{TST}, \quad (3.4)$$

i.e. as the instantaneous flux at the transition state times the fraction that actually makes it to the product state at time t . The transmission function $\kappa(t)$ is given by

$$\kappa(t) = \frac{\langle \delta[\xi(0)] \dot{\xi}(0) \theta[\xi(t)] \rangle}{\langle \delta[\xi(0)] \dot{\xi}(0) \theta[\dot{\xi}(0)] \rangle} = \frac{\langle \dot{\xi}(0) \theta[\xi(t)] \rangle_\xi}{\langle \dot{\xi}(0) \theta[\dot{\xi}(0)] \rangle_\xi}, \quad (3.5)$$

where $\langle \dots \rangle_\xi$ denotes a conditional average. Since most recrossings follow shortly after a crossing, $\kappa(t)$ quickly decays on the time scale of molecular vibrations from one to a plateau⁷ value which remains constant on that time scale. The transmission function stabilises since after some time the molecules have moved far enough from the transition state into one of the two wells for recrossings to become extremely rare. Of course, on the far longer time scale of $1/k_f$ recrossings do still occur, so the plateau is in fact decaying extremely slowly. The real transmission coefficient κ is equal to the plateau value of $\kappa(t)$, or more precisely to the extrapolation of the plateau to its value at $t = 0$. The reactive flux method ensures that the rate constant, i.e. the product κk_f^{TST} , is insensitive to the precise definition of the reaction coordinate and transition state.⁷

The problem usually encountered when performing MD simulations of reactions in condensed phases is the extremely small chance for molecules to surmount the barrier. In the expression for $\kappa(t)$ this problem does not occur, since all trajectories start at the barrier, making the improbable probable. Stabilising the transmission function on its plateau value typically requires the simulation of several thousand trajectories for a couple of picoseconds directly after the start at the transition state. Starting configurations in the transition plane are efficiently obtained by performing biased MD or Monte Carlo runs. The influence of the applied constraint or restraint on the sampled positions and velocities is simply corrected for. Good statistics and fast convergence are obtained when the plateau value is as high as

possible, i.e. when the TST rate is as small as possible. For a Cartesian dividing plane in configuration space this suggests identification of the reaction coordinate with the displacement along the unstable direction at the saddle point. The hyperplane perpendicular to the unstable mode which includes the saddle point then is the transition state.

The reactive flux method has been used to calculate the isomerisation rates for a number of isomerisation reactions, including those of *n*-butane,⁸ dichloro-ethane,⁹ cyclohexane,¹⁰⁻¹² cyclohexene¹³ and *n*-octane¹⁴ and even the side chain rotation of BPTI¹⁵ has been studied. Numerous other reactions, including chemical reactions, have been simulated too.^{16,17} In these examples the reaction coordinates are defined in terms of distances or dihedrals. A rare exception is cyclohexane, where a special set of coordinates and an accompanying potential were introduced.¹⁸ For some of the molecules the chosen reaction coordinate indeed defines a dividing surface that includes the saddle point, while for others it is an educated guess.

Defining a reaction coordinate in a complex isomerising molecule may prove difficult. Often a torsion is the slowest internal motion, suggesting a dihedral angle as the reaction coordinate. Concerted motions, however, may drastically complicate the choice. In this article it will be shown that it is advantageous to define the reaction coordinate via the unstable normal mode at the saddle point. This objective many-body reaction coordinate is calculated by a zero-point search. Its derivative, which is needed many times in the subsequent MD simulations, may then be obtained non-iteratively, in contrast with other iteratively determined coordinates. When properly implemented, a single MD program can be used to study a wide variety of reactions.

Normal modes and their properties are introduced in section 3.2. It proves simple to describe any molecular configuration uniquely by a translation, a rotation and the amplitudes of the rotated vibrational normal modes of the saddle point. The coefficient of the unstable mode is then used as a reaction coordinate. Constraining this mode, as to sample the transition state, can be done efficiently. The constraint and its side effects are discussed in section 3.3. A method for implementing the technique in an MD program is presented in section 3.4. In section 3.5 it is shown that the results of test runs with *n*-butane in carbon tetrachloride and with liquid *n*-butane are in good agreement with previously published results. As an example of a complicated reaction the isomerisation of a calix[4]arene in chloroform is discussed.

3.2 The reaction coordinate

As we remarked already in the previous section, the precise definition of the reaction coordinate is not crucial. A physically appealing reaction coordinate is the component along the unstable normal mode of the free molecule in its transition state. In this section we shall first make some remarks about normal mode analysis, mainly for the sake of setting our notation. Next we shall describe a method to calculate the value of this reaction coordinate for any molecule in whichever orientation and whichever configuration.

Suppose we are given the potential energy surface (PES) of a molecule containing N atoms in terms of its $3N$ Cartesian coordinates. We shall collect all coordinates in a $3N$ dimensional column vector \mathbf{X} of mass-weighted 3 dimensional column vectors: $\mathbf{X}^T = (m_1^{1/2}\mathbf{x}_1^T, m_2^{1/2}\mathbf{x}_2^T, \dots, m_N^{1/2}\mathbf{x}_N^T)$. At the saddle point \mathbf{X}^0 the gradient of the potential energy equals zero, and its Taylor expansion up to second order reads

$$E_{pot} = V(\mathbf{X}^0) + \frac{1}{2}(\mathbf{X} - \mathbf{X}^0)^T \mathbf{H}(\mathbf{X} - \mathbf{X}^0). \quad (3.6)$$

Here \mathbf{H} denotes the Hessian, a matrix containing all second order derivatives of the potential with respect to the mass-weighted coordinates. Diagonalising the Hessian yields $3N$ eigenvectors and eigenvalues. In absence of external fields the potential energy is independent of the position and orientation of the molecule, ensuring that at least six eigenvalues (assuming we are dealing with a non-linear molecule) will be equal to zero. The corresponding six eigenvectors can easily be constructed:

$$(\mathbf{E}^l)^T = \left(\sqrt{m_1}(\mathbf{e}^l)^T, \sqrt{m_2}(\mathbf{e}^l)^T, \dots, \sqrt{m_N}(\mathbf{e}^l)^T \right), \quad (3.7)$$

$$(\mathbf{S}^l)^T = \left(\sqrt{m_1}(\mathbf{e}^l \times \mathbf{r}_1^0)^T, \sqrt{m_2}(\mathbf{e}^l \times \mathbf{r}_2^0)^T, \dots, \sqrt{m_N}(\mathbf{e}^l \times \mathbf{r}_N^0)^T \right), \quad (3.8)$$

where \mathbf{e}^1 , \mathbf{e}^2 and \mathbf{e}^3 are three unit vectors along the Cartesian axes, and \mathbf{r}_i^0 is the position of atom i with respect to the centre of mass for a molecule in configuration \mathbf{X}^0 . Choosing $\mathbf{X} - \mathbf{X}^0$ proportional to one of the \mathbf{E}^l or \mathbf{S}^l amounts to translating or (infinitesimally) rotating the molecule as a whole away from its reference configuration. Noticing that E_{pot} remains unaltered under such an operation, one easily concludes that \mathbf{E}^l and \mathbf{S}^l are eigenvectors of \mathbf{H} with eigenvalue zero. The remaining $3N - 6$ eigenvectors correspond to internal vibrations,

$$(\mathbf{Q}^j)^T = \left(\sqrt{m_1}(\mathbf{q}_1^j)^T, \sqrt{m_2}(\mathbf{q}_2^j)^T, \dots, \sqrt{m_N}(\mathbf{q}_N^j)^T \right), \quad (3.9)$$

and can only be obtained by explicitly diagonalising \mathbf{H} . In a regular normal mode analysis, where \mathbf{X}^0 corresponds to an energy minimum, all eigenvalues will be non-negative, equal to the square of the oscillation frequencies. At the saddle point, however, one unstable direction, \mathbf{Q}^r , occurs, which may be recognised by its negative eigenvalue or imaginary frequency.

The orthogonality of eigenvectors, or the possibility to orthogonalise eigenvectors in case of degeneracy, has some interesting consequences. The scalar product of a vibration and a translation gives

$$\mathbf{Q}^j \cdot \mathbf{E}^l = \mathbf{e}^l \cdot \sum_{i=1}^N m_i \mathbf{q}_i^j = 0 \quad \forall l, j, \quad (3.10)$$

and the scalar product of a vibration and a rotation gives

$$\mathbf{Q}^j \cdot \mathbf{S}^l = \mathbf{e}^l \cdot \sum_{i=1}^N m_i \mathbf{r}_i^0 \times \mathbf{q}_i^j = 0 \quad \forall l, j. \quad (3.11)$$

These equations are known as the Eckart conditions.¹⁹ They state that a molecule does not translate nor rotate during an *infinitesimal* vibration. Put differently: vibrations are the result of internal forces while translations and rotations require external forces. Notice that the \mathbf{S}^l as defined above are not orthogonal among each other. By making linear combinations they are simply made orthogonal. Henceforth it will be assumed that all eigenvectors have been orthonormalised.

We now come to the definition of the reaction coordinate. When the molecule is close to the transition state we may perform a harmonic analysis as described above, and identify the reaction coordinate with

$$(\mathbf{X} - \mathbf{X}^0) \cdot \mathbf{Q}^r = \xi. \quad (3.12)$$

We then immediately face the problem of how to define \mathbf{X}^0 . Notice that this will not only affect the first factor of the scalar product on the left hand side of Eq. (3.12), but also the second factor, \mathbf{Q}^r . Because we want the reaction coordinate to describe a molecular property, independent of the position and rotation of the molecule, we demand

$$(\mathbf{X} - \mathbf{X}^0) \cdot \mathbf{E}^l = 0 \quad \forall l, \quad (3.13)$$

$$(\mathbf{X} - \mathbf{X}^0) \cdot \mathbf{S}^l = 0 \quad \forall l, \quad (3.14)$$

i.e. we assume that the state \mathbf{X} can be obtained from the state \mathbf{X}^0 without translating or rotating the molecule. Here too, the eigenvectors depend on \mathbf{X}^0 . Together with the fact that \mathbf{X}^0 should correspond to a saddle point these equations completely specify \mathbf{X}^0 .

Equation (3.13) is trivially satisfied when all coordinates refer to the centre of mass of the molecule, which we shall assume in the remaining part of this paper. To solve Eq. (3.14) for \mathbf{X}^0 , we introduce a reference geometry \mathbf{Y}^0 with the molecule in its saddle point, and write

$$\mathbf{X}^0 = \mathbf{A}\mathbf{Y}^0. \quad (3.15)$$

Here \mathbf{A} is a $3N$ dimensional rotation matrix, containing N copies of a three dimensional rotation matrix \mathbf{a} along the diagonal. Once the rotation matrix \mathbf{A} has been found, the normal modes of \mathbf{X}^0 are given by $\mathbf{A}\mathbf{E}^l$, $\mathbf{A}\mathbf{S}^l$ and $\mathbf{A}\mathbf{Q}^j$, where \mathbf{E}^l , \mathbf{S}^l and \mathbf{Q}^j are the normal modes belonging to the reference geometry \mathbf{Y}^0 . Equation (3.14) now reads

$$(\mathbf{X} - \mathbf{A}\mathbf{Y}^0) \cdot \mathbf{A}\mathbf{S}^l = 0 \quad \forall l, \quad (3.16)$$

and the reaction coordinate is given by

$$(\mathbf{X} - \mathbf{A}\mathbf{Y}^0) \cdot \mathbf{A}\mathbf{Q}^r = \xi. \quad (3.17)$$

These two equations combined uniquely define ξ for every configuration. A numerical method for solving Eq. (3.16) will be discussed in section 3.4.

In the neighbourhood of the transition state, where the harmonic expansion of the potential is valid, the reaction coordinate has a clear physical interpretation as the displacement along the unstable normal mode. Since \mathbf{Q}^r is tangent to the mass-weighted path of steepest descent, the definition of ξ is then closely related to the common intrinsic reaction coordinate²⁰ (IRC). Far away from the transition state, i.e. for large ξ , the coordinate loses its physical interpretation and reduces to a mere mathematical description of the molecular configuration. This does not affect the validity of our reaction coordinate, since for large ξ , i.e. for $t > 0$, Eq. (3.3) only requires the sign of ξ . Accuracy is therefore demanded only near the transition state, i.e. at $t = 0$ in Eqs. (3.1) and (3.3), and that is precisely where ξ is stringently defined. Elsewhere a rough estimate of the reaction coordinate will do. Note that Eqs. (3.16) and (3.17) can *not* ensure that ξ is positive (negative) throughout the entire product (reactant) region. This has to be verified before using the present definition of ξ .

Equations (3.16) and (3.17) may also be understood by using a slightly different point of view. It is clear that any configuration \mathbf{X} can be obtained from the reference geometry by a superposition of \mathbf{Y}^0 and all vibrations, followed by a rotation:

$$\mathbf{X} = \mathbf{A} \left(\mathbf{Y}^0 + \sum_{j=1}^{3N-6} \alpha_j \mathbf{Q}^j \right). \quad (3.18)$$

The amplitude of the unstable normal mode is then identified with the reaction coordinate, $\xi = \alpha_r$. By using the orthonormality of normal modes, the solution to this equation again yields the Eqs. (3.16) and (3.17).

3.3 Sampling the transition state

3.3.1 Constrained dynamics

In order to efficiently calculate the numerator and denominator on the right hand side of Eq. (3.5) we need to perform a simulation with the molecule constrained to the saddle plane $\xi = 0$. This we do by means of the SHAKE algorithm of Ryckaert *et al.*²¹ Suppose we apply L holonomic constraints $\sigma_l(\mathbf{X}) = 0$, $l = 1, \dots, L$. As a result every atom in the molecule experiences an additional force, a constraint force of the form $-\sum_{l=1}^L \lambda_l \nabla_i \sigma_l$, where the λ_l are L Lagrange multipliers. The λ_l are determined by imposing that the L constraints hold at every time. Several methods may be chosen to solve for the λ_l , the most common being that the constraints are treated one at a time. Because imposing one constraint may do harm to all others, one usually has to go through all constraints several times in a cyclical fashion. This iterative procedure allows for the λ_l to be calculated to lowest order only.

We shall now restrict our discussion to the constraint $\xi = 0$. The result of imposing this constraint is that a constraint force

$$\mathbf{F}_i^r = -\lambda_r \nabla_i \xi \quad (3.19)$$

applies to atom i . The Lagrange multiplier λ_r has to be chosen such that the constraint is satisfied at every instant. When using the Verlet algorithm the displacement during the interval $(t, t + \Delta)$ reads

$$\mathbf{x}_i(t + \Delta) = \mathbf{x}'_i(t + \Delta) - \frac{\Delta^2}{m_i} \lambda_r \nabla_i \xi(t), \quad (3.20)$$

where $\mathbf{x}'_i(t + \Delta)$ is the position atom i would have had at time $t + \Delta$ had there been no constraint force. Inserting this into the constraint equation $\xi = 0$ yields an expression for λ_r . Usually this expression is solved to first order by writing

$$\xi(t + \Delta) = \xi'(t + \Delta) - \lambda_r \Delta^2 \sum_{i=1}^N \frac{1}{m_i} \nabla_i \xi'(t + \Delta) \cdot \nabla_i \xi(t), \quad (3.21)$$

where $\xi'(t + \Delta)$ is the value of the constraint coordinate when the atoms are at the positions $\mathbf{x}'_i(t + \Delta)$. Putting the left hand side equal to zero yields λ_r to first order. In successive iterations the newly calculated $\mathbf{x}_i(t + \Delta)$ replace the old $\mathbf{x}'_i(t + \Delta)$.

The important object to calculate now is $\nabla_i \xi$. The main problem in evaluating the gradient of Eq. (3.17) lies in the derivative of the rotation matrix, which will be dealt with first. Since \mathbf{a} is a rotation matrix it satisfies $\mathbf{a}^T \mathbf{a} = \mathbf{I}$, from which, after differentiating with respect to the α -coordinate of atom i , follow the six conditions

$$\left(\frac{\partial \mathbf{a}}{\partial x_{i\alpha}} \right)^T \mathbf{a} + \mathbf{a}^T \left(\frac{\partial \mathbf{a}}{\partial x_{i\alpha}} \right) = \mathbf{0}. \quad (3.22)$$

Expressing the matrix derivative as the product

$$\frac{\partial \mathbf{a}}{\partial x_{i\alpha}} = \mathbf{b}_{i\alpha} \mathbf{a} \quad (3.23)$$

and substituting this into Eq. (3.22) we find

$$\mathbf{b}_{i\alpha}^T = -\mathbf{b}_{i\alpha}. \quad (3.24)$$

Any antisymmetric matrix can be expanded as a linear combination of three independent antisymmetric matrices \mathbf{e}^k , so

$$\mathbf{b}_{i\alpha} = \sum_{k=1}^3 c_{i\alpha}^k \mathbf{e}^k. \quad (3.25)$$

The unknown $c_{i\alpha}^k$ may be obtained from the definition of \mathbf{a} , Eq. (3.16). Differentiating this equation with respect to the α -coordinate of atom i and substituting Eqs. (3.23) and (3.25) we get, after changing the order of summation,

$$0 = m_i (\mathbf{a} \mathbf{s}'_i)_\alpha + \sum_{k=1}^3 c_{i\alpha}^k \left\{ (\mathbf{e}^k \mathbf{a}) : \left(\sum_{j=1}^N m_j \mathbf{s}'_j \mathbf{x}_j \right) \right\}. \quad (3.26)$$

For every i and α this expression constitutes a set of three equations, i.e. one for every l , in the three unknown $c_{i\alpha}^k$, $k = 1, 2, 3$. Notice that the expression between curly brackets can be regarded as an element of a matrix, \mathbf{M} , which does not depend on i nor on α . Equation (3.26) is then easily solved for $c_{i\alpha}^k$, yielding the same linear combination of $m_i(\mathbf{a}\mathbf{s}_i^l)_\alpha$'s for every i and α .

We now return to the definition of the reaction coordinate, Eq. (3.17). Differentiating and substituting Eqs. (3.23) and (3.25) yields

$$\frac{\partial \xi}{\partial x_{i\alpha}} = m_i (\mathbf{a}\mathbf{q}_i^r)_\alpha + \sum_{k=1}^3 c_{i\alpha}^k \left\{ (\boldsymbol{\varepsilon}^k \mathbf{a}) : \left(\sum_{j=1}^N m_j \mathbf{q}_j^r \mathbf{x}_j \right) \right\}. \quad (3.27)$$

Again, the factor between curly brackets can be regarded as an element of a vector, \mathbf{N}^r , which is independent of i and α . Upon substituting the $c_{i\alpha}^k$ found from Eq. (3.26), the final result reads

$$\nabla_i \xi = m_i \mathbf{a} \left(\mathbf{q}_i^r - \sum_{l=1}^3 d_l^r \mathbf{s}_i^l \right), \quad (3.28)$$

where the coefficients,

$$d_l^r = \sum_{k=1}^3 \mathbf{N}_k^r (M^{-1})_{kl}, \quad (3.29)$$

are independent of i . From a calculation point of view this is a very attractive expression, since the cumbersome d_l^r need to be evaluated only once for every \mathbf{X} . At the saddle point the gradient takes a particular simple form, since then $\mathbf{N}^r = \mathbf{0}$ and $d_l^r = 0$. Note that the constraint force is derived from an internal coordinate, and hence does not affect the angular momentum of the molecule. Therefore, one does not need to explicitly use this conservation property when defining the constraint force, as was done by Tobias and Brooks.²²

3.3.2 The conditional average at the transition state

In this subsection we present the formulas needed to calculate the conditional averages in Eq. (3.5). Things will be complicated a bit by the fact that apart from the constraint on ξ we will also make use of the usual constraints on the bond lengths involving hydrogen atoms. We therefore have one constraint $\xi = 0$ and L constraints $\sigma_l = 0$. We introduce the generalised coordinates $q_1, \dots, q_{3N-L-1}, \xi, \sigma_1, \dots, \sigma_L$, and write for the kinetic energy

$$T_{q\xi\sigma} = \frac{1}{2} \mathbf{p}_{q\xi\sigma}^T \mathbf{A}_{q\xi\sigma}^{-1} \mathbf{p}_{q\xi\sigma}, \quad (3.30)$$

where $\mathbf{p}_{q\xi\sigma}$ represents the column vector of all generalised momenta. One of Hamilton's equations of motion then reads

$$\mathbf{v}_{q\xi\sigma} = \frac{\partial T_{q\xi\sigma}}{\partial \mathbf{p}_{q\xi\sigma}} = \mathbf{A}_{q\xi\sigma}^{-1} \mathbf{p}_{q\xi\sigma}, \quad (3.31)$$

where $\mathbf{v}_{q\xi\sigma}$ is the column vector of all generalised velocities. We will make use of the following notation

$$\mathbf{A}_{q\xi\sigma} = \begin{pmatrix} \mathbf{A}_q & \mathbf{B}_{\xi\sigma} \\ \mathbf{B}_{\xi\sigma}^T & \mathbf{C}_{\xi\sigma} \end{pmatrix}, \quad (3.32)$$

$$\mathbf{A}_{q\xi\sigma}^{-1} = \begin{pmatrix} \mathbf{X}_q & \mathbf{Y}_{\xi\sigma} \\ \mathbf{Y}_{\xi\sigma}^T & \mathbf{Z}_{\xi\sigma} \end{pmatrix}, \quad (3.33)$$

where \mathbf{A}_q is the $(3N - L - 6) \times (3N - L - 6)$ left upper block of $\mathbf{A}_{q\xi\sigma}$, etc.

We are interested in the integral

$$\begin{aligned} & \int d\mathbf{q}d\mathbf{p}_q \int d\xi dp_\xi \int d\boldsymbol{\sigma}d\mathbf{p}_\sigma F \delta(\xi) \exp[-\beta(T_{q\xi\sigma} + \Phi)] \\ & \approx \int d\mathbf{q}d\mathbf{p}_q \int d\xi dp_\xi \int d\boldsymbol{\sigma}d\mathbf{p}_\sigma F \delta(\xi) \delta(\boldsymbol{\sigma}) \exp[-\beta(T_{q\xi\sigma} + \Phi)], \end{aligned} \quad (3.34)$$

where Φ is the potential energy, $\beta = 1/k_B T$, and F , the function to be averaged, may depend on all variables. In the second expression we have made the usual assumption for stiff variables. Because of the δ -functions, ξ and $\boldsymbol{\sigma}$ may be put equal to zero in F , $T_{q\xi\sigma}$ and Φ .

We intend to compute the integral (3.34) by using the constrained molecular dynamics simulations described in the previous section. Since in these simulations not only ξ and $\boldsymbol{\sigma}$ are constrained to zero, but also $\dot{\xi}$ and $\dot{\boldsymbol{\sigma}}$, it is advantageous to change coordinates from $(\mathbf{p}_q, p_\xi, \mathbf{p}_\sigma) = (\mathbf{p}_q, \mathbf{p}_{\xi\sigma})$ to $(\mathbf{p}_q, \xi, \dot{\boldsymbol{\sigma}}) = (\mathbf{p}_q, \mathbf{v}_{\xi\sigma})$ according to

$$\begin{pmatrix} \mathbf{p}_q \\ \mathbf{v}_{\xi\sigma} \end{pmatrix} = \begin{pmatrix} \mathbf{1} & \mathbf{0} \\ \mathbf{Y}_{\xi\sigma}^T & \mathbf{Z}_{\xi\sigma} \end{pmatrix} \begin{pmatrix} \mathbf{p}_q \\ \mathbf{p}_{\xi\sigma} \end{pmatrix}, \quad (3.35)$$

where the second line follows from Eqs. (3.31) and (3.33). The Jacobian of this transformation equals $|\mathbf{Z}_{\xi\sigma}|^{-1}$. The kinetic energy can be calculated by inverting Eq. (3.35) and introducing the result into Eq. (3.30):

$$T_{q\xi\sigma} = \frac{1}{2} \mathbf{p}_q^T \mathbf{A}_q^{-1} \mathbf{p}_q + \frac{1}{2} \mathbf{v}_{\xi\sigma}^T \mathbf{Z}_{\xi\sigma}^{-1} \mathbf{v}_{\xi\sigma}. \quad (3.36)$$

Integral (3.34) then reads

$$\begin{aligned} & \int d\mathbf{q}d\mathbf{p}_q \int d\xi d\dot{\xi} \int d\boldsymbol{\sigma}d\dot{\boldsymbol{\sigma}} F \exp[-\beta(T_q + \Phi)] \delta(\xi) \delta(\boldsymbol{\sigma}) |\mathbf{Z}_{\xi\sigma}|^{-1} \exp[-\frac{1}{2} \beta \mathbf{v}_{\xi\sigma}^T \mathbf{Z}_{\xi\sigma}^{-1} \mathbf{v}_{\xi\sigma}] \\ & \propto \int d\mathbf{q}d\mathbf{p}_q \int d\dot{\xi} \int d\dot{\boldsymbol{\sigma}} F P_{\xi\sigma}^c(\mathbf{q}, \mathbf{p}_q) |\mathbf{Z}_{\xi\sigma}|^{-1} \exp[-\frac{1}{2} \beta \mathbf{v}_{\xi\sigma}^T \mathbf{Z}_{\xi\sigma}^{-1} \mathbf{v}_{\xi\sigma}], \end{aligned} \quad (3.37)$$

where $T_q = \frac{1}{2} \mathbf{p}_q^T \mathbf{A}_q^{-1} \mathbf{p}_q$, and $P_{\xi\sigma}^c(\mathbf{q}, \mathbf{p}_q)$ is the probability distribution in $(\mathbf{q}, \mathbf{p}_q)$ -space as it is generated by a molecular dynamics simulation during which ξ and $\boldsymbol{\sigma}$ are constrained.²³

In the application ahead of us F will be $\dot{\xi}(0) \theta[\xi(t)]$. We shall assume that this function is rather independent of $\dot{\boldsymbol{\sigma}}$, i.e. we assume that the evolution of the reaction coordinate hardly

depends on the vibrations of the C–H and O–H bonds. In this case we can easily calculate the integral over $\dot{\boldsymbol{\sigma}}$ analytically. Defining

$$\mathbf{Z}_{\xi\sigma} = \begin{pmatrix} \mathbf{Z}_{\xi} & \mathbf{D} \\ \mathbf{D}^T & \mathbf{Z}_{\sigma} \end{pmatrix}, \quad (3.38)$$

$$\mathbf{Z}_{\xi\sigma}^{-1} = \begin{pmatrix} \mathbf{K}_{\xi} & \mathbf{L} \\ \mathbf{L}^T & \mathbf{M}_{\sigma} \end{pmatrix}, \quad (3.39)$$

we write

$$\mathbf{v}_{\xi\sigma}^T \mathbf{Z}_{\xi\sigma}^{-1} \mathbf{v}_{\xi\sigma} = \dot{\xi} \mathbf{Z}_{\xi}^{-1} \dot{\xi} + \left(\dot{\boldsymbol{\sigma}} + \mathbf{M}_{\sigma}^{-1} \mathbf{L}^T \dot{\xi} \right)^T \mathbf{M}_{\sigma} \left(\dot{\boldsymbol{\sigma}} + \mathbf{M}_{\sigma}^{-1} \mathbf{L}^T \dot{\xi} \right). \quad (3.40)$$

Introducing this result into Eq. (3.37) and performing the Gaussian integral over $\dot{\boldsymbol{\sigma}}$, we obtain, apart from a constant factor,

$$\begin{aligned} & \int d\mathbf{q} d\mathbf{p}_q \int d\dot{\xi} F P_{\xi\sigma}^c(\mathbf{q}, \mathbf{p}_q) \exp\left[-\frac{1}{2} \beta \dot{\xi} \mathbf{Z}_{\xi}^{-1} \dot{\xi}\right] |\mathbf{M}_{\sigma}|^{-1/2} |\mathbf{Z}_{\xi\sigma}|^{-1} \\ & \propto \int d\mathbf{q} d\mathbf{p}_q \int d\dot{\xi} F P_{\xi\sigma}^c(\mathbf{q}, \mathbf{p}_q) P(\dot{\xi}|\mathbf{q}) \mathbf{Z}_{\xi}^{1/2} |\mathbf{M}_{\sigma}|^{-1/2} |\mathbf{Z}_{\xi\sigma}|^{-1}. \end{aligned} \quad (3.41)$$

In the second expression $P(\dot{\xi}|\mathbf{q})$ is the normalised Gaussian probability density of the velocity $\dot{\xi}$ for a given value of \mathbf{q} . Using $\mathbf{Z}_{\xi} = |\mathbf{Z}_{\xi\sigma}| |\mathbf{M}_{\sigma}|$, which is proven in the appendix, we derive the final result

$$\begin{aligned} & \int d\mathbf{q} d\mathbf{p}_q \int d\xi d\mathbf{p}_{\xi} \int d\boldsymbol{\sigma} d\mathbf{p}_{\sigma} F \delta(\xi) \exp\left[-\beta(T_{q\xi\sigma} + \Phi)\right] \\ & \propto \int d\mathbf{q} d\mathbf{p}_q \int d\dot{\xi} F P_{\xi\sigma}^c(\mathbf{q}, \mathbf{p}_q) P(\dot{\xi}|\mathbf{q}) |\mathbf{Z}_{\xi\sigma}|^{-1/2}. \end{aligned} \quad (3.42)$$

This expression can easily be used in computations by means of molecular dynamics simulations. First a set of $(\mathbf{q}, \mathbf{p}_q)$ distributed according to $P_{\xi\sigma}^c(\mathbf{q}, \mathbf{p}_q)$ is generated by means of a molecular dynamics simulation during which both ξ and $\boldsymbol{\sigma}$ are constrained. Next, velocities $\dot{\xi}$ are drawn according to $P(\dot{\xi}|\mathbf{q})$. In order to calculate the velocities $\mathbf{v}_{q\xi\sigma}$ at this point, we notice that

$$\begin{pmatrix} \dot{\mathbf{q}} \\ \mathbf{v}_{\xi\sigma} \end{pmatrix} = \begin{pmatrix} \mathbf{A}_q^{-1} & -\mathbf{A}_q^{-1} \mathbf{B}_{\xi\sigma} \\ \mathbf{0} & \mathbf{1} \end{pmatrix} \begin{pmatrix} \mathbf{p}_q \\ \mathbf{v}_{\xi\sigma} \end{pmatrix}. \quad (3.43)$$

This result can easily be derived by using Eq. (3.31) in the form $\mathbf{p}_q = \mathbf{A}_q \dot{\mathbf{q}} + \mathbf{B}_{\xi\sigma} \mathbf{v}_{\xi\sigma}$. Equation (3.43) tells us that after the first constrained run $\dot{\mathbf{q}} = \mathbf{A}_q^{-1} \mathbf{p}_q$, and that after having drawn $\mathbf{v}_{\xi\sigma}$ we should add $-\mathbf{A}_q^{-1} \mathbf{B}_{\xi\sigma} \mathbf{v}_{\xi\sigma}$. Since we shall continue to constrain $\boldsymbol{\sigma}$ we only need the first column of $\mathbf{B}_{\xi\sigma}$. The changes in the generalised velocities are then transformed into the Cartesian velocities of the MD run by $\mathbf{v} = \mathbf{J} \mathbf{v}_{q\xi\sigma}$, where

$$\mathbf{J} = \frac{\partial\{\mathbf{x}_i\}}{\partial\{\mathbf{q}, \xi, \boldsymbol{\sigma}\}}. \quad (3.44)$$

In the final step F is calculated by means of a molecular dynamics run with $\boldsymbol{\sigma}$ constrained, multiplied by $|\mathbf{Z}_{\xi\sigma}|^{-1/2}$, and averaged.

We conclude this derivation with an expression for the matrix $\mathbf{A}_{q\xi\sigma}$ and its inverse. The kinetic energy of the molecule can be expressed in terms of the generalised velocities by combining Eqs. (3.30) and (3.31),

$$T = \frac{1}{2} \sum_{i=1}^N m_i \mathbf{v}_i^2 = \frac{1}{2} \mathbf{v}_{q\xi\sigma}^T \mathbf{A}_{q\xi\sigma} \mathbf{v}_{q\xi\sigma}. \quad (3.45)$$

Introducing the aforementioned relation between the Cartesian velocities and the generalised velocities one finds²³

$$\left(\mathbf{A}_q\right)_{jk} = \sum_{i=1}^N m_i \frac{\partial \mathbf{x}_i}{\partial q_j} \cdot \frac{\partial \mathbf{x}_i}{\partial q_k}, \quad (3.46)$$

and likewise for $\mathbf{B}_{\xi\sigma}$ and $\mathbf{C}_{\xi\sigma}$. It is then straightforward to prove that the elements of the inverse matrix are given by

$$\left(\mathbf{X}_q\right)_{jk} = \sum_{i=1}^N \frac{1}{m_i} \frac{\partial q_j}{\partial \mathbf{x}_i} \cdot \frac{\partial q_k}{\partial \mathbf{x}_i}, \quad (3.47)$$

and likewise for $\mathbf{Y}_{\xi\sigma}$ and $\mathbf{Z}_{\xi\sigma}$. A similar equation also holds for the width of $P(\dot{\xi}|\mathbf{q})$, which by using Eq. (3.28) is found to be

$$Z_\xi = 1 + \sum_{k=1}^3 \left(d_k^r\right)^2. \quad (3.48)$$

An obvious drawback of the method presented so far is that Eq. (3.43) explicitly requires an expression for the matrix $\mathbf{A}_{q\xi\sigma}$. Moreover, in order to transform all generalised velocities to the Cartesian velocities used in the simulation run, one needs the Jacobian matrix \mathbf{J} . If we use the normal mode based internal coordinates, Eq. (3.18), then the evaluation of \mathbf{J} is straightforward. Furthermore, at the saddle point we then have $Z_\xi = 1$ and $\mathbf{B}_{\xi\sigma} = \mathbf{0}$. The fluctuations around these values in a ξ -constrained run are small, as we will see in section 3.5.

An alternative expression for the constrained average was presented by Carter *et al.*²⁴ Similar to the steps leading from Eq. (3.34) to Eq. (3.37), where $\mathbf{p}_{q\xi\sigma}$ was replaced by $(\mathbf{p}_q, \mathbf{v}_{\xi\sigma})$, we can also make the transformation from $\mathbf{p}_{q\xi\sigma}$ to $(\mathbf{p}_{q\xi}, \boldsymbol{\sigma})$. Integration over $\boldsymbol{\sigma}$ then yields

$$\begin{aligned} & \int d\mathbf{q} d\mathbf{p}_q \int d\xi dp_\xi \int d\boldsymbol{\sigma} d\mathbf{p}_\sigma F \delta(\xi) \exp\left[-\beta(T_{q\xi\sigma} + \Phi)\right] \\ & \propto \int d\mathbf{q} d\mathbf{p}_{q\xi} F P_{\xi\sigma}^c(\mathbf{q}) P_\sigma(\mathbf{p}_{q\xi}|\mathbf{q}) |\mathbf{Z}_{\xi\sigma}|^{-1/2}, \end{aligned} \quad (3.49)$$

where $P_{\xi\sigma}^c(\mathbf{q})$ is the again the probability of finding a ξ and σ constrained molecule at point \mathbf{q} and $P_{\sigma}(\mathbf{p}_{q\xi}|\mathbf{q})$ is the momenta distribution of a σ constrained molecule at this point. The latter distribution can be sampled without prior knowledge on $\mathbf{A}_{q\xi\sigma}$ or \mathbf{J} by assigning a Maxwellian velocity to all atoms and SHAKEing the coordinates after a single MD step.²⁵ Our expression differs from the one by Carter *et al.*²⁴ by a factor of $|\mathbf{Z}_{\sigma}|^{1/2}$ since we integrated over the $\dot{\sigma}$ rather than demanding $\delta(\dot{\sigma})$.

3.4 Implementation

The numerical results presented in this paper were calculated using the GROMOS87²⁶ package. The molecular dynamics program was adapted to employ the above described reaction coordinate. Some details of the implementation will be discussed here.

Several algorithms have been developed to locate the required saddle point \mathbf{Y}^0 of a potential energy surface.²⁷⁻³⁰ We used the TRAVEL routine³⁰ implemented in the QUANTA/CHARMM package.³¹ The atomic coordinates were transferred to GROMOS and refined by minimising the potential-gradient using Newton-Raphson. The Hessian matrix of second derivatives of the potential energy was calculated by numerically differentiating the atomic forces with respect to the atomic coordinates. Standard routines³² were used to diagonalise the matrix, yielding both the eigenvalues and the eigenvectors. Because of the sixfold degeneracy of the zero frequency eigenvalue it is not simple to split the corresponding eigenvectors into rotational and translational modes. Therefore the rotational eigenvectors were evaluated directly using the orthonormalised version of Eq. (3.8). All modes were normalised to 1 a.m.u.^{1/2} nm.

The rotation matrix of a molecule with coordinates \mathbf{X} is found by solving Eq. (3.16). Using the orthogonality of \mathbf{Y}^0 and \mathbf{S}^k , Eq. (3.8), we find the three equations

$$\mathbf{a}:\left(\sum_{i=1}^N m_i \mathbf{s}_i^k \mathbf{x}_i\right) = 0. \quad (3.50)$$

All information about the orientation of the molecule is condensed in the bracketed term, which needs to be evaluated only once for each configuration. Several methods are available to solve this equation.^{18,19} In our calculations we have used a numerical zero-point search. A rotation matrix can be defined as a function of three parameters, e.g. the Euler angles, by writing each element as a function of these three parameters. Unfortunately, any three parameter definition will contain singularities which complicate numerical handling of the matrix.³³ This problem does not occur when using the four quaternions³⁴ q_i . In this definition the elements of the matrix are second order polynomials in the q_i 's. The redundancy of using a fourth parameters is elevated by the constraint

$$q_0^2 + q_1^2 + q_2^2 + q_3^2 - 1 = 0. \quad (3.51)$$

Eqs. (3.50) and (3.51) then constitute a set of four quadratic equations in four variables. The derivatives of these equations with respect to the quaternions are straightforward to calculate,

hence this set of coupled equations is efficiently solved numerically using the rapidly converging Newton-Raphson method.

A minor problem made its appearance during test runs: there are four solutions (eight if left-handed rotation matrices are also allowed) to Eq. (3.51), so care must be taken to pick the right one. During MD runs, when the changes in atomic coordinates between successive evaluations of the rotation are small, the correct matrix is simply identified as the one that best resembles its predecessor,

$$\mathbf{a}^T(t + \Delta)\mathbf{a}(t) \approx \mathbf{I}. \quad (3.52)$$

In practice, the correct matrix will be found directly when the solution to the previous matrix evaluation is used as the starting point of the next iteration procedure. A different technique is needed at the start of the MD run. We note that in many molecules part of the molecule is not affected by the reaction (in the current runs the starting configurations lie in the saddle plane, making this requirement less strict). A set of three orthonormal vectors can then be constructed from the relative positions of at least three atoms of the ‘rigid’ section of the saddle point configuration \mathbf{Y}^0 . For instance, in the case of the calix[4]arene of section 3.5.3 we used the hinge to hinge vectors. This procedure is also applied to the molecule of unknown rotation. Comparing the two sets of vectors yields a good initial guess at the rotation matrix.

The code was tested in a series of runs. It proved simple to reproduce the correct rotation matrix of randomly rotated excited molecules. The normal mode constraint was found to work well, also when combined with simultaneous constraints on the hydrogen bond lengths. In vacuum runs the angular momentum of molecules was unaffected by the constraints. Leuwerink and Briels³⁵ have successfully used the code to calculate the rotation autocorrelation function of 18-crown-6.

3.5 Results

The reaction coordinate has been applied to calculate the transmission function of three isomerisation models. Two models, namely *n*-butane in carbon tetrachloride and liquid *n*-butane, were taken from the literature, and the results show that the code reproduces known transmission coefficients in those cases where our reaction coordinate is similar to the conventional reaction coordinate. Some features of these reactions are discussed. A third model describes an isomerising calix[4]arene dissolved in chloroform.

3.5.1 Flexible *n*-butane in carbon tetrachloride

In an early paper combining the reactive flux method and full-MD simulations Rosenberg *et al.*⁸ calculated the transmission function of the trans-gauche isomerisation of *n*-butane dissolved in carbon tetrachloride (CCl₄). This model serves as our first test case. By using the united atom model the butane molecule is reduced to four interacting pointmasses, and the dihedral angle emerges as the designated reaction coordinate. The potential energy of the

molecule is modelled by the torsion potential of Ryckaert and Bellemans, in combination with harmonic potentials for bond stretching and angle bending.³⁶ The molecule is immersed in a box of 122 pointmasses, each representing a carbon tetrachloride molecule. All intermolecular interactions are described by Lennard-Jones potentials. Details on the force field can be found in the original article.

A butane molecule with a dihedral ϕ of 60° was made by hand. Starting from this configuration the saddle point was calculated by reducing the force down to $(\sum_{i=1}^N \mathbf{F}_i^2)^{1/2} = 2.4 \cdot 10^{-14} \text{ kJ mol}^{-1} \text{ nm}^{-1}$, resulting in a slightly shifted dihedral, $\phi = 59.96^\circ$. Normal modes and eigenfrequencies were obtained by diagonalising the Hessian matrix. The positive direction of the reaction coordinate was chosen to coincide with an increase in dihedral angle. From evaluating the derivatives $\partial\phi/\partial\alpha^j$ at the saddle point it follows that four out of six vibrational modes affect the dihedral, in a 1.00/0.31/0.24/0.09 ratio. Our reaction coordinate, therefore, differs from the obvious choice, the dihedral angle, even in the neighbourhood of the saddle point. Notice that it is possible to construct a set of orthonormal mass-weighted vectors, including \mathbf{E}^l and \mathbf{S}^l , such that at the saddle point only one vector,

$$(\mathbf{Q}^\phi)^T \propto \left(\sqrt{m_1} (\nabla_1 \phi)^T, \dots, \sqrt{m_N} (\nabla_N \phi)^T \right), \quad (3.53)$$

couples to the dihedral. Along this vector the decrease in torsion energy reaches a maximum, but the accompanying increase in bending and stretching potential energy is even bigger. Since this vector is strongly correlated to the unstable mode, $\mathbf{Q}^\phi \cdot \mathbf{Q}^r = 0.93$, it is to be expected that our reaction coordinate and the dihedral will lead to equivalent results.

A cubic carbon tetrachloride box was made by placing 125 particles at random in spheres centred at lattice points of a simple cubic lattice with the proper density. The excess potential energy was discharged by a short energy minimisation run and a consecutive MD run. Three particles were then removed to provide space for a butane molecule in its saddle point configuration. Again the excess potential energy was reduced, followed by a 0.1 ns equilibration MD run. The transition state was sampled in a production run of 10 ns, saving the positions and velocities of all atoms in the box at intervals of 1 ps. The acceptance criterion on the rotation matrix was such that the left hand side of Eqs. (3.50) and (3.51) did not exceed 10^{-6} and 10^{-8} respectively. The constraint on the normal mode was satisfied to within 10^{-10} . Due to inaccuracies of the rotation matrix the actual precision of the reaction coordinate is about $3 \cdot 10^{-8}$. In the MD runs the time step was 2 fs, the temperature was kept at 300 K using velocity scaling³⁷ with a time constant of 0.1 ps and the volume of the box was kept constant.

The dihedral distribution of the sampled saddle plane configurations is shown in Fig. 3.1. This broad distribution results from the coupling of the dihedral to the unconstrained normal modes. Obviously, the transition state differs from the dihedral constrained distribution of Rosenberg *et al.*⁸ Constraining the projection along the vector \mathbf{Q}^ϕ , i.e. using a basis where only one direction couples in first order to the dihedral, leads to a narrower distribution, see Fig. 3.1. The remaining dispersion reflects the second and higher order contributions of the other internal coordinates to the dihedral.

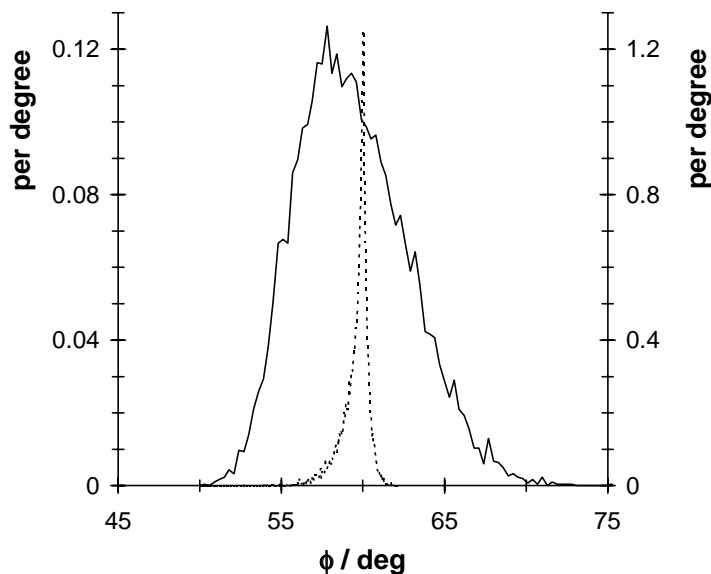


Figure 3.1. The distribution function of the dihedral angle during a constrained run, in which the unstable normal mode (solid line, left axis) or the dihedral mode (dotted line, right axis) is kept constant.

The sampled transition state configurations and corresponding velocities serve as the starting points of relaxation runs. As outlined in section 3.3.2, we start by supplying a velocity $\dot{\xi}$ sampled from $P(\dot{\xi}|\mathbf{q})$. The width of this distribution depends on \mathbf{q} , but in the constrained run the fluctuations in the width were found to be very small, $\langle Z_{\xi} \rangle = 1.005 \pm 0.006$. We used $Z_{\xi} = 1$. Next in line is the coupling of $\dot{\xi}$ to $\dot{\mathbf{q}}$, resulting in a velocity change $\delta\dot{q}_j = (-\mathbf{A}_q^{-1}\mathbf{B}_{\xi\sigma})_j \dot{\xi}$. By combining Eqs. (3.18) and (3.45), it follows that the matrix $\mathbf{A}_{q\xi\sigma}$ is diagonal, except for the three rows and the three columns containing derivatives with respect to the rotation angles. These were calculated numerically for the sampled configurations. The average velocity correction, $\langle \delta\dot{q}_j \rangle$, is easily shown to be zero. The standard deviation of the correction is small compared to the standard deviation of the existing velocities: for the rotation we find $(\langle \delta\dot{q}_j^2 \rangle / \langle \dot{q}_j^2 \rangle)^{1/2} \approx 0.06$, while for the vibrations this ratio is about $3 \cdot 10^{-3}$. The velocity of the centre of mass is unaffected. Since this effect is fairly small, and expected to be smaller for bigger molecules, we neglected it. In the final step the generalised velocity is transformed into Cartesian velocities by $\mathbf{v}_i = \mathbf{a}\mathbf{q}_i^r \dot{\xi}$ and superimposed on the already existing velocities.

The relaxing molecule is followed for 10 ps. During these runs the solvent is still temperature scaled. The solute is excluded from scaling, so it can only lose its excess energy by means of collisions with the solvent. Each transition state configuration is used as the starting point of only one relaxation run.

The time evolution of both reaction coordinates in four typical relaxation runs is displayed in Fig. 3.2. Figures 3.2(a) and (b) show the most common trajectories, in which a butane

molecule with a negative (positive) transient reaction velocity enters the trans (gauche+) well and remains there for some time. In Fig. 3.2(c) a butane molecule with a positive transient velocity recrosses the transition state after oscillating in the gauche+ well. Surprisingly, nearly all molecules showing this behaviour were found to recross after two, rather than one, oscillations in the gauche+ well. Figure 3.2(d) shows a direct gauche+ to gauche- transition without equilibration in the trans well. The plot also shows that the close harmony of the two reaction coordinates suddenly breaks down near the trans-gauche- barrier. In this region it proves difficult to find a rotation matrix that meets all requirements. Of the runs entering this region many crashed since they failed to find a proper rotation matrix, while in the surviving runs the reaction coordinate made a sudden change of direction, as in Fig. 3.2(d). In all runs that made it to the gauche- well the reaction coordinate was found to be positive; upon re-entering the trans well the reaction coordinate made a second jump to become negative again.

The transmission function is calculated from 3000 relaxation runs. In view of the above mentioned problems with the normal mode based reaction coordinate, we decided to use the dihedral angle as discriminator, see Eq. (3.55). In compliance with common practice both gauche configurations are regarded as product states of the reaction, i.e. $\xi = |\phi| - 60^\circ$. The resulting transmission function is shown in Fig. 3.3 as a solid line. Because the transition state was sampled with $\alpha_r = 0$, and the discriminator is taken to be $\xi = |\phi| - 60^\circ$, the

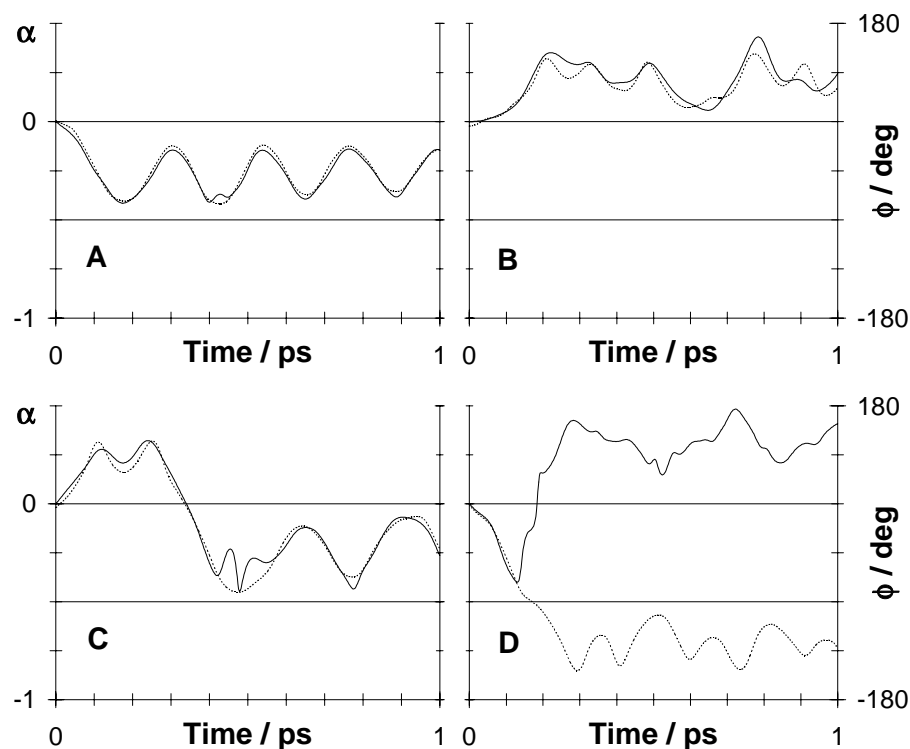


Figure 3.2. Four typical relaxation runs of butane in carbon tetrachloride, showing both the unstable mode reaction coordinate (solid line, left axis) and the dihedral angle (dotted line, right axis).

transmission function does not start at the value one at $t = 0$. Almost all molecules with a positive (negative) velocity $\dot{\alpha}_r(0)$ will quickly reach $\phi \geq 60^\circ$ ($\phi \leq 60^\circ$), so the function rapidly raises to nearly one. The function then decreases down to about 0.4 before levelling off to a slowly decaying plateau.

Rosenberg *et al.*⁸ fitted their 2.6 ps transmission function with

$$\kappa(t) = (1 - \kappa)e^{-k_1 t} + \kappa e^{-kt}. \quad (3.54)$$

The second exponential, with the relaxation rate $k = \kappa k^{TST}$ and $k^{TST} = k_f^{TST} + k_b^{TST}$, is the analytic long time solution to Eq. (3.5) for a system evolving to equilibrium, and the first exponential is added to match the transient decay to the plateau. In a free energy calculation^{8,38,39} it was found that $k^{TST} = 200 \text{ ns}^{-1}$, which was used in the fit to yield $k_1 = 7.1 \text{ ps}^{-1}$ and $\kappa = 0.361$. Using the same fit procedure, but shifted to the right by 0.05 ps for obvious reasons, we find $k_1 = 3.6 \text{ ps}^{-1}$ and $\kappa = 0.34$. The plateau values are in good agreement. However, on a logarithmic scale it is apparent that the final exponential decay of the plateau starts after about 5 ps. Fitting the 5-10 ps range with a single exponential yields $k = 29 \text{ ns}^{-1}$ and $\kappa = 0.28$, hence a small k^{TST} of 102 ns^{-1} . The fitted region of the plateau is too short and too noisy to get an accurate value for k ; the κ is far more reliable since it is insensitive to the details of the fit. We further want to remark that the free energy profile, i.e. k^{TST} , was calculated for a molecule with rigid bond lengths and rigid bending angles and may therefore differ from the free energy profile of the extremely flexible molecule discussed here, even after a correction for the different phase space distributions of the constrained and unconstrained runs.

Subdividing the transmission function into various contributions reveals some interesting

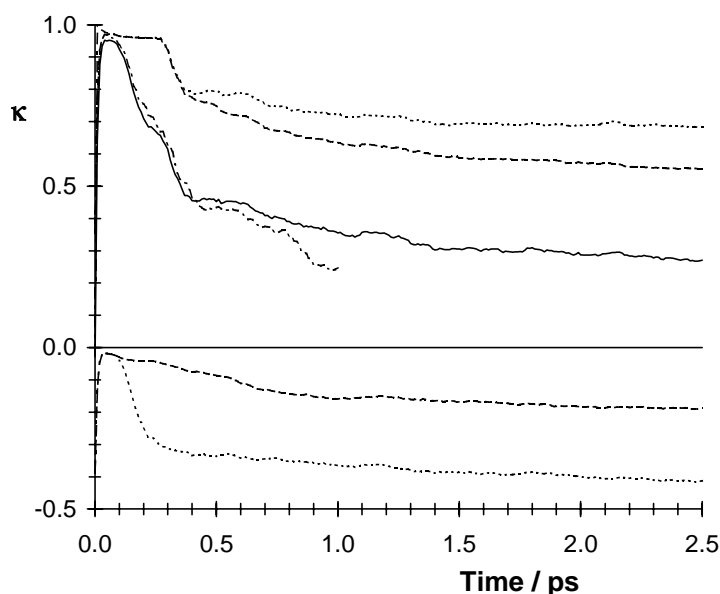


Figure 3.3. The transmission function (solid line) of butane in carbon tetrachloride for the first 2.5 ps. The meaning and interpretation of the other lines is given in the text.

features that are not apparent from the function itself. In Fig. 3.3 the upper (lower) dashed line represents the contribution f_+ (f_-) to κ of molecules that have reached gauche+ at time t , after having started with a positive (negative) transient velocity, i.e.,

$$f_{\pm}(t) = \pm \frac{\langle \delta[\alpha_r(0)] \dot{\alpha}_r(0) \theta[\pm \dot{\alpha}_r(0)] \theta[\phi(t) - 60^\circ] \rangle}{\langle \delta[\alpha_r(0)] \dot{\alpha}_r(0) \theta[\pm \dot{\alpha}_r(0)] \rangle}. \quad (3.55)$$

The upper dashed line nearly starts at the value one, so almost all molecules with a positive transient velocity are in the gauche+ well. After about 0.3 ps the line suddenly drops due to a massive recrossing, the elapsed time corresponding to twice the period of an oscillation in the gauche+ well, as in Fig. 3.2(c). The decrease of the function is larger than the actual fraction of recrossing trajectories, indicating that the recrossing trajectories have on average a higher initial velocity than the non-recrossing trajectories. As time goes by the function gradually decreases to its equilibrium value without showing any structure. The lower dashed line corresponds to molecules that have reached the gauche+ well after having started with a negative transient velocity. This line starts at zero and decreases only gradually. The mean transient velocity of these trajectories is only about a third of the average transient velocity, meaning that this kind of trajectory is much more likely than it appears from the plot. The gradual decrease of the line is predominantly caused by an increase in the average transient velocity, rather than by the small rise in the number of molecules reaching gauche+.

The dotted lines give the contribution to κ of those molecules that have reached either one of the two gauche wells, again grouped according to their transient velocity. They differ from the dashed lines by those molecules that have reached the gauche- well. At the bottom of the plot the difference between the dotted and the dashed line rapidly increases after about 0.1 ps due to direct gauche+ to gauche- transitions, as in Fig. 3.2(d). The average transient velocity of these trajectories is well above the overall average, since direct gauche+ to gauche- transitions account for only 17% of the trajectories with a negative transient velocity. The upper dotted line and the upper dashed line coincide for the first 0.4 ps and then slowly grow apart. It takes about 0.2 ps before the first molecules with a (small) positive transient velocity reach gauche-. After 0.4 ps their numbers start to increase and so does their average transient velocity: it looks as though a considerable fraction of the molecules that leave gauche+ after a double oscillation proceed directly to the gauche- well. The transmission function, the solid line, is obtained as the sum of the two dotted lines. It is seen then that the rapid decline between 0.1 and 0.4 ps is the combined effect of two independent processes. From the above discussion and the plots of individual relaxation runs it is obvious that the reaction tends to the low friction regime.

We also calculated the transmission function using the unstable normal mode as the reaction coordinate to monitor the relaxation runs. In view of the particular problems of this coordinate, as discussed above, we assumed that:

- i) Molecules with a positive reaction coordinate are in a product well. Considering the jumpy behaviour of the coordinate in the gauche- well, this properly includes gauche- as being a product.

- ii) Crashed runs are in a product configuration for the rest of the run. Since runs are found to crash when a molecule enters the gauche– well, this is correct as long as the molecule does not return to the trans well (which does occur after 0.5 ps).

Figure 3.3 shows the transmission function calculated from 1000 relaxation runs of 1 ps as a dash-dotted line. There is a good resemblance to the solid line. The difference between the two curves after about 0.5 ps is attributed to the failure of the second assumption. In the 1 ps interval already 14% of the runs aborted prematurely.

In a third set of relaxation runs the usual technique of replacing all velocities of the sampled transition state configurations by velocities sampled from a Maxwellian distribution was used, Eq. (3.49). The transient velocity of the reaction coordinate was obtained by projecting the assigned Cartesian velocities onto the unstable normal mode. The transmission function, which is not shown here, was identical to the one discussed above to within about 0.01. This indicates that the assumptions underlying our velocity assignment are justified.

3.5.2 Liquid rigidified *n*-butane

As a second test-case we study the isomerisation process of liquid *n*-butane. The appealing feature of this model is the high number of barrier crossings at little computational expense. This allows for a direct determination of the rate constant from the time evolution of the fractions trans and gauche. Edberg *et al.*² studied the relaxation of non-equilibrium boxes with all molecules initially in the same configuration. Brown and Clarke¹ showed that the rate constant can also be calculated from an equilibrium run by studying the relaxation to equilibrium of those molecules that are trans (gauche) at some time *t*.

The butane model employed in this section is the one by Brown and Clarke.¹ The butane molecule consists of four pointmasses interacting by Lennard-Jones potentials. The bond lengths and the bending angles are rigidified by means of five distance constraints, leaving the dihedral as the sole internal degree of freedom. The torsional energy is modelled by the Ryckaert-Bellemans potential. The saddle point of this molecule is exactly identical to the one of the previous section. We now ought to calculate the unstable normal mode \mathbf{Q}^c of the constrained molecule, a mode that does not couple to the constrained coordinates. Instead, we will make use of the unstable normal mode \mathbf{Q}^r of the unconstrained molecule. This mode, in comparison with the other normal modes, is indeed only weakly coupled to the constrained coordinates. For a molecule as simple as the current butane model it is straightforward to calculate the accuracy of this approximation, $\mathbf{Q}^c \cdot \mathbf{Q}^r = 0.995$, so it will be of little effect.

A simulation box was made by placing 108 randomly orientated molecules, all in the saddle point configuration, at random points within spheres centred around the lattice points of a simple cubic lattice. The unstable normal mode of the first molecule is constrained in the runs to come, while the dihedrals of the remaining 107 bath molecules are free. The excess energy of the box was released by an energy minimisation, followed by a 0.5 ns equilibration MD run. In a subsequent 3 ns production run the saddle plane was sampled, saving a configuration every picosecond. A thermostat³⁷ maintained an average temperature of

291.6 K. Because of the five distance constraints on each molecule, the effect of constraining the normal mode of the first molecule is identical to making this molecule completely rigid. In the production run the dihedral angle of the first molecule fluctuated within 0.001° of the saddle point value.

At the start of a relaxation run the normal mode constraint on the first molecule is lifted. Since the molecule is at the saddle point it is evident that $Z_\xi = 1$ and $\delta\dot{q}_j = 0$. A Maxwellian velocity $\dot{\xi}$ is assigned to the unstable mode. This velocity then ought to be transformed into atomic Cartesian velocities by $\mathbf{v}_i = \mathbf{a}\mathbf{q}_i^c \dot{\xi}$, but, here too, we made the approximation $\mathbf{v}_i = \mathbf{a}\mathbf{q}_i^r \dot{\xi}$. As a check on the validity of this assumption we calculated the resulting dihedral velocity $\dot{\phi}$ using the virtual time step method:²⁵ a molecule *in vacuo* is placed at the saddle point, velocities are assigned using the above approximation, positions are advanced by a 2 fs MD step without forces, constraints are applied, and the change in the dihedral is calculated. The distribution of the dihedral velocities, averaged over 16,000 trials, was found to be a Gaussian with $\langle |\dot{\phi}| \rangle = 4.46$ rad/ps, in excellent agreement with the 4.445 rad/ps found by Brown and Clarke.⁴⁰

The transmission function, depicted in Fig. 3.4 as a solid line, was calculated from 3000 relaxation runs of 5 ps. In these runs the dihedral angle of the previously constrained first molecule was used as the reaction coordinate; unlike with the other butane model, this time the transition at $t = 0$ is smooth. The decaying plateau was fitted with an exponential in the range 2.5–5.0 ps, yielding $\kappa = 0.32$ and $k = 35$ ns⁻¹. Again, the upper and lower parts of the figure are obtained by splitting the transmission function into contributions from trajectories with positive or negative transient velocities; the dashed lines correspond to molecules which have reached the gauche+ well, and the dotted lines to molecules which have reached either the gauche+ or the gauche- well. Like before, a number of molecules with a positive initial

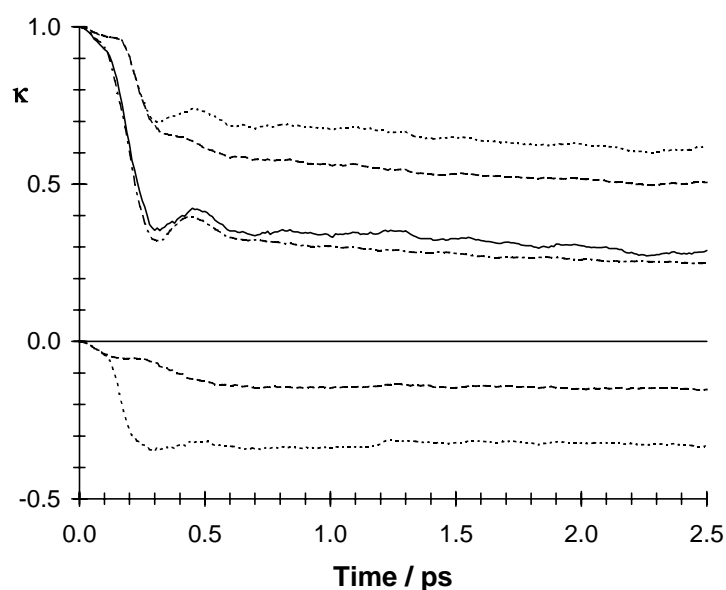


Figure 3.4. The transmission function (solid line) of liquid butane. The meaning and interpretation of the other lines is given in the text.

velocity are found to recross the barrier after oscillating in the gauche+ well. But this time they oscillate only once due to the absence of other degrees of freedom, so the decay of the upper dashed line sets in earlier than in Fig. 3.3. A few of these molecules even manage to pass through the trans well into gauche-, causing the upper dotted and dashed lines to rapidly grow apart after 0.3 ps, and making the total transmission function rise for a short while. The latter rise is enhanced by molecules with a negative transient velocity that follow a trans-gauche- trans route.

As a comparison, we have also calculated the reaction rate from a 2 ns equilibrium run. The temperature of this box was kept at 291.6 K using a time constant of 10 ps. We observed $N_{BC} = 16,415$ barrier crossings in this run. The TST rate constant was calculated by directly evaluating Eq. (3.1), and by¹

$$k^{TST} = \frac{N_{BC}}{2N_{mol} \langle X_T \rangle t_{run}} \frac{1}{1 - \langle X_T \rangle}, \quad (3.56)$$

where $\langle X_T \rangle$ is the average fraction of trans molecules. Both produced a value of 160 ns^{-1} . The true rate constant was obtained from the bulk relaxation,¹

$$\frac{R_{TT}(t) - \langle X_T \rangle^2}{\langle X_T \rangle - \langle X_T \rangle^2} = e^{-kt} \quad (3.57)$$

where $R_{TT}(t)$ is the fraction of molecules that are in the trans conformation at time 0 and also at time t . A fit over the interval 10-50 ps yields $k = 47 \text{ ns}^{-1}$, which together with $k^{TST} = 160 \text{ ns}^{-1}$ yields a κ of 0.29. This means that the plateau of the transmission function predicts the correct κ , while the absolute rate is in error. The reason for this is poor statistics, the transmission function is too short and too noisy to really probe the exponential decay.

This long run also offers an alternative route to the transmission function, by following the dihedral of a molecule after it incidentally crosses a barrier. Selecting those molecules that are in one well at time t and in another at time $t+\Delta$ biases the distribution of crossing velocities, but this is simply corrected for.⁴⁰ The transmission function, shown in Fig. 3.4 as a dash-dot line, resembles the result found in the relaxation runs. On a logarithmic scale the linear decay sets in at 2.5 ps, so we fitted the plateau over the range 2.5–10 ps to find $\kappa = 0.28$ and $k = 47 \text{ ns}^{-1}$, in good agreement with the bulk data.

3.5.3 Calix[4]arene

As an example of a really complex reaction we will now discuss the isomerisation of a calix[4]arene. This molecule consists of four phenol groups, each of which is connected to two neighbouring phenols by methyl bridges located ortho to the hydroxyl group, see Fig. 3.5. In supramolecular chemistry they are being used as building blocks for larger molecules that are designed for the complexation of cations and neutral molecules. Various sidegroups can be attached at the upper and lower rim, replacing the explicitly named hydrogens in Fig. 3.5, to influence the characteristics of the molecule. We will use hydrogen

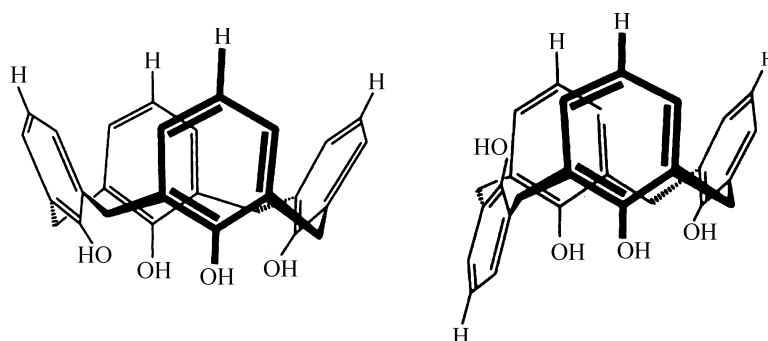


Figure 3.5. The cone (left) and paco (right) conformation of a calix[4]arene.

sidegroups only. The most interesting feature in the current context is that this molecule has four stable conformations. The favourable configuration is one in which all phenol groups point in the same direction. This conformation, the so-called ‘cone’, is stabilised by a cyclic array of four hydrogen bonds at the lower rim. Its chalice-like shape gives its name to this class of molecules. Flipping one phenol group, with two methyl bridges acting as hinges and the hydroxyl group swinging through the annulus, yields the partial cone or ‘paco’. It is this particular reaction step that will be studied here. In a following reaction step either one of the two neighbouring phenol groups can flip over to form the ‘1,2-alternate’, or the opposing phenol group can rotate to form the ‘1,3-alternate’. After two more steps the cone is transformed into an inverted cone. The rate of this inversion process has been measured by ^1H NMR to be about 150 s^{-1} at room temperature.^{41,42}

Computational studies on the conformations of calix[4]arenes with various sidegroups have mainly focused on the energy minima and the resulting conformational distribution, using a variety of force fields.^{43–46} In a recent article by Fischer *et al.*⁴⁷ the saddle points and the reaction paths between the local minima of the PES were calculated using the Conjugated Peak Refinement algorithm. The cone to paco transition was found to be the rate limiting step for cone inversion, but this energy-based picture could change if entropic effects are included. With the all-hydrogen CHARMM parameter set 22^{47,48} the saddle point lies 15.2 kcal/mol above the minimum of the cone and 5.6 kcal/mol above the minimum of the paco. This saddle point was taken as the starting point of the present calculations, employing the same force field. The accuracy of the saddle point after minimising the gradient is $(\sum_i \mathbf{F}_i^2)^{1/2} = 5.8 \cdot 10^{-10}\text{ kJ mol}^{-1}\text{ nm}^{-1}$. All $3N$ normal modes of the molecule were calculated by diagonalising the Hessian matrix. The eigenvalues of the zero-frequency normal modes were smaller than any other frequency by almost six orders of magnitude. The unstable normal mode, \mathbf{Q}^r , pointed in the direction of the paco.

Since we intend to do MD runs with a molecule with L constraints on the bonds containing hydrogen, we should have calculated the $3N - L$ normal modes $\tilde{\mathbf{Q}}^j$ of the σ -constrained molecule. Only for these modes will the velocity transformation $\mathbf{v}_i = \mathbf{a}\tilde{\mathbf{q}}_i^r \dot{\xi}$ hold (to lowest order). If we use $\mathbf{v}_i = \mathbf{a}\mathbf{q}_i^r \dot{\xi}$ on the regular modes, then SHAKEing the molecule will eliminate the velocities along σ , hence effectively reduce $\dot{\xi}$. We then would have to go through the

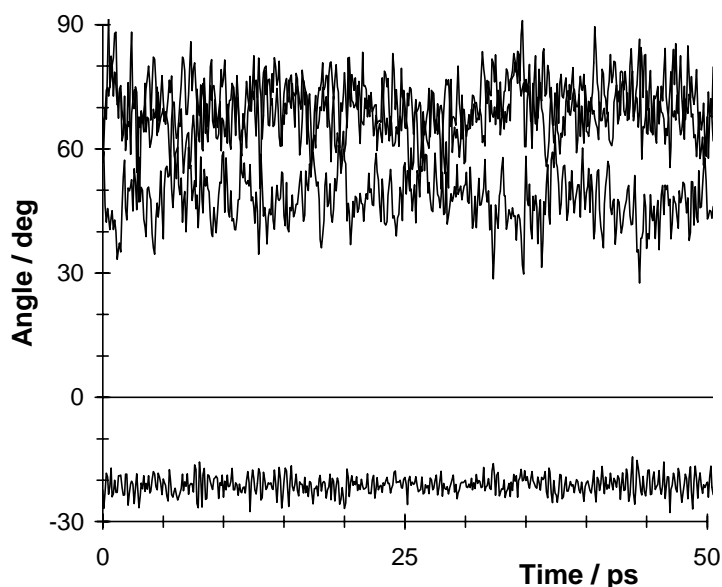


Figure 3.6. The four angles between each of the four benzene rings and the central annulus of a calix[4]arene as a function of time for a constrained dynamics run in chloroform.

elaborate process of evaluating \mathbf{J} and $\mathbf{A}_{q\xi\sigma}$ before being able to assign a velocity. Fortunately, nature offers a helping hand. The $3N - 6$ vibrational modes of the unconstrained molecule are subdivided into two groups. The low frequency modes, the $3N - L - 6$ modes with wavenumbers up to 1600 cm^{-1} , are only very weakly coupled to the bonds with hydrogens. The high frequency modes, the L modes with wavenumbers over 2800 cm^{-1} , are strongly coupled to the bonds with hydrogens. This suggests that the low frequency modes of the unconstrained molecule will be nearly identical to the modes of the constrained molecule. We, therefore, will make use of $\mathbf{v}_i = \mathbf{a}\mathbf{q}_i^r \dot{\xi}$ and neglect the small effects of the σ constraints.

The calix[4]arene was dissolved in a bath of chloroform (CHCl_3) molecules. The chloroform potential by Dietz and Heinzinger^{49,50} was used. Each chloroform molecule is treated as a rigid five-sided entity, modelling the atoms by a mass, charge and Lennard-Jones parameters. A cubic solvent box of 216 molecules was made by placing randomly orientated molecules at random positions within cubes centred at the lattice sites of a simple cubic lattice. The size of the box was chosen to match the experimental density of 1489 kg m^{-3} at 293 K and 1 bar. The excess potential energy of the box was released by a couple of energy minimisation steps, followed by a short NVT MD run. The calix[4]arene was combined with several copies of (fractions of) the solvent box to form a truncated octahedral box of roughly 4.4 nm, containing about 320 chloroform molecules. Again, the excess potential energy was reduced by a minimisation run, followed by a 150 ps NPT equilibration run. In the subsequent production run of 500 ps the configuration was saved every 1 ps. This procedure of making a box and sampling the transition state was repeated four times. All 24 hydrogen bonds of the calix[4]arene and 9 distances in each chloroform molecule were constrained to a relative accuracy of 10^{-5} . The unstable mode was constrained to within 10^{-8} , the rotation matrix was

calculated with a tolerance of 10^{-10} . A constant pressure³⁷ was maintained by scaling the box, using a compressibility of $10^{-9} \text{ m}^2 \text{ N}^{-1}$ and a time constant of 0.5 ps. The temperature³⁷ was fixed at 300 K with a time constant of 0.1 ps. A time step of 2 fs was used. Intermolecular interaction were cut off beyond 1.3 nm, and the dielectric constant equalled one.

The dynamics of the calix[4]arene in the constrained runs was visualised on a SGI workstation. It clearly showed that the motion of the partially rotated phenol group was confined. To give an impression of what is going on, we have calculated the four angles between the annulus and the phenols. Planes were fitted to the six carbon atoms of each phenol group. In the annulus a plane was fitted to the four methyl hinges. These planes were obtained by numerically minimising the sum of the squared perpendicular distances between the plane and the atoms. Figure 3.6 shows the resulting four angles as a function of time during a constrained run, $\xi = 0$. The rotated phenol dangles at an angle of -21° , the opposing phenol oscillates at 45° and the two neighbouring phenols are at about 70° . In the two minima the rotated phenol is at either 58° (cone) or -77° (paco). The oscillations of the rotated group are mainly caused by deformations of the annulus, while for the other groups there are also contributions from low frequency vibrations that lead to periodic back and forth rotation of the phenols.

Two typical relaxation runs of a calix[4]arene in chloroform are shown in Fig. 3.7. In the first plot the molecule quickly adopts the cone conformation. In the second plot it takes a while before the molecule leaves the saddle region and ends up as a paco. The reaction coordinate (dashed line) and the angle of the rotated phenol behave remarkably similar. Therefore, the angle would probably have done a good job when used as the reaction coordinate. However, its cumbersome calculation, and the lack of a non-numerical method to evaluate the derivatives needed in constrained runs, are serious drawbacks.

In Fig. 3.8 the transmission function for a calix[4]arene *in vacuo* is presented. The saddle

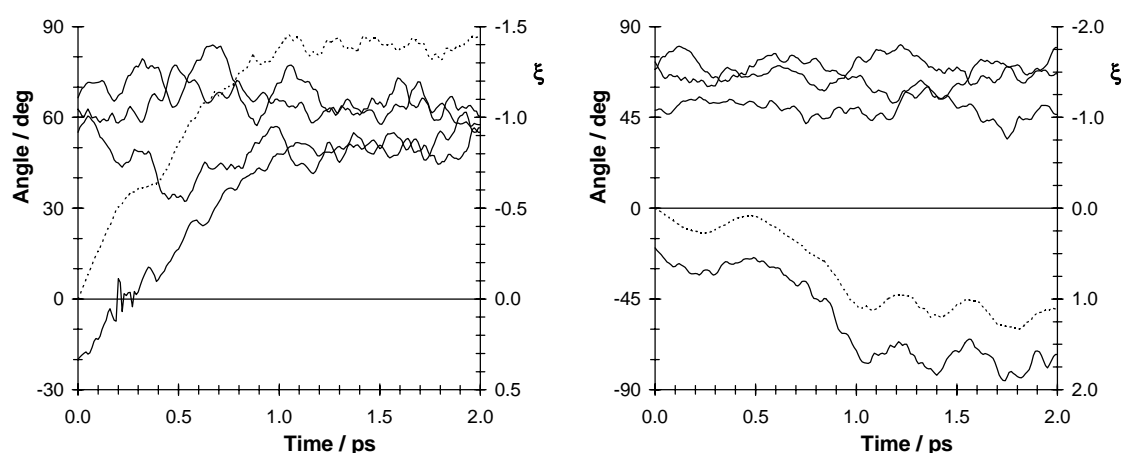


Figure 3.7. Two typical relaxation runs of a calix[4]arene in chloroform. The solid lines denote the angle between each benzene and the central annulus, the dotted line shows the reaction coordinate. The angle of the flipping benzene ring follows the reaction coordinate closely.

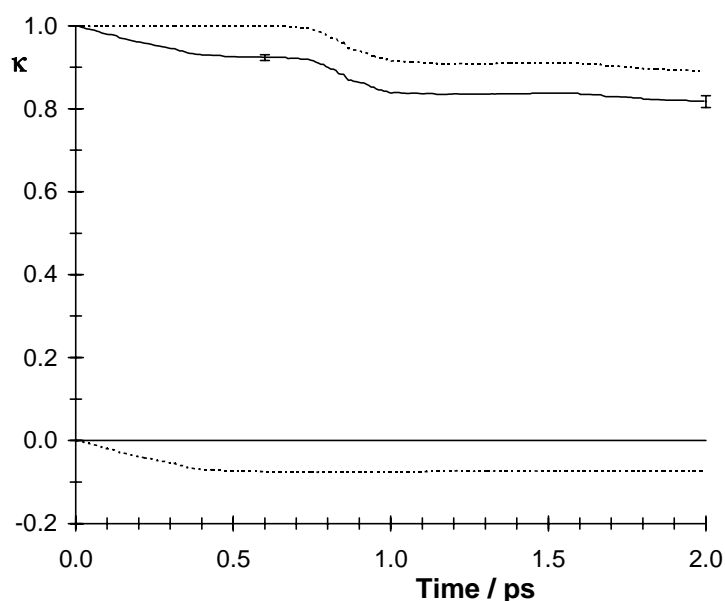


Figure 3.8. The transmission function of a calix[4]arene in vacuo (solid line). The dotted lines correspond to molecules that have reached the *paco* conformation with a positive (top) or negative (bottom) transient velocity.

plane was sampled in a constant energy simulation with an average temperature of 301 K. The angular momentum was eliminated at the start of this run and remained virtually zero throughout the run. After a 0.2 ns equilibration run followed a 4 ns production run in which configurations were saved every 2 ps. Each of these 2000 configurations served as the starting point for one relaxation run, with $Z_{\xi} = 1$ and $\delta\dot{q}_j = 0$. The figure shows that after the transient decay a plateau sets in with $\kappa = 0.923 \pm 0.007$. This high transmission coefficient indicates that the used transition state is indeed near the optimum, ‘the watershed’. Virtually all molecules with a positive transient velocity end up as *paco*. Nearly a quarter of all molecules with a negative transient velocity recross the barrier, but they reduce κ by only 0.08 since their average transient velocity is about 30% of the mean transient velocity. The characteristics of the PES near the saddle point seem to play an important role. The sudden decrease of κ at 0.8 ps is caused by particles that recross the transition state after an oscillation in the *paco* well. Apparently, the flow of the high excess energy to the bath of internal vibrations of the molecule is inefficient. The error in κ was estimated by the variation in κ ’s calculated from sets of randomly selected relaxation runs.

We calculated 2000 relaxation runs of a calix[4]arene in chloroform. In the 2 ps relaxation runs the solute was excluded from temperature scaling. The transmission function, Fig. 3.9, smoothly decreases from one to a stable plateau of $\kappa = 0.43 \pm 0.02$. The trajectories that resulted in the *paco* conformation at time t were subdivided into those with a positive or a negative transient velocity. Both groups, shown as dotted lines, behave as expected. The mean transient velocity of the first group lies 10% above average, that of the second group lies 20% below average. Molecules with a high transient velocity were found to recross the

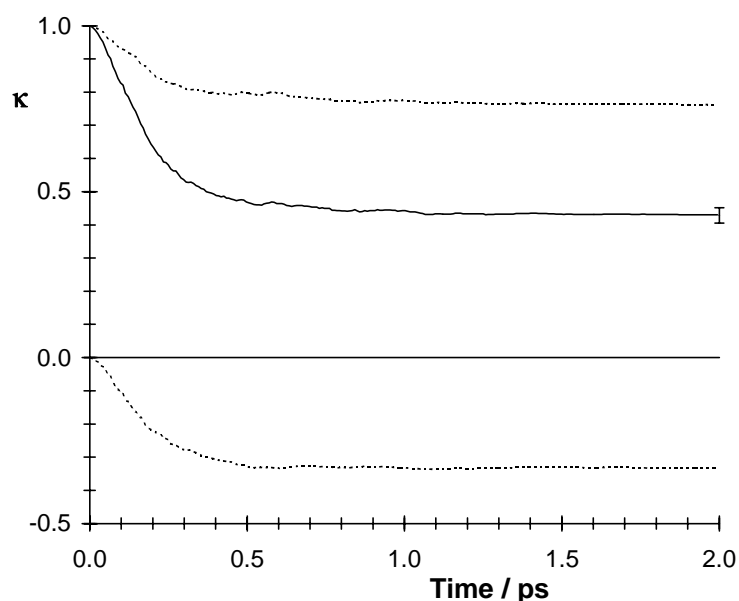


Figure 3.9. The transmission function of a calix[4]arene in chloroform (solid line). The dotted lines have the same meaning as in Fig. 3.8.

transition state less often than molecules with a low transient velocity. Of all molecules with a positive transient velocity some 60% end up as a *paco* conformer without ever recrossing. Those with a negative transient velocity recross more often, only 45% does not recross. As a result, the majority of trajectories will end up in the *paco* well: 70 (40)% of those with a positive (negative) transient velocity.

Analysis of the individual trajectories revealed that the two wells act as nearly perfect sinks. Only molecules that are still close to the transition state, $|\xi| < 0.5$ so $\Delta E \approx 2.0$ kcal/mol, were observed to recross. This region is rapidly cleared in the relaxation runs, after 1 ps only 10% still remains and after 2 ps just 1%. So, 95% of all recrossings occurred within 1 ps after the start of the run. Molecules outside this region only rarely (about one in every hundred) recross the transition state. Comparing this with the *vacuo* relaxation runs makes it clear that the solvent bath must be absorbing the liberated energy efficiently. It is to be expected that the plateau of the transmission function will be a constant for quite some time to come. Indeed, extending 100 runs to 15 ps hardly altered the plateau.

In some studies on transmission functions a relatively small set of transition state configurations is created with a short constrained or restrained MD or MC run. Each of these configurations is then used as the starting point of a dozen relaxation runs.^{8,12} New initial velocities for *all* atoms in the simulation box are sampled from a Maxwellian distribution, Eq. (3.49), so the dozen relaxation runs are relatively uncorrelated. The velocity assignment used in this paper, affecting only *one* internal velocity, hardly randomises the starting point. It is therefore to be expected that relaxation runs based on the same transition state configuration will yield highly correlated trajectories. To test this hypothesis, 25 independent configurations were used as the starting point of 10 relaxation runs each. For most of the 10

trajectories the time evolution of the reaction coordinate is more or less the same, but runs with a high transient velocity were sometimes seen to deviate from the main stream. The same 25 configurations were also each used to start 10 relaxation runs with a Maxwellian velocity for all atoms. These trajectories were found to be less correlated. Surprisingly then, the transmission functions calculated for both sets of 250 runs are similar.

Sofar, little has been said about the $|\mathbf{Z}_{\xi\sigma}|$ of Eq. (3.42). We first take a look at \mathbf{Z}_{σ} , Eq. (3.38). The L constrained bond lengths are commonly defined as $\sigma_l = (\mathbf{r}_{l,H} - \mathbf{r}_{l,A})^2 - l_{AH}^2$, where l_{AH} is the equilibrium length of the A–H bond.²³ It then follows that the diagonal elements of \mathbf{Z}_{σ} are constants, $4l_{AH}^2(m_H^{-1} + m_A^{-1})$. Since only four atoms are involved in two distance constraints, namely the carbons of the methyl hinges, there are only eight non-vanishing off-diagonal elements. They are of the form $4l_C^2 m_C^{-1} \cos\phi_{HCH}$, which amounts to about $-1/40^{\text{th}}$ of the diagonal elements. These elements are not constants, but the harmonic bending potential limits the fluctuations. The Z_{ξ} , Eq. (3.48), is nearly constant during the constrained run at 1.00010 ± 0.00011 . From the above discussion on low frequency and high frequency modes it follows that the elements of \mathbf{D} are of the order $\sum_k d_k^r d_k^l$, Eq. (3.29); the exact value amounts to about $0 \pm 1 \cdot 10^{-3}$. We then arrive at the final result, $\langle |\mathbf{Z}_{\xi\sigma}| \rangle = 3.658 \pm 0.002 \cdot 10^{-32}$. Because of the relatively very small fluctuations this term can safely be neglected when calculating the constrained average.

In the so-called [1₄]metacyclophane the hydroxyl groups at the lower rim of the calix[4]arene have been replaced by hydrogens. This molecule is extremely flexible due to the absence of stabilising hydrogen bonds. The energy barriers between the local minima, 3.8 kcal/mol,⁴⁷ are only slightly higher than those of *n*-butane. A short constrained MD run showed that this molecule is much too floppy to be studied with the reactive flux method. Even with a constraint on the unstable normal mode of the cone to paco saddle point, the molecule is still flexible enough to allow for spontaneous conformational changes. This clearly shows the limited effect of the normal mode constraint on the remaining vibrations of the molecule. In principle, this problem could also have occurred with the calix[4]arene, but there the energy barriers are high enough to suppress side-reactions.

3.6 Conclusions

A new versatile reaction coordinate was introduced that can be used on a wide variety of reactions. In combination with the reactive flux method the transmission functions of several reactions have been calculated. The results for isomerising *n*-butane are in good agreement with results found previously. A calix[4]arene served as an example of a more complex isomerising molecule. Two pitfalls of the technique, in fact problems of any reaction coordinate, were discussed: i) the sign of the reaction coordinate need not be the same throughout the entire reactant or product well, and ii) simultaneous reactions in the molecule are not suppressed. Provided these two problems do not arise, the reaction coordinate is found to be a very efficient one. The coordinate is shown to yield a high plateau value, at least for reactions *in vacuo*, at small computational expense. In the following chapter the

calculation of the free energy of a solvated calix[4]arene will be discussed using the same reaction coordinate.

3.7 Appendix: calculation of Z_ξ .

Starting with the identity

$$\begin{pmatrix} Z_\xi & \mathbf{0} \\ \mathbf{D}^T & \mathbf{1} \end{pmatrix} = \mathbf{Z}_{\xi\sigma} \mathbf{Z}_{\xi\sigma}^{-1} \begin{pmatrix} Z_\xi & \mathbf{0} \\ \mathbf{D}^T & \mathbf{1} \end{pmatrix}, \quad (3.58)$$

replacing $\mathbf{Z}_{\xi\sigma}^{-1}$ by equation (3.39) and evaluating all resulting matrix products by using the combination rules that follow from $\mathbf{Z}_{\xi\sigma} \mathbf{Z}_{\xi\sigma}^{-1} = \mathbf{1}$ yields

$$\begin{pmatrix} Z_\xi & \mathbf{0} \\ \mathbf{D}^T & \mathbf{1} \end{pmatrix} = \mathbf{Z}_{\xi\sigma} \begin{pmatrix} \mathbf{1} & \mathbf{L} \\ \mathbf{0} & \mathbf{M}_\sigma \end{pmatrix}. \quad (3.59)$$

Taking the determinant produces the final result,

$$Z_\xi = |\mathbf{Z}_{\xi\sigma}| |\mathbf{M}_\sigma|. \quad (3.60)$$

3.8 References

- ¹ D. Brown and J. H. R. Clarke, *J. Chem. Phys.* **92**, 3062 (1990).
- ² R. Edberg, D. J. Evans and G. P. Morriss, *J. Chem. Phys.* **87**, 5700 (1987).
- ³ P. Hänggi, P. Talkner and M. Borkovec, *Rev. Mod. Phys.* **62**, 251 (1990).
- ⁴ H. Eyring, *J. Chem. Phys.* **3**, 107 (1935).
- ⁵ J. Horiuti, *Bull. Chem. Soc. Jpn.* **13**, 210 (1938)
- ⁶ T. Yamamoto, *J. Chem. Phys.* **33**, 281 (1960).
- ⁷ D. Chandler, *J. Chem. Phys.* **68**, 2959 (1978).
- ⁸ R. O. Rosenberg, B. J. Berne and D. Chandler, *Chem. Phys. Lett.* **75**, 162 (1980).
- ⁹ I. Benjamin and A. Pohorille, *J. Chem. Phys.* **98**, 236 (1993).
- ¹⁰ R. A. Kuharski, D. Chandler, J. A. Montgomery Jr., F. Rabii and S. J. Singer, *J. Phys. Chem.* **92**, 3261 (1988).
- ¹¹ D. Chandler and R. A. Kuharski, *Faraday Discuss. Chem. Soc.* **85**, 329 (1988).
- ¹² M. A. Wilson and D. Chandler, *Chem. Phys.* **149**, 11 (1990).
- ¹³ J. M. Depaepe, J.-P. Ryckaert and A. Bellemans, *Mol. Phys.* **78**, 1575 (1993).
- ¹⁴ K. D. Hammonds, I. R. McDonald and J.-P. Ryckaert, *Chem. Phys. Lett.* **213**, 27 (1993).
- ¹⁵ I. Ghosh and J. A. McCammon, *Biophys. J.* **51**, 637 (1987).
- ¹⁶ R. M. Whitnell and K. R. Wilson, *Rev. Comp. Chem.* **IV**, 67 (1993).
- ¹⁷ J. B. Anderson, *Adv. Chem. Phys.* **XCI**, 381 (1995).
- ¹⁸ H. M. Pickett and H. L. Strauss, *J. Am. Chem. Soc.* **92**, 7281 (1970).
- ¹⁹ C. Eckart, *Phys. Rev.* **47**, 552 (1935).
- ²⁰ K. Fukui, *Acc. Chem. Res.* **14**, 363 (1981).

- ²¹ J.-P. Ryckaert, G. Ciccotti and H. J. C. Berendsen, *J. Comp. Phys.* **23**, 327 (1977).
- ²² D. J. Tobias and C. L. Brooks III, *J. Chem. Phys.* **89**, 5115 (1988).
- ²³ G. Ciccotti and J.-P. Ryckaert, *Comp. Phys. Rep.* **4**, 347 (1986).
- ²⁴ E. A. Carter, G. Ciccotti, J. T. Hynes and R. Kapral, *Chem. Phys. Lett.* **156**, 472 (1989).
- ²⁵ J.-P. Ryckaert and G. Ciccotti, *Mol. Phys.* **58**, 1125 (1986).
- ²⁶ W. F. van Gunsteren and H. J. C. Berendsen, *Groningen Molecular Simulation Library*, Groningen, The Netherlands, 1987.
- ²⁷ C. J. Cerjan and W. H. Miller, *J. Chem. Phys.* **75**, 2800 (1981).
- ²⁸ S. Bell and J. S. Crighton, *J. Chem. Phys.* **80**, 2464 (1984).
- ²⁹ F. Jensen, *J. Chem. Phys.* **102**, 6706 (1995).
- ³⁰ S. Fischer and M. Karplus, *Chem. Phys. Lett.* **194**, 252 (1992).
- ³¹ B. R. Brooks, R. E. Bruccoleri, B. D. Olafson, D. J. States, S. Swaminathan and M. Karplus, *J. Comp. Chem.* **4**, 187 (1983).
- ³² W. H. Press, B. P. Flannery, S. A. Teukolsky and W. T. Vetterling, *Numerical recipes* (Cambridge University Press, Cambridge, U. K., 1986).
- ³³ D. J. Evans, *Mol. Phys.* **34**, 317 (1977).
- ³⁴ H. Goldstein, *Classical mechanics* (Addison-Wesley, Reading MA, 1980).
- ³⁵ F. T. H. Leuwerink and W. J. Briels, *J. Chem. Phys.* **103**, 4637 (1995).
- ³⁶ We used a bending potential that is quadratic in the angle θ rather than quadratic in $\cos\theta$. The force constant was adapted accordingly, $k'_\theta = k_\theta \sin\theta_0$.
- ³⁷ H. J. C. Berendsen, J. P. M. Postma, W. F. van Gunsteren, A. DiNola and J. R. Haak, *J. Chem. Phys.* **81**, 3684 (1984).
- ³⁸ D. W. Rebertus, B. J. Berne and D. Chandler, *J. Chem. Phys.* **70**, 3395 (1979).
- ³⁹ D. Chandler and B. J. Berne, *J. Chem. Phys.* **71**, 5386 (79).
- ⁴⁰ D. Brown and J. H. R. Clarke, *J. Chem. Phys.* **93**, 4117 (1990); **94**, 4684 (1991).
- ⁴¹ C. D. Gutsche and L. J. Bauer, *J. Am. Chem. Soc.* **107**, 6052 (1985).
- ⁴² K. Araki, S. Shinkai and T. Matsuda, *Chem. Lett.* **1989**, 581 (1989).
- ⁴³ P. D. J. Grootenhuis, P. A. Kollman, L. C. Groenen, D. N. Reinhoudt, G. J. van Hummel, F. Uguzzoli and G. D. Andreotti, *J. Am. Chem. Soc.* **112**, 4165 (1990).
- ⁴⁴ T. Harada, J. M. Rudzinski and S. Shinkai, *Chem. Soc. Perkin Trans. 2* **1992**, 2109 (1992).
- ⁴⁵ T. Harada, J. M. Rudzinski, E. Osawa and S. Shinkai, *Tetrahedron* **49**, 5941 (1993).
- ⁴⁶ J. Royer, F. Bayard and C. Decoret, *J. Chim. Phys.* **87**, 1695 (1990).
- ⁴⁷ S. Fischer, P. D. J. Grootenhuis, L. C. Groenen, W. P. van Hoorn, F. C. J. M. van Veggel, D. N. Reinhoudt and M. Karplus, *J. Am. Chem. Soc.* **117**, 1611 (1995).
- ⁴⁸ J. C. Smith and M. Karplus, *J. Am. Chem. Soc.* **114**, 801 (1992).
- ⁴⁹ W. Dietz and K. Heinzinger, *Ber. Bunsenges. Phys. Chem.* **88**, 543 (1984); **89**, 968 (1985).
- ⁵⁰ I. G. Tironi and W. F. van Gunsteren, *Mol. Phys.* **83**, 381 (1994).

Chapter 4

Free energy and conformational transition rates of calix[4]arene in chloroform^{*}

Abstract

In a previous article we introduced a reaction coordinate based on the unstable normal mode at the saddle point of the potential energy surface. We here calculate the free energy distribution along this coordinate for the isomerisation of calix[4]arene *in vacuo* and in chloroform using umbrella sampling, with one umbrella covering the entire range of the reaction coordinate. An excellent first guess at this umbrella is obtained by performing a normal mode analysis at various points along the reaction path. The isomerisation rate constant of this reaction is determined using the reactive flux method, and is found to be in good agreement with experimental data. The rate was found to be independent of the location of the transition state, as it should be.

4.1 Introduction

The forward rate constant k_f of a reaction, i.e. the fraction of reactants turned into products per unit of time, in a solvent is a complicated function of the internal potential of the reacting solute molecule(s), the solute-solvent interactions and the solvent-solvent interactions. Molecular dynamics simulations (MD) are perfectly well suited for the numerical analysis of such involved situations. Based on the statistical mechanical ideas discussed below, it is possible to deduce from a total of about 10 nanosecond simulation time a reaction rate that is slower by many orders of magnitude. The particular reaction studied here is the isomerisation of a calix[4]arene *in vacuo* and in chloroform.

In Eyring's transition state theory¹ (TST) a hyperplane, the transition state, is introduced to split configuration space into a reactant space and a product space. This plane is characterised by $\xi(\{\mathbf{x}_i\}) = \xi^\ddagger$, where the reaction coordinate $\xi(\{\mathbf{x}_i\})$ is a function of the atomic coordinates. Product space and reactant space are defined by $\xi > \xi^\ddagger$ and $\xi < \xi^\ddagger$

^{*} W. K. den Otter and W. J. Briels, J. Chem. Phys. **107** 4968 (1997).

respectively. The forward rate constant is calculated as the instantaneous product-bound flux through the transition state, normalised by the population of the reactant space:²

$$k_f^{TST} = \frac{\langle \delta[\xi(0) - \xi^\ddagger] \dot{\xi}(0) \theta[\dot{\xi}(0)] \rangle}{\langle \theta[\xi^\ddagger - \xi(0)] \rangle}. \quad (4.1)$$

Here the angular brackets denote a canonical average and θ is the Heaviside function.

The TST expression is conveniently rewritten as

$$k_f^{TST} = \frac{\langle \delta[\xi(0) - \xi^\ddagger] \dot{\xi}(0) \theta[\dot{\xi}(0)] \rangle \langle \delta[\xi(0) - \xi^\ddagger] \rangle}{\langle \delta[\xi(0) - \xi^\ddagger] \rangle \langle \theta[\xi^\ddagger - \xi(0)] \rangle}. \quad (4.2)$$

The second term on the right hand side is the probability of finding the molecule at the transition state, $P(\xi^\ddagger)$, divided by the probability for the molecule to be in reactant space,

$$P_R = \int_{-\infty}^{\xi^\ddagger} P(\xi) d\xi. \quad (4.3)$$

We will discuss two techniques for the calculation of the probability distribution $P(\xi)$: normal mode analysis in section 4.2.2, and umbrella sampling in section 4.2.3. The first term on the right hand side of Eq. (4.2), the average positive velocity of the reaction coordinate at the transition state, will be addressed in section 4.2.4. The particular reaction coordinate that we will use is discussed in section 4.2.1. Numerical results for the probability function and the TST isomerisation rate of a calix[4]arene *in vacuo* and in chloroform are presented in section 4.3.

Transition state theory, by focusing on the instantaneous forward flux, neglects the fact that some fraction of this flux will recross the transition state shortly (order of a picosecond) after having crossed it. Likewise, the forward flux also contains a contribution of ‘product molecules’ that have crossed the transition state with a negative velocity shortly before they recross with a positive velocity. These recrossings are the result of the normal dynamics of a reacting molecule, induced by both the internal interactions of the molecule and its interactions with the solvent. To a macroscopic observer, though, these rapid recrossings are invisible, irrelevant. He defines the rate by the number of molecules that are in the reactant well at time $t = 0$ and are in the product well at time t , normalised by the overall number of molecules in the reactant well at time $t = 0$. Only if there are no recrossings will his rate equal the TST rate, otherwise TST overestimates the true rate.

In the reactive flux method (RF) the aforementioned macroscopic definition of the rate is related to the microscopic behaviour of a single molecule in a solvent by means of Onsager’s regression hypothesis.^{3,4} The resulting rate expression is

$$k_f^{RF}(t) = \frac{\langle \delta[\xi(0) - \xi^\ddagger] \dot{\xi}(0) \theta[\xi(t) - \xi^\ddagger] \rangle}{\langle \theta[\xi^\ddagger - \xi(0)] \rangle}. \quad (4.4)$$

In comparison with TST, attention has shifted from those molecules that cross the transition state with a positive velocity to those molecules that actually end up in the product space at some time t after crossing the transition state in whatever direction. The rate is often expressed as

$$k_f^{RF}(t) = \kappa(t) k_f^{TST}, \quad (4.5)$$

$$\kappa(t) = \frac{\langle \delta[\xi(0) - \xi^\ddagger] \dot{\xi}(0) \theta[\xi(t) - \xi^\ddagger] \rangle}{\langle \delta[\xi(0) - \xi^\ddagger] \dot{\xi}(0) \theta[\dot{\xi}(0)] \rangle}, \quad (4.6)$$

where $\kappa(t)$ is the transmission function. On the time scale of the recrossings, about a picosecond, the transmission function decays from unity at $t = 0$ to the so-called plateau level. The true rate constant is found by inserting this plateau value into Eq. (4.5). Actually, the plateau is not constant but decaying on the time scale of the reaction, but for most reactions this is too slow to be seen in MD simulations. In a previous article⁵ we discussed the calculation of the transmission function of the reaction studied here.

From Eqs. (4.1) and (4.4) one could infer that the calculated rate depends on the definition of the transition state, i.e. on ξ^\ddagger and $\xi(\{\mathbf{x}_i\})$ (for simplicity we will neglect the latter dependence). The rate should of course depend on this definition, since it is embodied in the definition of the number of reactant molecules, P_R , and hence in the therefrom derived rate. But, provided the free energy barrier is high and ξ^\ddagger lies somewhere near the top, the number of reactants is virtually independent to the precise location of ξ^\ddagger , and so must the rate be. The TST rate obviously strongly depends on ξ^\ddagger ; in the RF method the dynamics incorporated in the transmission function blurs the picture. Miller⁶ showed, using Liouville's theorem, that the RF rate is independent of the precise location of the transition state. Chandler⁴ arrived at the same conclusion in a discussion based on the separation in time scales between recrossing and reactive events. In section 4.3.3 this independence is verified numerically.

4.2 Theory

4.2.1 Reaction coordinate

We here briefly discuss the unstable normal mode reaction coordinate; an elaborate introduction is to be found in a previous article.⁵ The reasoning behind this reaction coordinate is the fact that in a reactive system most reactant to product trajectories will surmount the potential energy barrier somewhere near the lowest point of the barrier, i.e. the saddle point. It is therefore natural to construct a reaction coordinate based on the properties of the saddle point. The Taylor expansion of the potential energy around a saddle point, \mathbf{X}^0 , up to second order reads

$$\Phi(\mathbf{X}) = \Phi(\mathbf{X}^0) + \frac{1}{2}(\mathbf{X} - \mathbf{X}^0)^T \mathbf{H}(\mathbf{X} - \mathbf{X}^0). \quad (4.7)$$

For notational convenience, we collect all coordinates of the reacting molecule in a single $3N$ dimensional column vector of mass-weighted atomic coordinates, $\mathbf{X}^T = (m_1^{1/2}\mathbf{x}_1^T, m_2^{1/2}\mathbf{x}_2^T, \dots, m_N^{1/2}\mathbf{x}_N^T)$. The Hessian matrix, \mathbf{H} , contains all second order derivatives of the potential energy with respect to the components of \mathbf{X} . Its eigenvectors are orthogonal, or orthogonalisable in case of degeneracy, since the Hessian is symmetric. Henceforth, all eigenvectors will be assumed to be normalised. We shall assume that there is no external field.

The set of $3N$ eigenvectors can be split into three groups. First, there are three independent vectors \mathbf{E}^l that correspond to an overall translation of the molecule. Obviously, they leave the potential energy unchanged and therefore are eigenvectors of \mathbf{H} with eigenvalues zero, as follows from Eq. (4.7) after replacing $\mathbf{X} - \mathbf{X}^0$ by \mathbf{E}^l . Similarly, there are three independent (assuming a non-linear molecule) eigenvectors \mathbf{S}^k corresponding to infinitesimal rotations of the molecule. If $\mathbf{r}_i^0 = \mathbf{x}_i^0 - \mathbf{x}_{com}^0$ is the vector pointing from the centre of mass of the molecule to atom i , then an infinitesimal rotation around an axes \mathbf{e}_k through the centre of mass leads to the atomic displacements

$$(\mathbf{S}^k)^T = \left(\sqrt{m_1}(\mathbf{e}_k \times \mathbf{r}_1^0)^T, \sqrt{m_2}(\mathbf{e}_k \times \mathbf{r}_2^0)^T, \dots, \sqrt{m_N}(\mathbf{e}_k \times \mathbf{r}_N^0)^T \right). \quad (4.8)$$

Obviously, assuming orthonormality of the eigenvectors \mathbf{S}^k , the three \mathbf{e}_k are not orthogonal. The six modes of the first two groups are degenerate, they all have eigenvalue zero, if there is no external field. Finally, the remaining $3N - 6$ eigenvectors \mathbf{Q}^j are the normal modes of vibration.

At an energy minimum all vibrational modes have a non-negative eigenvalue, but at a first order saddle point there will be exactly one mode, \mathbf{Q}^r , with a negative eigenvalue. It is this unstable normal mode that we are interested in; it points downhill, from the saddle point towards the reactant and product wells, while all other modes are pointing uphill. Motion of the molecule along this mode, therefore, corresponds to a reaction. The reaction coordinate of a molecule with coordinates \mathbf{X} might now be defined as the projection of the displacement with respect to the saddle point configuration onto the unstable normal mode,

$$\xi = (\mathbf{X} - \mathbf{X}^0) \cdot \mathbf{Q}^r. \quad (4.9)$$

This coordinate, however, is not invariant under rotations of the molecule \mathbf{X} . This problem is solved by making the saddle point \mathbf{X}^0 depend on \mathbf{X} . First we note that the rotated saddle point $\mathbf{A}\mathbf{R}^0$, where \mathbf{A} is a $3N$ dimensional rotation matrix containing N copies of a regular three dimensional rotation matrix \mathbf{a} down the diagonal, and \mathbf{R}^0 is a mass-weighted column vector of the \mathbf{r}_i^0 , is also a saddle point. The normal modes of this rotated configuration simply are \mathbf{E}^l , $\mathbf{A}\mathbf{S}^k$ and $\mathbf{A}\mathbf{Q}^j$. We next define the reaction coordinate by

$$\xi = (\mathbf{X} - \mathbf{A}\mathbf{R}^0) \cdot \mathbf{A}\mathbf{Q}^r. \quad (4.10)$$

The rotation matrix \mathbf{A} , which is a function of just three parameters, is determined from the three equations

$$0 = (\mathbf{X} - \mathbf{AR}^0) \cdot \mathbf{AS}^k, \quad k \in \{1,2,3\}, \quad (4.11)$$

and assures rotational invariance. One may check that the above two equations are invariant under translation, as follows from the orthogonality of the eigenvectors of the Hessian.

The inverse transformation reads

$$\mathbf{X} = \mathbf{AR} + \sum_{l=1}^3 \gamma_l \mathbf{E}^l, \quad \mathbf{R} = \mathbf{R}^0 + \sum_{j=1}^{3N-6} \alpha_j \mathbf{Q}^j, \quad (4.12)$$

where the centre of mass of \mathbf{R} evidently lies at the origin. The reaction coordinate is one of the deviations, $\xi = \alpha_r$. At this point the reader might argue that the reaction coordinate now is dimensionless, while in Eq. (4.10) it seems to have a dimension of kg m^2 . However, the orthonormality of the vectors \mathbf{Q}^j that is assumed in going from Eq. (4.12) to Eq. (4.10) cancels the dimensionality.

In the following we will make use of the derivative of ξ with respect to \mathbf{X} . From the orthogonality of the rotation matrix in combination with the derivatives of Eqs. (4.10) and (4.11) it follows that

$$\nabla_{\mathbf{X}} \xi = \mathbf{A} \left(\mathbf{Q}^r - \sum_{k=1}^3 d_k^r \mathbf{S}^k \right). \quad (4.13)$$

The expression relating d_k^r to \mathbf{X} , \mathbf{A} , \mathbf{S}^k and \mathbf{Q}^r is given in a previous article.⁵

4.2.2 Theory of small vibrations

The free energy of a classical molecule *in vacuo* can be calculated in reasonable approximation by the theory of small vibrations. If we assume that the potential energy function around the energy minimum is quadratic, and if we neglect the coupling between rotations and vibrations, then the well-known semi-classical partition function of the minimum reads⁷

$$\begin{aligned} Q &= \frac{1}{h^{3N}} \int d\mathbf{x} \int d\mathbf{p}_x \exp[-\beta H(\mathbf{x}, \mathbf{p}_x)] \\ &= \left(\frac{2\pi M k_B T}{h^2} \right)^{3/2} V \cdot \frac{\pi^{1/2}}{\sigma} \left(\frac{8\pi^2 k_B T}{h^2} \right)^{3/2} (I_A I_B I_C)^{1/2} \\ &\quad \times \prod_{i=1}^{3N-6} \frac{k_B T}{\hbar \omega_i} \cdot \omega_e \exp[-E_{\min}/k_B T]. \end{aligned} \quad (4.14)$$

Here $\beta = 1/k_B T$, T is the absolute temperature, k_B is the Boltzmann constant, H is the Hamiltonian, h is the Planck constant, $\hbar = h/2\pi$, M is the total mass of the molecule, V is the volume of the box, σ is the symmetry number, the I_X are the momenta of inertia, the ω_i are the eigenfrequencies of vibration (the square roots of the non-zero eigenvalues of the Hessian), ω_e is the electronic degeneracy and E_{\min} is the energy at the potential minimum.

We will now give a derivation of this expression, such that it later can be generalised to calculate a ξ -dependent partition function.

To solve the integral of Eq. (4.14) we use the generalised coordinates of Eq. (4.12), where now the configuration \mathbf{R}^0 is assumed to be a local minimum of the potential function, and \mathbf{S}^k , \mathbf{E}^l and \mathbf{Q}^j are evaluated at this point. The obvious reason is that the potential energy in terms of these coordinates reduces to a simple formula,

$$\Phi \cong E_{min} + \frac{1}{2} \sum_{j=1}^{3N-6} \omega_j^2 \alpha_j^2, \quad (4.15)$$

provided the vibrations are small. After the canonical transformation of Eq. (4.14) from Cartesian coordinates to mass-weighted Cartesian coordinates the integration over the conjugate momenta yields $(2\pi k_B T)^{3N/2}$. The subsequent transformation of the coordinates to the generalised coordinates ψ_k , α_j and γ_l is accompanied by the Jacobi matrix

$$\mathbf{J} = \frac{\partial \mathbf{X}}{\partial \{\psi_k, \alpha_j, \gamma_l\}} = \mathbf{A}(\Psi^k \quad \mathbf{Q}^j \quad \mathbf{A}^{-1}\mathbf{E}^l), \quad (4.16)$$

where the rightmost matrix is expressed in terms of $3 + (3N - 6) + 3$ column vectors, and the three ψ_k parameterise the rotation matrix \mathbf{A} . Since the derivative of the rotation matrix with respect to its k^{th} argument can be written as the product of the rotation matrix and an antisymmetric matrix, \mathbf{B}_k , we find

$$\Psi^k = \mathbf{B}_k(\boldsymbol{\psi})\mathbf{R} = \sum_{l=1}^3 \boldsymbol{\varepsilon}^l \mathbf{R} c_{lk}(\boldsymbol{\psi}). \quad (4.17)$$

Here the $\boldsymbol{\varepsilon}^l$ are three $3N$ dimensional matrices containing N copies of a three dimensional antisymmetric matrix, an infinitesimal rotation generator,⁸ down the diagonal. The Jacobi matrix can then be written as

$$\mathbf{J} = \mathbf{A}(\boldsymbol{\varepsilon}^k \mathbf{R} \quad \mathbf{Q}^j \quad \mathbf{A}^{-1}\mathbf{E}^l) \begin{pmatrix} \mathbf{c} & \mathbf{0} & \mathbf{0} \\ \mathbf{0} & \mathbf{1} & \mathbf{0} \\ \mathbf{0} & \mathbf{0} & \mathbf{1} \end{pmatrix}. \quad (4.18)$$

If the Euler angles⁸ are used to parameterise the rotation matrix, then $0 \leq \psi_1 \leq 2\pi$, $0 \leq \psi_2 \leq \pi$, $0 \leq \psi_3 \leq 2\pi$, and $|\mathbf{c}| = \sin \psi_2$. Obviously, $|\mathbf{A}| = |\mathbf{a}|^N = 1$.

For small vibrations we may approximate \mathbf{R} by \mathbf{R}^0 in Eq. (4.18). Then $\boldsymbol{\varepsilon}^k \mathbf{R}$ is of the form of Eq. (4.8), hence perpendicular to both $\mathbf{A}^{-1}\mathbf{E}^l$ and \mathbf{Q}^j . Denoting the second matrix on the right-hand side of Eq. (4.18) by \mathbf{m} , and using $|\mathbf{m}| = |\mathbf{m}^T \mathbf{m}|^{1/2}$ in combination with these orthogonality relations and the orthonormality of the eigenvectors of the Hessian, the resulting Jacobian reads

$$|\mathbf{J}| = |\mathbf{I}^0|^{1/2} \sin \psi_2 = (I_A^0 I_B^0 I_C^0)^{1/2} \sin \psi_2. \quad (4.19)$$

The inertia tensor \mathbf{I}^0 is the upper left 3×3 submatrix of $\mathbf{m}^T \mathbf{m}$, with elements $I_{lk}^0 = (\boldsymbol{\epsilon}^l \mathbf{R}^0) \cdot (\boldsymbol{\epsilon}^k \mathbf{R}^0)$, and the I_x^0 are the eigenvalues of this tensor. The integrals over the generalised coordinates are straightforward, and combination with the previously evaluated integral over the momenta leads to Eq. (4.14). One should keep in mind that in a cubic box of side L the coordinates γ_i run from 0 to $L\sqrt{M}$ due to the normalisation of the translational eigenvectors. The integrals over the α_j are supposed to run from minus infinity to plus infinity.

In order to be able to calculate the numerator in the second factor in Eq. (4.2), we now derive an expression for the partition function as a function of the reaction coordinate,

$$Q(\xi^*) = \frac{1}{h^{3N}} \int d\mathbf{x} \int d\mathbf{p}_x \exp[-\beta H(\mathbf{x}, \mathbf{p}_x)] \delta[\xi(\mathbf{x}) - \xi^*], \quad (4.20)$$

using the same assumptions that were used in the above derivation of Eq. (4.14). This partition function is often expressed in terms of a free energy by

$$A(\xi^*) = -k_B T \ln Q(\xi^*). \quad (4.21)$$

We first transform to mass-weighted coordinates, and define a standard minimum \mathbf{R}^* on the hyperplane $\xi(\mathbf{X}) = \xi^*$. This minimum is found by varying the α_j in Eq. (4.12), while keeping α_r equal to ξ^* . The minimum \mathbf{R}^* is not rotated with respect to \mathbf{R}^0 , and their centres of mass coincide. In the present partition function the configuration \mathbf{R}^* plays a role analogous to that of \mathbf{R}^0 in Eq. (4.14). In the appendix it is shown that

$$Q(\xi^*) = \left(\frac{2\pi M k_B T}{h^2} \right)^{3/2} V \cdot \frac{\pi^{1/2}}{\sigma} \left(\frac{8\pi^2 k_B T}{h^2} \right)^{3/2} (I_A^* I_B^* I_C^*)^{1/2} \\ \times \prod_{i=1}^{3N-7} \frac{k_B T}{\hbar \omega_i^*} \cdot \omega_e \exp[-E^*/k_B T] \cdot \left| \nabla_{\mathbf{R}^*} \xi \right|^{-1} \cdot (2\pi k_B T)^{1/2} h^{-1}, \quad (4.22)$$

where a superscript asterisk denotes a quantity that is to be calculated at \mathbf{R}^* . An alternative expression for the partition function is also derived in the appendix.

To locate the minimum \mathbf{R}^* on the hyperplane $\xi(\mathbf{X}) = \xi^*$ we used a standard minimum search routine in combination with a constraint on the reaction coordinate. The resulting configuration was further refined by reducing the projection of the gradient of the potential onto the tangent hyperplane. This was achieved by an iterative Newton-Raphson zero point search, using forces and Hessians calculated in the plane spanned by the basisvectors \mathbf{T}^l defined in the appendix. Since the tangent hyperplane is only locally correct, each iterated point was reset to $\xi(\mathbf{X}) = \xi^*$ by a SHAKE-routine,^{5,9} followed by a recalculation of the normal to the hyperplane, \mathbf{N} , and of the basisvectors \mathbf{T}^l . If these minimisations are performed in the full $3N$ dimensional space, then the molecule will rotate inevitably. This is easily corrected for, either by rotating the vectors \mathbf{N} and \mathbf{T}^l , or by counter-rotating the molecule after each step. This effect does not arise if the minimum is directly located in the $3N - 6$ dimensional α -space.

Eqs. (4.14) and (4.22) obviously do not take into account the anharmonicity of the force field, nor the coupling between rotations and vibrations. The inclusion of interactions with a solvent is difficult. In the next section an alternative technique is discussed which does not suffer from these drawbacks.

4.2.3 Umbrella sampling

A straightforward way of obtaining the correct probability distribution $P(\xi)$ of a (dissolved) molecule is to calculate this distribution directly from a long MD run. The MD run should include numerous barrier crossings to ensure that both wells and the barrier region are sampled sufficiently. For reactions with a high barrier, exceeding several $k_B T$, such a run would last prohibitively long. Two techniques are commonly employed to circumvent this problem.¹⁰⁻¹² In the potential of mean force method the derivative of the free energy with respect to the reaction coordinate is calculated in a series of ξ -constrained runs and then integrated. We will use the second method, and apply an ‘umbrella potential’, a modification to the force field that can easily be corrected for, to effectively reduce the barrier.

We are interested in the probability distribution of the reaction coordinate,

$$P(\xi^*) = \int d\mathbf{X} p(\mathbf{X}) \delta[\xi(\mathbf{X}) - \xi^*]. \quad (4.23)$$

Here

$$p(\mathbf{X}) = \frac{1}{Z} \exp[-\beta\Phi(\mathbf{X})] \quad (4.24)$$

is the Boltzmann factor for a molecule in configuration \mathbf{X} with potential Φ , and Z is a normalisation factor. \mathbf{X} represents all coordinates, including the solvent coordinates, and Φ includes solvent-solvent and solute-solvent interactions. In the barrier region this probability becomes extremely small, too small to be sampled efficiently. Addition of an umbrella potential, U , changes the Boltzmann factor into

$$p_U(\mathbf{X}) = \frac{1}{Z_U} \exp[-\beta\{\Phi(\mathbf{X}) + U(\mathbf{X})\}]. \quad (4.25)$$

The umbrella potential is used to favour the distribution p_U in areas that would otherwise have been difficult to sample. The requested probability distribution of the reaction coordinate is readily obtained from the biased distribution by combining Eqs. (4.23) through (4.25) into

$$P(\xi^*) = \frac{Z_U}{Z} \int d\mathbf{X} p_U(\mathbf{X}) \exp[\beta U(\mathbf{X})] \delta[\xi(\mathbf{X}) - \xi^*]. \quad (4.26)$$

The normalisation factors Z_U and Z do not have to be calculated independently, only the factor which normalises the final distribution $P(\xi^*)$ is needed.

In many applications the umbrella potential is chosen to be a function of the reaction coordinate ξ only, in which case the exponential in the integral of Eq. (4.26) becomes a

constant.^{13,14} For molecules with more than two local minima, as in our case, it may prove necessary to use a somewhat more complicated umbrella potential to suppress unwanted side reactions.

Often a series of L umbrellas of the form $\Phi_l(\xi) = \frac{1}{2}k_l(\xi - \xi_l)^2$, $l = 1, \dots, L$, is used. At each l a small area of configuration space, a so-called ‘window’, is sampled, resulting in a distribution $P_l(\xi)$ for each window. The various distributions are then combined into the overall distribution, using the overlap of successive windows to match the partial distributions.¹⁵ We use a single umbrella covering the whole range of ξ . Only if the diffusion along the reaction coordinate is relatively fast this method will work, so care must be taken to make the reaction coordinate distribution in the biased run as flat as possible.

4.2.4 Transition state crossing velocity

The first term on the right hand side of Eq. (4.2) is most easily calculated by using the mass-weighted coordinates introduced above. The velocity of the reaction coordinate can be expressed in terms of the mass-weighted Cartesian momenta as

$$\dot{\xi} = \nabla_x \xi \cdot \dot{\mathbf{X}} = \nabla_x \xi \cdot \mathbf{p}_x, \quad (4.27)$$

and the kinetic energy of the molecule reduces to $E_{kin} = \mathbf{p}_x \cdot \mathbf{p}_x$. These equations remain the same if the coordinate system is rotated. We now apply a rotation such that the first mass-weighted coordinate axis lies parallel to $\nabla_x \xi$; all other axes are then perpendicular to the gradient. Integration over the momentum parallel to this axis, using

$$\int_0^{\infty} dp p \exp[-ap^2] = \frac{1}{2\sqrt{\pi a}} \int_{-\infty}^{\infty} dp \exp[-ap^2], \quad (4.28)$$

yields the average positive crossing velocity

$$\frac{\langle \delta[\xi(0) - \xi^\ddagger] \dot{\xi}(0) \theta[\dot{\xi}(0)] \rangle}{\langle \delta[\xi(0) - \xi^\ddagger] \rangle} = \sqrt{\frac{k_B T}{2\pi}} \frac{\langle \delta[\xi(0) - \xi^\ddagger] |\nabla_x \xi| \rangle}{\langle \delta[\xi(0) - \xi^\ddagger] \rangle}. \quad (4.29)$$

The length of the gradient, Eq. (4.42), is seen to act as the reciprocal effective mass of the reaction coordinate. Combining Eqs. (4.2), (4.14), (4.22) and (4.29) yields the classical analogue to Eyring’s expression.

It is common practice to express the rate constant in terms of a free energy difference between the transition state and the reactant well, $\Delta A^\ddagger = A^\ddagger - A_R$, as in

$$k_f = \frac{k_B T}{h} \exp\left[-\frac{\Delta A^\ddagger}{k_B T}\right]. \quad (4.30)$$

This free energy difference should not be confused with the free energy difference calculated by means of Eqs. (4.2) and (4.21). First, the free energy A^\ddagger is based on the partition function of a molecule which is constrained to $\xi(\mathbf{X}) = \xi^\ddagger$ and which explicitly excludes any motion along the reaction coordinate, $\dot{\xi} = 0$. In the harmonic approximation

$$A^\ddagger = -k_B T \ln \left[Q(\xi^\ddagger) \frac{h}{\sqrt{2\pi k_B T}} \right]. \quad (4.31)$$

Using this result, the transition state theory value of the rate constant in the harmonic approximation takes the form of Eq. (4.30). Second, in the literature on experiments the ΔA^\ddagger includes the transmission factor.

4.3 Results

The techniques introduced above are now applied to the isomerisation reaction of calix[4]arene.¹⁶ This molecule consists of four phenol groups, each of which is connected to two neighbouring phenols by methyl bridges located ortho to the hydroxyl group, see Fig. 4.1. In supramolecular chemistry they are being used as building blocks. The interesting property in the current context is the fact that they have four stable conformations. The ‘cone’ conformation, with all phenol groups pointing in the same direction, is most abundant. It is stabilised by a cyclic array of four hydrogen bonds. The partial cone, ‘paco’ for short, is formed by rotating one phenol group, with the methyl groups acting as hinges and the hydroxyl group moving through the central annulus. In this process two hydrogen bonds are broken. We will focus here on this reaction step. In a following reaction step one of the phenol groups nearest to the rotated phenol can rotate and form the ‘1,2-alternate’, or the opposing phenol group can rotate to form the ‘1,3-alternate’. After two more steps all phenol groups have rotated, and the final ‘inverted cone’ conformation is reached. This name will be used to distinguish it from the initial ‘cone’ configuration.

All simulations were done with a modified version of GROMOS87.¹⁷ Several routines were adapted or added for the handling of the normal mode reaction coordinate. The calix[4]arene was modelled with the all-atom CHARMM parameter set 22.¹⁸ The saddle point of the cone to paco reaction was calculated with the Conjugate Peak Refinement algorithm.^{18,19} The unstable normal mode of the saddle point, \mathbf{Q}^r , was chosen to point towards the paco well. All normal modes were normalised to 1 a.m.u.^{1/2} nm. In the MD runs all bonds involving hydrogen atoms were constrained to constant lengths using SHAKE,⁹ and in several runs the reaction coordinate was also constrained. The effect of these constraints on the sampling of

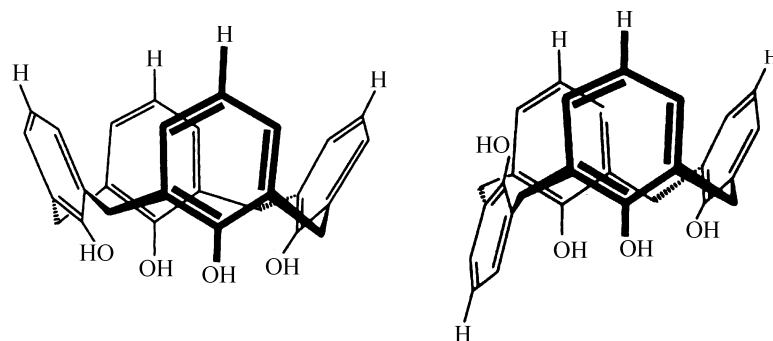


Figure 4.1. The cone (left) and partial cone (paco, right) conformation of a calix[4]arene.

phase space was shown to be very small, so we applied no corrections. We refer to a previous article⁵ for more details.

In section 4.3.1 the free energy profile of a calix[4]arene *in vacuo* is calculated using the theory of small vibrations. The runs with umbrella sampling, both *in vacuo* and in chloroform, are described in section 4.3.2. Combining the free energy and the transmission function allows us to calculate the reaction rates of section 4.3.3.

4.3.1 Small vibrations

The minimum energy of a calix[4]arene *in vacuo* as a function of the reaction coordinate was calculated by two series of ξ -constrained energy minimisations. Starting at the saddle point, the value of ξ was increased (decreased) by 0.01 up to a maximum value of 2 (-2), and a minimum was located at each value. The resulting function is shown in Fig. 4.2 by the dotted line, while the plot is shifted vertically to place the saddle point at zero energy. The local minima of the cone and paco conformations are seen to be at 15.2 and 5.6 kcal/mol respectively below the saddle point, in agreement with the results of previous unconstrained minimisation runs.¹⁸ At both extremes of the ξ -axis, with energies exceeding the saddle point value, the minimum search algorithm ran into problems. In these areas, as a result of the constraint on the reaction coordinate, the strain on the molecules was so extreme that the molecule ‘spontaneously’ changed into another conformation. These areas are irrelevant to the problem at hand, so these problems are of no consequence. For energies below the saddle point value, in the range $-1.71 \leq \xi \leq 1.53$, the minimisation produces a smooth energy profile.

Next, each minimum in the intermediate range was refined by a Newton-Raphson zero point search in $3N$ dimensions, as described in section 4.2.2. After each iteration step SHAKE was applied to prevent the molecule from slowly drifting away from the hyperplane. The Hessian \mathbf{H}^* , as defined in the appendix, of the converged configurations were diagonalised to obtain the eigenfrequencies of vibration. All frequencies were positive, so Eq. (4.22) could be used to evaluate the partition function. The absolute values of the rotational eigenfrequencies, which should have been zero, were found to be smaller than the lowest vibrational eigenfrequency by 4 to 5 orders of magnitude for most configurations, indicating that the constrained minima were indeed well converged.

The free energy function *in vacuo* was calculated by means of Eq. (4.22). In Fig. 4.2 this function is shown as a dashed line, shifted vertically in order to make it pass through the origin. The difference with the minimum energy function is considerable, ranging from +1.2 kcal/mol near the cone minimum to -0.5 kcal/mol near the paco minimum. This difference is predominantly of vibrational origin, i.e. it reflects the ξ -dependence of the eigenfrequencies of vibration perpendicular to the gradient of ξ . The other two ξ -dependent terms, due to rotation and due to the gradient of ξ , vary by just 2.9% and 0.8%, respectively, of the variation of the vibrational contribution. The top of the free energy function has shifted from the origin towards $\xi = -0.06$, as can be seen in the inset of Fig. 4.2. The

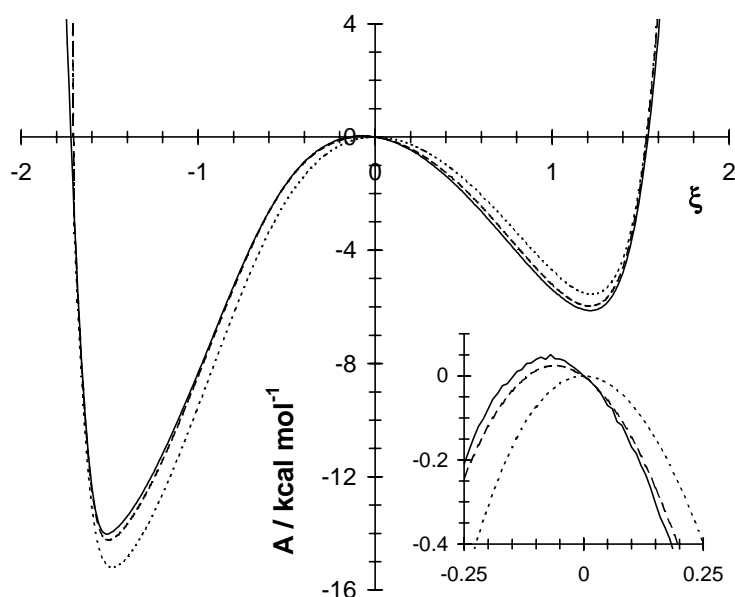


Figure 4.2. Minimum energy (dotted), free energy according to normal mode analysis (dashed) and free energy according to umbrella sampling (solid) for a calix[4]arene in *vacuo*. The inset shows the three functions near the saddle point.

transmission function calculated *in vacuo* with $\xi^\ddagger = 0$ must therefore yield a transmission coefficient less than unity, as was indeed found.⁵

In an alternative calculation the potential energy as a function of the α_j , Eq. (4.12), was minimised using Newton-Raphson, at intervals of 0.01 for ξ . The partition function was then calculated according to Eq. (4.47) of the appendix. The resulting minimum energy and free energy distributions are identical to the ones discussed above, but the two methods are clearly different in the assignment of the rotational and vibrational free energy.

Replacing the vibrational partition function by its quantised version is of little effect on the free energy function: after forcing the function to pass through the origin, the differences with the semi-classical result range from about +0.25 kcal/mol for the cone to -0.2 kcal/mol for the paco. However, now the two expressions for the partition function differ by at most 0.02 kcal/mol. Omission of the 24 highest frequencies is of little influence, namely of the order of 0.06 kcal/mol for the quantised partition function and 0.008 kcal/mol for the semi-classical partition function. These 24 modes correspond to the stretching of bonds including hydrogen atoms; bonds that will be constrained in the MD simulations.

4.3.2 Umbrella sampling

As the initial trial umbrella for the umbrella sampling *in vacuo* served the above calculated minimum energy function,¹³ $U(\mathbf{X}) = f(\xi)$. At first a tenth order polynomial was used to fit the function in the interval where ξ ranges from -1.7 to +1.5, i.e. the region in which the potential energy is less than the saddle point energy. The umbrella was supplemented with two Fermi-Dirac functions at both extremes to delimit the range of

accessible ξ -values to those values that are relevant to the isomerisation rate. The least-squares fitted polynomial oscillated around the minimum energy function with an amplitude of about 0.25 kcal/mol. These oscillations were clearly visible in the sampled probability distribution, which contained corresponding maxima and minima. Upon examination of the trajectory it became clear that the molecule was hopping from one local minimum to the next. Since the time spent in the evaluation of the umbrella potential is negligible in comparison with the overall execution time, a more complicate umbrella, which represented the minimum energy function better, was used next. The cone well and the paco well were both fitted with a fifteenth order polynomial. In the saddle point region, which was covered by both fits, a third order ‘switch’ polynomial was used to make a smooth transition from one fit to the other. With this umbrella the time evolution of the reaction coordinate was effectively smoothed.

A second problem arose during the simulations. When the reaction coordinate reached a value of about 0.7, it proved possible for a phenol ring neighbouring the freely rotating ring to flip over. Thus the calix[4]arene reached the 1,2-alternate configuration, where it was captured for the rest of the MD-run. The reason for this problem was that the umbrella not only lowers the energies of the paco and the barrier conformations to the energy of the cone conformations, but it also lowers other saddle points to within a few $k_B T$ of the cone conformations. We therefore located the saddle point of the paco to 1,2-alternate transition, in the absence of an umbrella, using the TRAVEL algorithm and refined it with Newton-Raphson. Because of the circular orientation of the hydrogen bonds at the lower rim of the calix[4]arene there are two saddle points, depending on which neighbouring phenol ring is being rotated. One saddle point is located at $\xi = 1.02$ with an energy of 0.5 kcal/mol below the saddle point of the cone to paco transition, the other saddle point is located at $\xi = 0.96$ with an energy of 0.3 kcal/mol above the saddle point of the cone to paco transition. This second saddle point was not mentioned by Fischer *et al.*¹⁸ The umbrella potential was next extended to

$$U(\mathbf{X}) = f(\xi) + f_1(\xi_1) + f_2(\xi_2), \quad (4.32)$$

where f_1 and f_2 are two Fermi-Dirac functions used to delimit the range of accessible values of the reaction coordinates ξ_1 and ξ_2 calculated with respect to the saddle points of the paco to 1,2-alternate transitions. Analysis of the configurations sampled in simulations showed that these two reaction coordinates are well behaved and of constant sign throughout the cone and paco wells. Inclusion of the two potentials hardly effected the motion of the molecule for most of the time, but it effectively suppressed the rare but fatal transitions to the 1,2-alternate. Of course, the two additional potential functions were corrected for in the evaluation of the probability distribution of ξ , see Eq. (4.26).

A calix[4]arene *in vacuo* with the above described umbrella potential was equilibrated at a temperature of 300 K using velocity scaling. When a steady temperature was reached the velocity scaling was turned off, the angular velocity was eliminated and the molecule was simulated for 30 ns. The resulting biased probability distribution $P_f(\xi)$, corrected for f_1 and

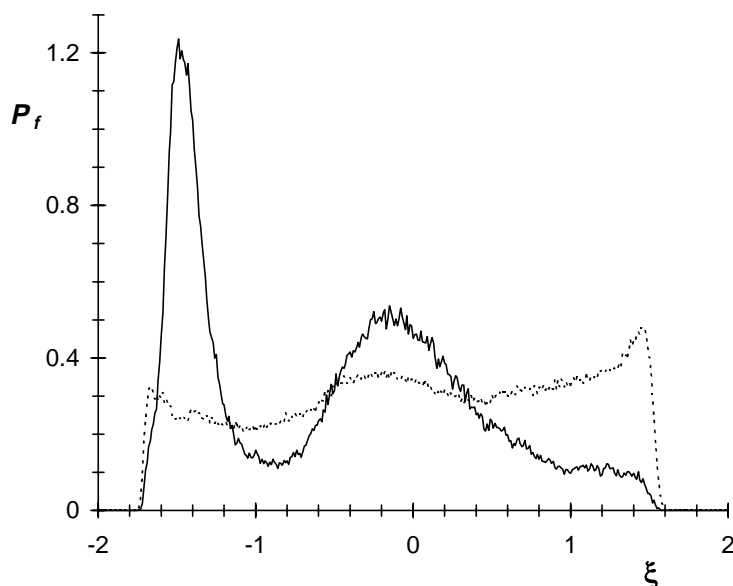


Figure 4.3. Probability distributions $P_f(\xi)$ in vacuo (dotted) and in chloroform (solid), calculated with the same umbrella potential. The areas under both graphs are identical.

f_2 but not for f , contained some strongly preferred regions. The vast majority of the sampled configurations was distributed over the paco well, and a peak was found at the outer extreme of the cone well. The cone well itself, i.e. the region with the highest population in the unbiased distribution, was sampled very poorly. To improve the sampling of this region, the sofar sampled probability distribution was transformed into a potential which was added to the existing umbrella. A second 30 ns run and a repeat of this recipe eventually lead to the relatively flat distribution $P_f(\xi)$ of Fig. 4.3. The resulting free energy profile after correction for f is shown in Fig. 4.2 as a solid line. Note the excellent resemblance to the normal mode based free energy function, they differ by less than 0.3 kcal/mol, and the less striking resemblance to the minimum energy function.

The final vacuum umbrella was also used in a run of a calix[4]arene dissolved in chloroform (CHCl_3). The run was performed at a constant temperature of 300 K and a constant pressure of 1 bar, bonds containing hydrogen atoms were constrained, the time step was 2 fs, long range interactions were cut off beyond 1.3 nm and the periodic box was a truncated octahedron containing 324 rigid solvent molecules. The system was equilibrated for 150 ps, followed by a production run of 2 ns. The sampled probability distribution $P_f(\xi)$ is shown in Fig. 4.3 as a solid line. Comparison with the vacuum distribution shows that the solvent environment induces a preference for the cone and the saddle point configurations. Fortunately, the differences with the vacuum run are fairly small since otherwise it would have been impossible to make the leap from vacuum to solvent without breaking up the range of the umbrella into smaller parts. Once more, the sampled probability distribution was turned into a potential and added to the umbrella. This umbrella was then used in a 5 ns

simulation to sample the conclusive distribution of the reaction coordinate of the dissolved molecule.

4.3.3 Rate constants

In this section the free energy profiles of the previous two sections are used to calculate rate constants according to transition state theory. The transmission coefficient is calculated next, and the reactive flux rate is obtained by multiplication of this coefficient with the transition state theory rate constant.

We first discuss the isomerisation rate of a calix[4]arene *in vacuo*. The partition function of the cone well, Q_{cone} , is equal to the integral of the partition function $Q(\xi)$, Eq. (4.20), over the interval from minus infinity to ξ^\ddagger . Because of the depth of the well the result is virtually independent of ξ^\ddagger . With $\xi^\ddagger = 0$ and the approximation of small vibrations we find $A_{cone} = 172.7$ kcal/mol, and similarly, $A_{paco} = 180.6$ kcal/mol. Direct evaluation of the free energies with the full normal mode analysis of Eq. (4.14) yields almost identical values. Next, we look at the transition state theory rate constant as a function of ξ^\ddagger . Approximating $|\nabla\xi| = |\mathbf{Q}^r|$, which is exact at the saddle point, we find that transition state theory predicts a minimum rate constant of 167 s^{-1} at $\xi = -0.06$, corresponding to the maximum of the free energy in Fig. 4.2. If, following Eyring, we use $\xi^\ddagger = 0$ as the transition state, we find $A(0) = 185.9$ kcal/mol and $k_f^{TST} = 174 \text{ s}^{-1}$. Using the free energy A_{cone} obtained with Eq. (4.14) in this case, i.e. using the textbook equation in which the rate constant is expressed in terms of the energies and the eigenfrequencies of the reactant well and the saddlepoint,^{2,20} we find a value of 177 s^{-1} .

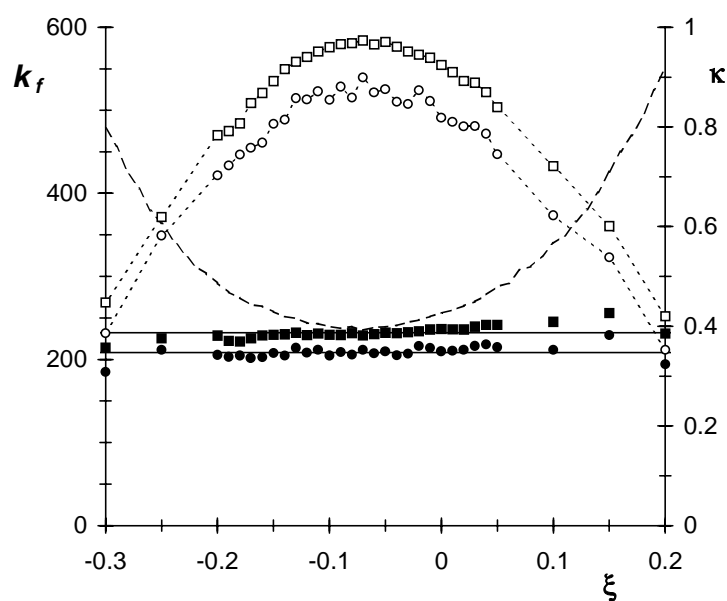


Figure 4.4. Transition state theory rate (dashed line), transmission coefficients (open markers) and reactive flux rates (solid markers) as a function of the location of the transition state in vacuo, for $t = 0.6$ ps (squares) and $t = 2.0$ ps (circles).

The changes of the free energy profile in going from the normal mode analysis to the umbrella sampling method are found to be fairly small. Nevertheless, the population of the paco well nearly doubles from $1.8 \cdot 10^{-6}$ to $3.4 \cdot 10^{-6}$, while $A_{paco} - A_{cone}$ changes from 7.9 to 7.5 kcal/mol. At $\xi = 0$ the population rises by about 50%, while $A(0) - A_{cone}$ changes from 13.1 to 12.9 kcal/mol, and the rate rises to $k_f^{TST} = 256 \text{ s}^{-1}$. Combination with the previously established transmission coefficient⁵ of 0.923 at $t = 0.6 \text{ ps}$ yields the reactive flux method rate of 237 s^{-1} . The transmission coefficient after 2 ps is slightly lower, $\kappa = 0.82$, and leads to $k_f^{RF} = 209 \text{ s}^{-1}$.

In principle the rate constant should be independent of the precise choice of the transition state, as long as this state is close enough to the top of the free energy barrier. To test this requirement in the case of the reactive flux method and to verify our results, we have calculated the rate constant as a function of ξ^\ddagger *in vacuo*. At various values the transmission function was evaluated by performing 2000 relaxation runs following the procedure outlined in a previous article. These transmission functions behaved as expected. For positive ξ^\ddagger virtually all molecules with a positive transient velocity, $\dot{\xi}(0)$, ended up as a paco. A considerable amount of those with a negative transient velocity also ended up as paco, and their number increased with increasing ξ^\ddagger . For negative ξ^\ddagger it was the other way round: many molecules with a positive transient velocity were found to recross the transition state, while molecules with a negative transient velocity recrossed only rarely. As reported earlier, a significant fraction of the molecules entering the paco well was found to return to the cone after a single oscillation of about 0.7 ps in the paco well. We therefore calculated the reactive flux rate constant using two transmission coefficients, namely the value of $\kappa(t)$ at 0.6 ps, as if the wells are perfect sinks, and the one at 2.0 ps. In Fig. 4.4 it is evident that the rates hardly depend on the transition state, as it should be.

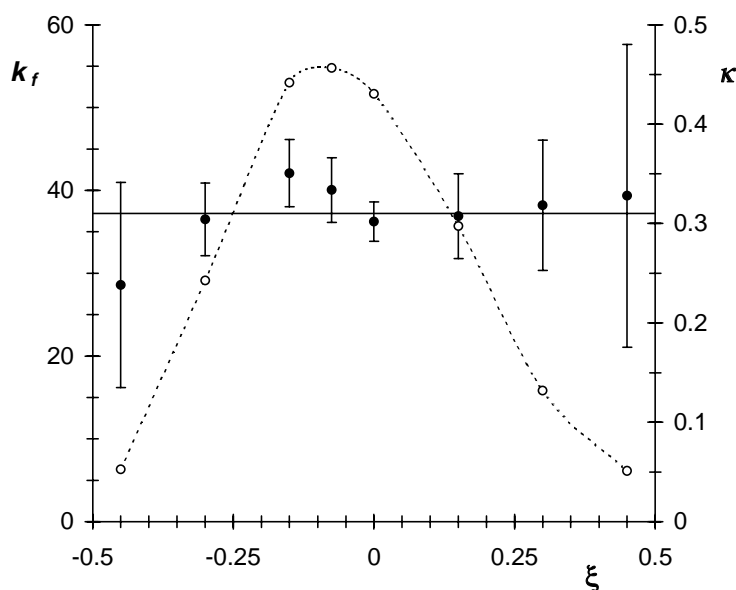
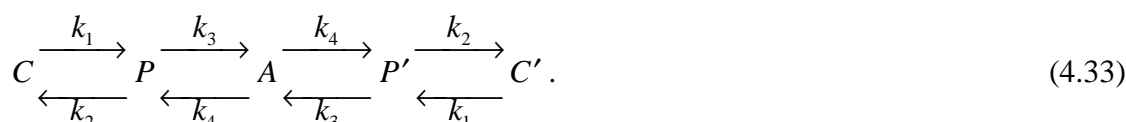


Figure 4.5. Transmission coefficient (open markers) and reactive flux rate (solid markers) as a function of the location of the transition state of a calix[4]arene in chloroform.

The effect of the chloroform solvent on the calix[4]arene is to shift the probability distribution to the cone conformation, leading to an equilibrium constant of $2.4 \cdot 10^{-7}$ and $A_{paco} - A_{cone} = 9.1$ kcal/mol. With $A(0) - A_{cone} = 13.6$ kcal/mol the transition state rate decreases to 84 s^{-1} . The transmission function for this system⁵ was found to be 0.43, so the reactive flux rate equals 36 s^{-1} . The solvent is thus seen to reduce the reaction rate by a factor of six.

In a previous article we calculated the transmission coefficient in chloroform from a set of 2000 relaxation runs. The transition velocities $\dot{\xi}(0)$ were sampled from a Gaussian distribution and according to Eq. (4.6) these velocities were used as weight factor in an average over all runs. In order to reduce the number of relaxation runs we here used the product of the Gaussian and the weight factor as the new probability distribution from which velocities were drawn. Between 500 and 1000 relaxations runs were found to suffice for an accurate calculation of the transmission coefficient. The effects of the transition state on the transmission function and the reactive flux rate are shown in Fig. 4.5. In the range of ξ^\ddagger between +0.45 and -0.45 the transmission function is seen to vary by a factor of ten. The reactive flux rate constant, on the other hand, is fairly constant.

Isomerisation rates of calix[4]arenes with various sidegroups and in various solvents have been measured with $^1\text{H-NMR}$.²¹⁻²⁴ With the calix[4]arene of this paper, however, comparison of the theoretical and experimental transition rates is complicated by the fact that the paco conformation is only very short-lived. Hence, only the cone to inverted cone rate is experimentally accessible. This inversion results from a series of independent reactions with one phenol ring flipping over in each step,¹⁸ as illustrated in Fig. 4.6. Because of symmetry, the flowchart can be reduced to



Here C denotes the cone with all four phenol rings pointing upwards, P denotes the set of four conformations with three phenol rings pointing upwards, A denotes the set of six alternate conformations with two phenol rings pointing upwards, and C' and P' are defined likewise as inverted paco and inverted cone. The five time constants of the relaxation processes of this system are obtained as the eigenvalues of the matrix of the transition probabilities. The relevant eigenvalue is

$$\begin{aligned}
 k &= \frac{1}{2} \left[(k_1 + k_2 + k_3) - \sqrt{(k_1 + k_2 + k_3)^2 - 4k_1k_3} \right] \\
 &\approx k_1 \frac{k_3}{k_2 + k_3},
 \end{aligned} \quad (4.34)$$

where in the second line it is assumed that k_1 is much smaller than the other k -s. The corresponding eigenvector describes the exchange of molecules between C and C' with accompanying changes in P smaller by a factor of $k_1/(k_2 + k_3)$ and no changes in A . In

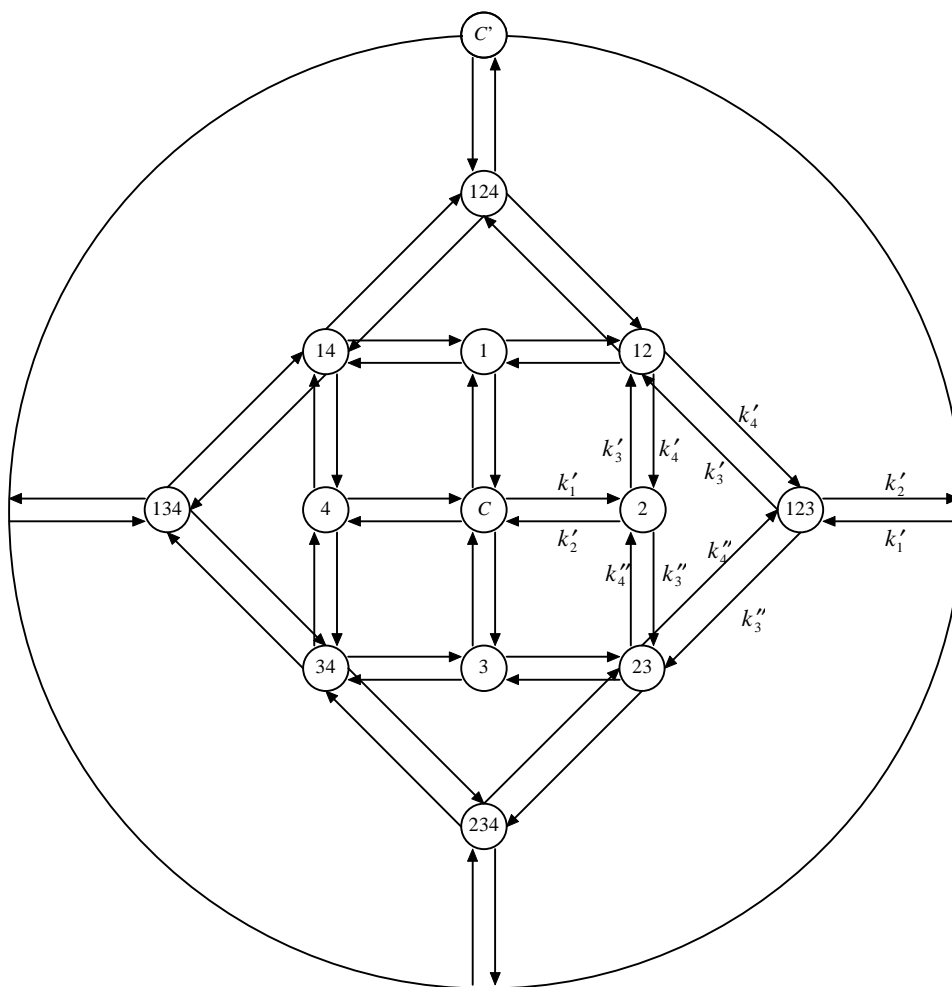


Figure 4.6. Flowchart of the various stable conformations and the possible interconversions of a calix[4]arene. In the cone conformation (C) all phenol rings are pointing upwards, in conformation '1' the ring numbered 1 is pointing downwards, etc. The entire outer circle corresponds to the inverted cone (C'), in which all phenols are pointing downward. The 1,3-alternate conformations are not shown.

Fig. 4.6 the rates of going from one particular conformation, e.g. a paco with phenol ring number 2 rotated, to another particular confirmation are marked by (double) primes. These primed rates can be calculated with the techniques described in this paper, while the unprimed rates are the experimentally accessible rates.²⁴ We now want to find a relation between k and k_1' .

There are four possible routes leading from the cone to the paco, so $k_1 = 4k_1'$. Rather than calculating k_2 and k_3 exactly, we will estimate their values from transition state theory based on normal mode analysis. The rate of the paco to cone transition then is $k_2 = k_2' = 1.1 \cdot 10^8 \text{ s}^{-1}$, $\Delta A^\ddagger = 6.6 \text{ kcal/mol}$. The rate of the paco to alternate transition equals the sum of the two different paco to 1,2-alternate transitions, $k_3 = k_3' + k_3''$, with $k_3' = 2.1 \cdot 10^8 \text{ s}^{-1}$, $\Delta A^\ddagger = 6.2 \text{ kcal/mol}$ and $k_3'' = 1.1 \cdot 10^8 \text{ s}^{-1}$, $\Delta A^\ddagger = 6.6 \text{ kcal/mol}$. With

Table 4.1. Computed and experimental reaction rates.

Method	$k^{\text{TST}} / \text{s}^{-1}$	κ	$k^{\text{RF}} / \text{s}^{-1}$
Vacuum normal modes	174		
Vacuum umbrella sampling, $t = 0.6$ ps	256	0.92	237
Vacuum umbrella sampling, $t = 2.0$ ps	256	0.82	209
Chloroform umbrella sampling	84	0.43	36
$^1\text{H-NMR}$ experiment			7 - 63

$\Delta A^\ddagger = 12.4$ kcal/mol, the path to 1,3-alternate transition is too slow to be of any influence. Substitution of these rates in the second line of Eq. (4.34) yields $k = 2.99k_1'$, so as a rule of thumb the experimentally observed cone to inverted cone rate k equals three times the cone to paco reaction rate k_1' . Of course, this estimate should not be taken for granted, but it gives a reasonable approximation of the effect that is to be expected in exact calculations.

Gutsche and Bauer²¹ measured a ΔA^\ddagger of 14.9 kcal/mol, $k = 189 \text{ s}^{-1}$, at the coalescence temperature of 36 °C. Araki *et al.*²² found a slightly higher coalescence temperature of 44 °C, and rate of 20 s^{-1} , $\Delta A^\ddagger = 15.7$ kcal/mol, at 24 °C. With the rule of thumb they yield a cone to paco rate k_1' of 63 and 7 s^{-1} respectively. These figures compare surprisingly well with the 36 s^{-1} calculated with the reactive flux method. The various rate constants are summarised in Table 4.1.

4.4 Conclusions

The reaction coordinate based on the unstable normal mode at the saddle point of the potential energy surface is shown to be a very convenient reaction coordinate, both in the calculation of the probability distribution along the reaction coordinate and in the calculation of transmission coefficients. The free energy function obtained by a normal mode analysis as a function of ξ proves to be an excellent first guess at the umbrella function. The reaction rates calculated with the reactive flux method for a calix[4]arene *in vacuo* and in chloroform are virtually independent of the chosen transition state. The isomerisation rate of the solvated molecule is in good agreement with experimental data.

4.5 Appendix: Normal mode analysis and $Q(\xi)$.

In this appendix we will calculate the partition function $Q(\xi^*)$, defined by Eq. (4.20), within the harmonic approximation. To this end we first locate the minimum energy configuration \mathbf{R}^* , as indicated in section 4.2.2. We next perform a normal mode analysis in the neighbourhood of \mathbf{R}^* . We approximate the hyperplane $\xi(\mathbf{X}) = \xi^*$ by a tangent plane at \mathbf{R}^* . The unit vector normal to this hyperplane at \mathbf{R}^* follows from the gradient of ξ , Eq. (4.13),

$$\mathbf{N} = \frac{\mathbf{Q}^r - \sum_{k=1}^3 d_k^r \mathbf{S}^k}{1 + \sum_{k=1}^3 (d_k^r)^2}. \quad (4.35)$$

The tangent plane is spanned by a set of $3N - 1$ unit vectors perpendicular to \mathbf{N} ,

$$\mathbf{T}^l = \begin{cases} \mathbf{E}^k & k = 1, 2, 3 \\ \mathbf{Q}^j & j = 1, \dots, 3N - 6; \quad j \neq r, \\ \mathbf{S}^k + d_k^r \mathbf{Q}^r & k = 1, 2, 3 \end{cases} \quad (4.36)$$

where the final three vectors still need to be orthonormalised. The eigenfrequencies of vibration, ω_j^* , in the hyperplane

$$\mathbf{X} = \mathbf{R}^* + \sum_{l=1}^{3N-1} \tau_l \mathbf{T}^l \quad (4.37)$$

are found by diagonalising the $3N - 1$ dimensional Hessian at \mathbf{R}^* ,

$$H_{kl}^* = \frac{\partial^2 \Phi}{\partial \tau_k \partial \tau_l}. \quad (4.38)$$

Each $3N - 1$ dimensional eigenvector is next transformed into a $3N$ dimensional atomic displacements vector by summing over the \mathbf{T}^l using the components of the eigenvector as weight factors. The displacement vectors are again subdivided into three groups, the translational vectors \mathbf{E}^{*l} , identical to the \mathbf{E}^l , and the rotational vectors \mathbf{S}^{*k} , of the form of Eq. (4.8) with \mathbf{r}_i^0 replaced by \mathbf{r}_i^* , all having eigenfrequency zero, and the vibrational vectors \mathbf{Q}^{*j} all having positive eigenfrequencies. Analogously to Eq. (4.12), we now express any configuration as

$$\mathbf{X} = \mathbf{A}^* \mathbf{R} + \sum_{l=1}^3 \gamma_l^* \mathbf{E}^{*l}, \quad \mathbf{R} = \mathbf{R}^* + \sum_{j=1}^{3N-7} \alpha_j^* \mathbf{Q}^{*j} + \beta^* \mathbf{N}, \quad (4.39)$$

where the rotation matrix \mathbf{A}^* is determined by

$$0 = (\mathbf{X} - \mathbf{A}^* \mathbf{R}^*) \cdot \mathbf{A}^* \mathbf{S}^{*k}, \quad k \in \{1, 2, 3\}. \quad (4.40)$$

It is obvious that $\xi(\mathbf{X})$ (with ξ still defined with respect to \mathbf{R}^0) is a function of the α_j^* and β^* only, and does not depend on \mathbf{A}^* . Because of the construction of the \mathbf{Q}^{*j} , we have

$$\xi(\mathbf{X}) = \xi^* + \beta^* \left| \nabla_{\mathbf{R}^*} \xi \right|, \quad (4.41)$$

up to first order in α_j^* and β^* , where it was used that \mathbf{N} is a unit vector parallel to $\nabla_{\mathbf{X}} \xi$.

The integrals of the partition function in Eq. (4.20) are solved analogously to those in Eq. (4.14). The sole exception is the integral over β^* which, because of the delta-function, yields not a frequency factor but $|\nabla_{\mathbf{R}^*} \xi|^{-1}$, with

$$|\nabla_{\mathbf{R}^*} \xi| = \left[\sum_{i=1}^N \left(\frac{\partial \xi}{\sqrt{m_i} \partial \mathbf{x}_i} \right)^2 \right]^{1/2} = \left[1 + \sum_{k=1}^3 (d_k^r)^2 \right]^{1/2}. \quad (4.42)$$

We then arrive at

$$Q(\xi^*) = \left(\frac{2\pi M k_B T}{h^2} \right)^{3/2} V \cdot \frac{\pi^{1/2}}{\sigma} \left(\frac{8\pi^2 k_B T}{h^2} \right)^{3/2} (I_A^* I_B^* I_C^*)^{1/2} \\ \times \prod_{i=1}^{3N-7} \frac{k_B T}{\hbar \omega_i^*} \cdot \omega_e \exp[-E^*/k_B T] \cdot |\nabla_{\mathbf{R}^*} \xi|^{-1} \cdot (2\pi k_B T)^{1/2} h^{-1}. \quad (4.43)$$

We end this appendix with the derivation of an alternative expression for the above integral. Rather than introducing a new set of coordinates based on \mathbf{R}^* , we keep on using the coordinates defined with respect to \mathbf{R}^0 . The delta-function in the partition function is then trivially dealt with. The Jacobi matrix of the transformation from mass-weighted coordinates to generalised coordinates is again given by Eq. (4.18). However, for small vibrations around \mathbf{R}^* the approximation of \mathbf{R} by \mathbf{R}^* leads to three vectors $\boldsymbol{\varepsilon}^k \mathbf{R}^*$ that are no longer orthogonal to the \mathbf{Q}^j . Expressing these vectors in the \mathbf{R}^0 -based vectors yields

$$\mathbf{J} = \mathbf{A} \begin{pmatrix} \boldsymbol{\varepsilon}^k \mathbf{R}^0 & \mathbf{Q}^j & \mathbf{A}^{-1} \mathbf{E}^l \end{pmatrix} \begin{pmatrix} (\mathbf{I}^0)^{-1} \boldsymbol{\sigma}^* & \mathbf{0} & \mathbf{0} \\ \boldsymbol{\rho}^* & \mathbf{1} & \mathbf{0} \\ \mathbf{0} & \mathbf{0} & \mathbf{1} \end{pmatrix} \begin{pmatrix} \mathbf{c} & \mathbf{0} & \mathbf{0} \\ \mathbf{0} & \mathbf{1} & \mathbf{0} \\ \mathbf{0} & \mathbf{0} & \mathbf{1} \end{pmatrix}, \quad (4.44)$$

$$|\mathbf{J}| = |\boldsymbol{\sigma}^*| (I_A^0 I_B^0 I_C^0)^{-1/2} \sin \psi_2, \quad (4.45)$$

where

$$\boldsymbol{\sigma}_{lk}^* = (\boldsymbol{\varepsilon}^l \mathbf{R}^*) \cdot (\boldsymbol{\varepsilon}^k \mathbf{R}^0), \quad \boldsymbol{\rho}_{ij}^* = (\boldsymbol{\varepsilon}^i \mathbf{R}^*) \cdot \mathbf{Q}^j, \quad (4.46)$$

and the $(\mathbf{I}^0)^{-1}$ arises because the $\boldsymbol{\varepsilon}^k \mathbf{R}^0$ are not orthogonal. Performing the integration over the generalised coordinates and multiplying with the integral over the momenta gives

$$Q(\xi^*) = \left(\frac{2\pi M k_B T}{h^2} \right)^{3/2} V \cdot \frac{\pi^{1/2}}{\sigma} \left(\frac{8\pi^2 k_B T}{h^2} \right)^{3/2} (I_A^0 I_B^0 I_C^0)^{-1/2} \\ \times \prod_{i=1}^{3N-7} \frac{k_B T}{\hbar \omega_i^{**}} \cdot \omega_e \exp[-E^*/k_B T] \cdot |\boldsymbol{\sigma}^*| (2\pi k_B T)^{1/2} h^{-1}. \quad (4.47)$$

The required eigenfrequencies are found as the square roots of the eigenvalues of the $3N - 7$ dimensional Hessian at \mathbf{R}^* ,

$$H_{jk}^{**} = \frac{\partial^2 \Phi}{\partial \alpha_j \partial \alpha_k}, \quad j, k \neq r, \quad (4.48)$$

and differ from the eigenfrequencies used in Eq. (4.22).

4.6 References

- ¹ H. Eyring, *J. Chem. Phys.* **3**, 107 (1935).
- ² P. Hänggi, P. Talkner and M. Borkovec, *Rev. Mod. Phys.* **62**, 251 (1990).
- ³ T. Yamamoto, *J. Chem. Phys.* **33**, 281 (1960).
- ⁴ D. Chandler, *J. Chem. Phys.* **68**, 2959 (1978).
- ⁵ W. K. den Otter and W. J. Briels, *J. Chem. Phys.* **106**, 5494 (1997) (Chapter 3).
- ⁶ W. H. Miller, *Acc. Chem. Res.* **9**, 306 (1976).
- ⁷ D. A. McQuarrie, *Statistical Mechanics* (Harper and Row, New York, NY, 1976).
- ⁸ H. Goldstein, *Classical Mechanics* (Addison–Wesley, Reading, MA, 1980).
- ⁹ J. Ryckaert, G. Ciccotti and H. J. C. Berendsen, *J. Comput. Phys.* **23**, 327 (1977).
- ¹⁰ D. L. Beveridge and F. M. DiCapua, *Annu. Rev. Biophys. Biophys. Chem.* **18**, 431 (1989).
- ¹¹ W. F. van Gunsteren, T. C. Beutler, F. Fraternali, P. M. King, A. E. Mark and P. E. Smith in *Computer Simulations of Biomolecular Systems: Theoretical and Practical Applications*, edited by W. F. van Gunsteren, P. K. Weiner and A. J. Wilkinson (ESCOM, Leiden, The Netherlands, 1993), pp. 315.
- ¹² T. P. Straatsma, *Rev. Comp. Chem.* **9**, 81 (1996).
- ¹³ J.–M. Depaepe, J.–P. Ryckaert, E. Paci and G. Ciccotti, *Mol. Phys.* **79**, 515 (1993).
- ¹⁴ R. W. W. Hooft, B. P. van Eijck and J. Kroon, *J. Chem. Phys.* **97**, 6690 (1992).
- ¹⁵ S. Kumar, D. Bouzida, R. H. Swendsen, P. A. Kollman and J. M. Rosenberg, *J. Comp. Chem.* **13**, 1011 (1992).
- ¹⁶ C. D. Gutsche, J. S. Rogers, D. Stewart and K.–A. See, *Pure & Appl. Chem.* **62**, 485 (1990).
- ¹⁷ H. J. C. Berendsen and W. F. van Gunsteren, *GROMOS Reference Manual* (University of Groningen, Groningen, The Netherlands, 1987).
- ¹⁸ S. Fischer, P. D. J. Grootenhuys, L. C. Groenen, W. P. van Hoorn, F. C. J. M. van Veggel, D. N. Reinhoudt and M. Karplus, *J. Am. Chem. Soc.* **117**, 1611 (1995).
- ¹⁹ S. Fischer and M. Karplus, *Chem. Phys. Lett.* **194**, 252 (1992).
- ²⁰ S. Glasstone, K. J. Laidler and H. Eyring, *The Theory of Rate Processes* (MacGraw–Hill, New York, NY, 1941).
- ²¹ C. D. Gutsche and L. J. Bauer, *J. Am. Chem. Soc.* **107**, 6052 (1985).
- ²² K. Araki, S. Shinkai and T. Matsuda, *Chem. Lett.* **1989**, 581 (1989).
- ²³ W. P. van Hoorn, W. J. Briels, J. P. M. van Duynhoven, F. C. J. M. van Veggel and D. N. Reinhoudt, to be published.
- ²⁴ J. Blixt and C. Detellier, *J. Am. Chem. Soc.* **116**, 11957 (1994).

Chapter 5

Solvent effect on the isomerisation rate of calix[4]arene studied by molecular dynamics simulations^{*}

Abstract

The isomerisation rates of a calix[4]arene in benzene and in chloroform have been calculated using molecular dynamics simulations. The reaction coordinate that is employed is based on the unstable normal mode at the saddle point of the potential energy surface. The free energy as a function of this coordinate has been calculated by means of umbrella sampling. Comparison of the free energies in the solvents with those in vacuum reveals that both solvents destabilise the paco conformation and stabilise the transition state region. In chloroform the calix[4]arene shows a stronger preference for the cone conformation than in benzene or in vacuum. The isomerisation rate has been determined by the reactive flux method. Both solvents yield comparable transmission coefficients. The calculated rates are in perfect agreement with experimental data.

5.1 Introduction

Calix[4]arenes, cyclic arrays of four phenol rings, are versatile molecules:¹ they are used as building blocks in supramolecular chemistry, they can selectively bind ions, they show non-linear optical behaviour and they can take on various conformations. The latter property will be studied in this paper. In the cone conformation all phenol rings are orientated in the same direction, see Fig. 5.1. The molecule is then stabilised by four internal hydrogen bonds at the lower rim of the molecule. In the partial cone conformation, ‘paco’ for short, one of the phenol rings is rotated with respect to the other three phenol rings. During the isomerisation from cone to paco the methyl groups between the phenol rings act as the hinges around which the phenol ring rotates, and the hydroxyl moiety moves through the

^{*} W. K. den Otter and W. J. Briels, submitted to J. Am. Chem. Soc.

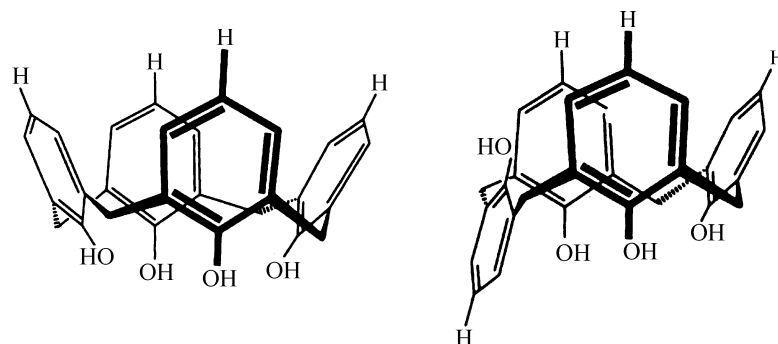


Figure 5.1. Cone (left) and paco (right) conformations of a calix[4]arene.

central annulus. The paco conformation has only two internal hydrogen bonds, making it energetically less stable than the cone conformation by about 10 kcal/mol. The energy barrier between the two conformations is about 15 kcal/mol, so the isomerisation rate at 300 K is of the order of 100 s^{-1} . This energy barrier makes it impossible to calculate the isomerisation rate by simply monitoring the conformation of the molecule during a long molecular dynamics simulations (MD). Currently simulations up to a dozen nanoseconds are feasible, but the isomerisation reaction requires simulations of the order of a second long. In this article we apply statistical mechanical theories which make it possible to calculate very slow reaction rates by simulations of only a few nanoseconds.

In section 5.2 the statistical mechanical ideas underlying reaction rate calculations are introduced. An important quantity in this theory is the reaction coordinate. We have recently introduced a convenient definition of this coordinate, based on the unstable normal mode at the saddle point of the potential energy surface. This definition is computationally efficient, and can be applied to a wide variety of reactions. Simulations of a calix[4]arene *in vacuo* and in two solvents are discussed in section 5.3, and compared with experiments.

5.2 Theory

5.2.1 Reaction rate

The forward reaction rate is defined as the fraction of reactants that turns into products per unit of time. We shall assume that the rate is predominantly determined by the (free) energy barrier separating reactants from products. In order to calculate the reaction rate, we first of all need a method of telling reactants and products apart. We therefore introduce the reaction coordinate, ξ , which is taken to be a function of the coordinates of the reacting molecule only. The reaction coordinate is defined in such a way that it is larger than ξ^\ddagger for products and smaller than ξ^\ddagger for reactants. Conformations with $\xi = \xi^\ddagger$ are at the dividing plane between reactants and products, the so-called transition state, which is located in the sparsely

populated area at the top of the energy barrier. The definition of the reaction coordinate employed in this article is deferred till the next section.

In Eyring's transition state theory (TST) the rate is expressed as the instantaneous product bound flux through the transition state, normalised by the number of reactant molecules:²

$$k_f^{TST} = \frac{1}{2} \left\langle \left| \dot{\xi} \right| \right\rangle_{\xi^\ddagger} \frac{P(\xi^\ddagger)}{\int_{-\infty}^{\xi^\ddagger} P(\xi) d\xi}, \quad (5.1)$$

where $\dot{\xi} = d\xi/dt$. The first factor on the right hand side is half the average absolute velocity of molecules at the transition state, which, because of symmetry, equals the average velocity of molecules crossing the transition state with a positive velocity. Once the definition of the reaction coordinate is chosen, this factor is readily evaluated. In the second factor we have used the probability distribution of the reaction coordinate in the canonical ensemble,

$$P(\xi) = \frac{1}{Q} h^{-3N} \iint \delta[\xi(\mathbf{X}) - \xi] \exp[-\beta H(\mathbf{X}, \mathbf{p}_x)] d\mathbf{X} d\mathbf{p}_x, \quad (5.2)$$

where H is the Hamiltonian, \mathbf{X} is the collection of all $3N$ coordinates of the reacting molecule and the solvent, \mathbf{p}_x are the conjugate momenta, δ is the Dirac delta function, h is Planck's constant and $\beta = 1/k_B T$ with T the absolute temperature and k_B Boltzmann's constant. The partition function Q arises as the normalisation factor of the distribution. The second factor in Eq. (5.1) is therefore to be interpreted as the probability for a molecule in the reactant state to reach the transition state. Two methods for calculating the probability distribution are discussed in section 5.2.3.

It is a well known fact that transition state theory overestimates the true reaction rate.³ The underlying reason simply is the implicit assumption of TST that each molecule crossing the transition state with a positive velocity will end up in the product well. However, there is a chance that a molecule crossing the transition state with a positive velocity rapidly recrosses the transition state before settling in the product well. Likewise, a molecule crossing the transition state with a negative velocity can recross the transition state with a positive velocity to return to the product state. Both these cases contribute to the TST rate, but neither of them corresponds to a reaction, as the molecule returns to its initial state. In textbooks this fact is compensated for ad hoc by multiplying the TST rate with a transmission coefficient, κ , whose value lies between zero and one:³

$$k_f = \kappa k_f^{TST}. \quad (5.3)$$

It is less well known that the transmission coefficient can be calculated exactly, under the condition that classical mechanics adequately describes the motion of the molecule. From Onsager's regression hypothesis it follows that^{2,4}

$$\kappa = \lim_{t \rightarrow \infty} \kappa(t), \quad (5.4)$$

$$\kappa(t) = \frac{\langle \delta[\xi(0) - \xi^\ddagger] \dot{\xi}(0) \theta[\xi(t) - \xi^\ddagger] \rangle}{\langle \delta[\xi(0) - \xi^\ddagger] \dot{\xi}(0) \theta[\dot{\xi}(0)] \rangle}, \quad (5.5)$$

where θ is the Heaviside step function, t and 0 denote the time, and the pointed brackets indicate a canonical average. The denominator of Eq. (5.5) is the average velocity of molecules crossing the transition state at time 0 in the positive direction, i.e. the first factor on the right hand side of Eq. (5.1). The numerator is the average velocity of molecules crossing the transition at time 0 of those molecules that are in the product state some time t after crossing the transition state, regardless of the initial crossing direction. One readily sees that in the limit of t going to zero the numerator equals the denominator. At longer times the contributions of recrossing trajectories will start to diminish the transmission coefficient (it may temporarily increase, though, depending on the characteristics of the reaction). After some time, which is longer than the typical time of the molecular motions but much shorter than the time constant of the reaction, the transmission coefficient will stabilise at a plateau level. At this point all molecules which crossed the transition state at time 0 have reached either the product well or the reactant well, and will stay there for a long while until they incidentally escape. The numerator of Eq. (5.5) then contains contributions only from those molecules that originated in the reactant well and have settled in the product well, hence the name reactive flux method (RF). By inserting the plateau value of the transmission coefficient into Eq. (5.3) we find the exact rate. Note that the transmission coefficient is easily calculated by MD simulations: first one samples configurations in the dividing plane, and next one calculates relaxation runs to see where each of these configurations ends up about a picosecond later.

From Eq. (5.1) it follows that the TST rate constant depends on the precise definition of the dividing plane between reactants and products. Obviously, the dividing plane must lie near the top of the energy barrier to cohere with the intuitive notion of reactants and products. But, there is no clear reason why one plane in this region should be preferred over another, or to put it differently, why one TST rate is better than another. The only thing one knows for sure is that even the lowest TST rate will still overestimate the true rate. It has been shown that the reactive flux method does not suffer from these problems: provided the dividing plane lies near the top of the barrier, the reactive flux method will always yield the same rate constant.^{4,5} The only problem is that the number of relaxation runs required to accurately calculate the transmission coefficient increases exponentially as the plateau value of the transmission coefficient decreases. We therefore now set forth to find a reaction coordinate which yields a high plateau value, i.e. a low TST rate.

5.2.2 Reaction coordinate

In the previous section we have pointed at the significance of the dividing plane to the reaction rate. A particularly important point in the dividing plane is the saddle point, the lowest point on the top of the energy barrier: any molecule going from the reactant state to

the product state must at least rise to the energy of the saddle point to overcome the reaction barrier. According to the Boltzmann distribution, molecules crossing the barrier will do so preferably with the least amount of energy, so the majority of the molecules will surmount the barrier in the vicinity of the saddle point. It is only natural, therefore, to introduce a reaction coordinate based on the properties of the saddle point, as will be done next.

Suppose we have located the first order saddle point, \mathbf{R}^0 , of the potential energy surface of an N atom molecule. For notational convenience and to make the results more transparent, we have collected all $3N$ coordinates into a single mass-weighted column vector, $\mathbf{R}^0 = (m_1^{1/2}(\mathbf{r}_1^0)^t, \dots, m_N^{1/2}(\mathbf{r}_N^0)^t)^t$, where \mathbf{r}_i^0 is the column vector of the coordinates of atom i with mass m_i . We shall assume that there is no external potential acting on the molecule. At the saddle point the gradient of the potential energy is zero, so a Taylor expansion up to second order of the potential energy yields an energy of

$$\Phi(\mathbf{X}) = \Phi(\mathbf{R}^0) + \frac{1}{2}(\mathbf{X} - \mathbf{R}^0)^T \mathbf{H}(\mathbf{X} - \mathbf{R}^0) \quad (5.6)$$

at a point \mathbf{X} close to the saddle point. The Hessian matrix, \mathbf{H} , contains all second derivatives of the potential energy with respect to the mass-weighted Cartesian coordinates. This matrix is then diagonalised to find its eigenvectors and eigenvalues, just as one normally does for a molecule at the potential energy minimum.

The eigenvectors of the Hessian can be subdivided into two groups. The first group contains the three eigenvectors which correspond to a rigid body translation and the three eigenvectors which correspond to a rigid body rotation. In the absence of an external field, one easily sees that the potential energy of the molecule does not change during these moves, hence the eigenvalues of these six eigenvectors are all equal to zero. The second group contains the $3N - 6$ eigenvectors with a non-zero eigenvalue, the normal modes of vibration.³ These vibrations are, in first order approximation, independent of one another; the eigenvalues are the squares of the frequencies of vibration, which are experimentally accessible. If the Hessian were to be evaluated at a local minimum of the potential energy surface, then all eigenvalues would be positive: move along any normal mode and the potential energy will rise. At a first order saddle point, however, there is exactly one eigenvector with a negative eigenvalue, i.e. an imaginary eigenfrequency. Move along this direction, henceforth called the unstable direction \mathbf{Q}^r , and the potential energy will fall. In other words, in this direction the molecule is going from the saddle point towards the product (or reactant) well. As an illustration of this unstable normal mode, the resulting atomic displacements of a calix[4]arene at the cone to paco saddle point are depicted in Fig. 5.2.

We now define the reaction coordinate as the displacement of the molecule, with respect to the saddle point, along the unstable direction. For a molecule with coordinates \mathbf{X} we thus arrive at the projection

$$\xi = \frac{(\mathbf{X} - \mathbf{R}^0) \cdot \mathbf{Q}^r}{\mathbf{Q}^r \cdot \mathbf{Q}^r}. \quad (5.7)$$

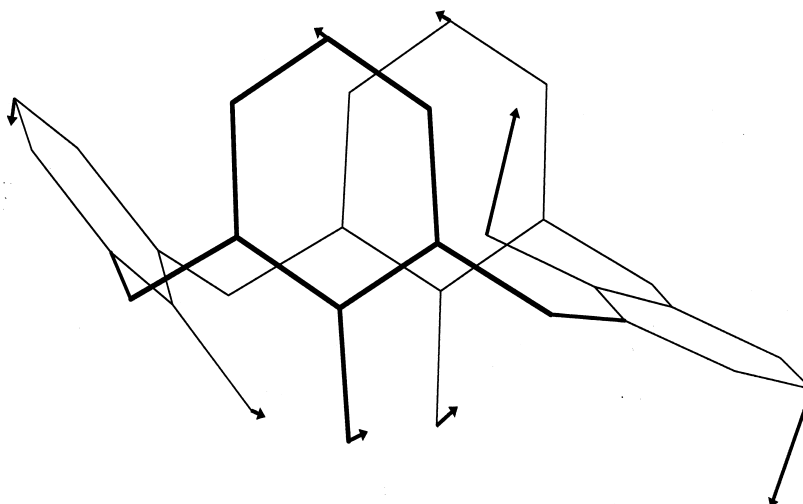


Figure 5.2. Saddle point configuration of a calix[4]arene. The arrows attached to the atoms indicate the displacements of the atoms under the unstable normal mode \mathbf{Q}^r .

The particularly simple form of this equation arises because the eigenvectors of the Hessian are orthogonal.

At this point the reader might argue that the above definition of the reaction coordinate is intuitively appealing, but that under practical conditions the definition is useless since it is not invariant under rotations. To solve this problem we exploit the freedom in choosing the saddle point configuration: the rotated saddle point, $\mathbf{AR}^u = (m_1^{1/2}(\mathbf{ar}_1^u)^t, \dots, m_N^{1/2}(\mathbf{ar}_N^u)^t)^t$ where \mathbf{a} is an ordinary three dimensional rotation matrix, is also a saddle point. One readily verifies that the eigenvectors of the Hessian are rotated in the same manner, so the unstable normal mode of the rotated saddle point is \mathbf{AQ}^r . By inserting these two rotated vectors into Eq. (5.7), the reaction coordinate becomes a function of the coordinates \mathbf{X} and the rotation matrix \mathbf{a} ,

$$\xi = \frac{(\mathbf{X} - \mathbf{AR}^0) \cdot \mathbf{AQ}^r}{\mathbf{Q}^r \cdot \mathbf{Q}^r}. \quad (5.8)$$

We now must find a connection between \mathbf{X} , \mathbf{R}^0 and \mathbf{a} to make the definition of the rotation matrix, and hence the definition of the reaction coordinate, unequivocal. Analogous to Eq. (5.8), we may calculate the ‘rotation’ of the molecule with respect to \mathbf{AR}^0 as the projection of the displacement $\mathbf{X} - \mathbf{AR}^0$ onto the three rotated rotational eigenvectors of the Hessian. The correct rotation matrix \mathbf{a} is then defined as the one which makes all three projections simultaneously equal to zero. A more elaborate discussion of this topic, as well as an algorithm to calculate the rotation matrix, are given elsewhere.⁶

5.2.3 Free energy

It is common practice to convert probability distributions and partition functions, as defined by Eq. (5.2), into free energies,

$$A(\xi) = -k_B T \ln P(\xi) + c, \quad (5.9)$$

where c is an irrelevant constant arising from the partition function Q . The RF rate then reads⁷

$$k_f = \kappa \sqrt{\frac{k_B T}{2\pi}} \langle |\nabla_{\mathbf{x}} \xi| \rangle_{\xi^\ddagger} \exp\left[-\frac{A(\xi^\ddagger) - A_R}{k_B T}\right], \quad (5.10)$$

where we have combined Eqs. (5.1) through (5.3). Here A_R is the free energy of the reactant well, obtained by replacing $P(\xi)$ in Eq. (5.9) by the denominator of Eq. (5.1). With the reaction coordinate as defined in section 5.2.2 we find $|\nabla_{\mathbf{x}} \xi| = 1 \text{ kg}^{-1/2} \text{ m}^{-1}$ at the saddle point, and this value increases only slightly on taking the average over the saddle plane. In the experimental literature a slightly different definition of the free energy is commonly used by writing a measured reaction rate as

$$k_f = \frac{k_B T}{h} \exp\left[-\frac{\Delta A^\ddagger}{k_B T}\right]. \quad (5.11)$$

By comparing these two expressions we find

$$\Delta A^\ddagger = A(\xi^\ddagger) - k_B T \ln \left[\sqrt{\frac{h^2}{2\pi k_B T}} \langle |\nabla_{\mathbf{x}} \xi| \rangle_{\xi^\ddagger} \right] - A_R - k_B T \ln \kappa. \quad (5.12)$$

The second term on the right hand side removes from $A(\xi^\ddagger)$ the contribution of the velocity $\dot{\xi}$, so the free energy difference ΔA^\ddagger is based on the probability of finding a molecule at the transition state with zero crossing velocity, while the free energy $A(\xi^\ddagger)$ is based on the probability for the molecule to be at the transition state regardless of the crossing velocity. Notice that ΔA^\ddagger also includes a contribution from the transmission coefficient, while $A(\xi^\ddagger)$ does not.

Perhaps the best known method of calculating the free energy of a molecule *in vacuo*, i.e. A_R , is to perform a normal mode analysis.³ Combining contributions from the $3N - 6$ eigenfrequencies of vibration, the inertia tensor and the total mass of the molecule gives the desired result. The assumptions underlying this theory are that the amplitudes of the vibrations are small, and that there is no coupling between rotations and vibrations. As we have shown elsewhere,⁷ it is straightforward to calculate the free energy as a function of the reaction coordinate under the same conditions. The basic task is to calculate the $3N - 7$ eigenfrequencies of vibrations in the hyperplane of configurations with a prescribed value of the reaction coordinate, and to calculate the moments of inertia of the corresponding deformed molecule. The method is reliable and fast for calculations *in vacuo*, but it is of

little practice for a molecule in a solvent, since the inclusion of solvent effects in the theory is virtually impossible.

If we were to directly sample the probability distribution of the reaction coordinate of the solvated molecule in one single long simulation, then the height of the energy barrier between reactants and products would obviously create insurmountable difficulties. The barrier region would be sampled very poorly, and the molecule might even stay in one conformation for the entire run. In fact, this is precisely the problem that we try to avoid by using reaction rate theory. Suppose now that we add to the existing potential energy surface a so-called umbrella potential,⁸ $U(\mathbf{X})$. The probability distribution of the system with the umbrella reads as

$$P_U(\xi) = \frac{1}{Q_U} h^{-3N} \iint \delta[\xi(\mathbf{X}) - \xi] \exp[-\beta\{H(\mathbf{X}, \mathbf{p}_x) + U(\mathbf{X})\}] d\mathbf{X} d\mathbf{p}_x. \quad (5.13)$$

In case the umbrella is a function of the reaction coordinate only, $P(\xi)$ may be calculated according to

$$P(\xi) = c P_U(\xi) \exp[\beta U(\mathbf{X})], \quad (5.14)$$

where c is a proportionality constant. The probability distribution of ξ in the biased run is thus seen to be easily converted into the probability distribution of the unbiased run. This remains true regardless of the kind of umbrella potential used, so we are free to choose the umbrella that suits us the best. The best choice is $U(\xi) = -A(\xi)$, since it renders P_U independent of ξ . In the biased run the barrier between reactants and products then effectively vanishes, and both configurations can be sampled efficiently with a single long simulation. In such a simulation the reaction coordinate behaves like a diffusing particle. An obvious problem is that we do not know $A(\xi)$ in advance, but by making a good initial guess, like according to the above discussed normal mode method, we can get close enough for the method to work properly. Alternatively, we may choose the umbrella in such a way that only a small range of ξ , a so-called window, is sampled. Combining the probability distributions from overlapping windows by making them match in the overlap region then yields the desired result. Since diffusion over long distances is a slow process, it may be advantageous to combine both methods: use a good guess of the free energy as umbrella and partitionate the range into windows that are rapidly sampled.

5.3 Results

The calix[4]arene was modelled with the all-atom CHARMM parameter set 22.⁹ The saddle points on the potential energy surface of a calix[4]arene *in vacuo* were calculated using the conjugate peak refinement algorithm^{9,10} implemented in QUANTA/CHARMM.¹¹ All other calculations were done with GROMOS87,¹² which we adapted to meet our specific needs. The saddle points were transported to GROMOS87, and further refined using Newton-Raphson to

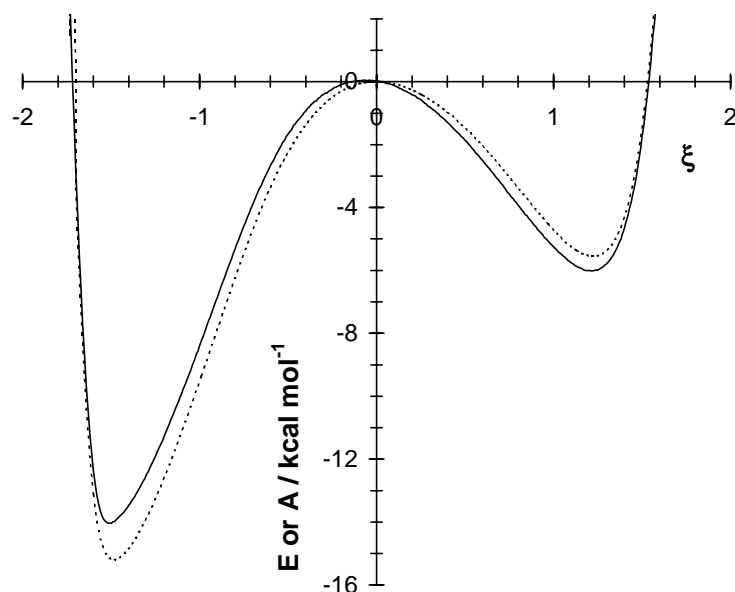


Figure 5.3. Minimum energy (dotted) and free energy as calculated by means of umbrella sampling (solid) as a function of the reaction coordinate for a calix[4]arene in vacuo.

minimise the gradient of the potential. The normal modes were calculated, and the positive value of the reaction coordinate were chosen to correspond to the paco conformation.

5.3.1 Free energy

The minimum energy conformations as a function of the reaction coordinate for the molecule *in vacuo* were calculated using Newton-Raphson in which the reaction coordinate was kept at a prescribed value. For each conformation a normal mode analysis was performed to calculate the free energy as a function of the reaction coordinate at 300 K. Both functions are plotted in Fig. 5.3. The free energy difference between the paco well and the cone well is 7.9 kcal/mol. From the free energy difference between the saddle plane and the cone well, $A(0) - A_{\text{cone}} = 13.1$ kcal/mol, follows the reaction rate $k_f^{TST} = 174$ s⁻¹.

The free energy function obtained by the normal mode analysis was used as the umbrella potential in a vacuum simulation. For this purpose the free energy function was fitted with two fifteenth order polynomials, one for the cone well and the saddle point region, and one for the paco well and the saddle point region. In the saddle point region a third order polynomial was used to make a smooth transition from one fit to the other. High order polynomials were used because they made possible a smooth fit; previously we had noticed that small deviations in the fit were very much reflected in the probability distribution P_U . The motion of the reaction coordinate was limited to the region between roughly -1.8 and +1.6 to prevent the molecule from sampling highly improbable conformations, and to reduce the chances of 'spontaneous' conformational transitions due to the high stress in the molecule at these extremes. This was done by adding two Fermi-Dirac-like functions to the umbrella, chosen such that they were virtually zero in the region of interest and rapidly

increased at the borders. During the simulation the lengths of the bonds involving a hydrogen atom were constrained. Langevin dynamics with a friction constant of 1 ps^{-1} was used to maintain a temperature of 300 K, to promote the energy exchange between vibrational modes, and to make the molecule rotate with a variable angular momentum. The simulation lasted 30 ns, with a time step of 2 fs. The probability distribution of the biased run was very flat, see Fig. 5.4, indicating that the umbrella function is an excellent approximation of the real free energy. Inserting the distribution in Eq. (5.14), we find $A(0) - A_{\text{cone}} = 12.9 \text{ kcal/mol}$, and $k_f^{\text{TST}} = 241 \text{ s}^{-1}$.

During the simulation we encountered the problem that molecules in the $\xi \approx 0.5$ region occasionally made transitions from a paco conformation to a 1,2-alternate conformation. In this conformation two neighbouring phenol rings are pointing upwards and the other two are pointing downwards. Once the molecule had reached the 1,2-alternate conformation it never returned to the paco conformation. There are two ways for a paco conformation to transform into a 1,2-alternate, depending on whether the rotating phenol ring neighbours the rotated phenol ring of the original paco on the left or on the right.⁷ Both 1,2-alternates have the same energy, but the transition states between each of them and the paco have slightly different energies because of the orientation of the hydrogen bonds. The reason for the occurrence of the unwanted side-reactions was that our umbrella not only had lowered the cone to paco transition state, but also the two paco to 1,2-alternate transition states. To prevent these rare side reactions we expanded the umbrella by adding two Fermi-Dirac-like potentials, each depending on the reaction coordinate corresponding to one of the two saddle points of the paco to 12-alternate barrier. Equations (5.13) and (5.14) were adapted accordingly.

In order to calculate the isomerisation rate of a calix[4]arene dissolved in benzene, we first simulated a box of pure benzene. The force field parameters of the benzene molecules

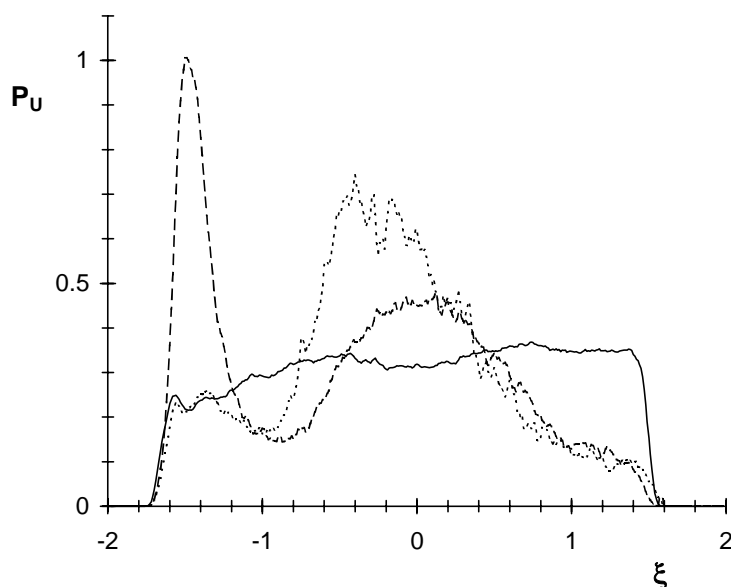


Figure 5.4. Probability distributions P_u in vacuo (solid), chloroform (dashed) and benzene (dotted), all corresponding to the same umbrella. The areas under the curves are equal.

were identical to those of the benzene in the calix[4]arene. The non-bonded parameters of this model have been used previously in Monte Carlo¹³ and MD¹⁴ simulations of liquid benzene. The cubic simulation box contained 343 molecules, a thermostat¹⁵ kept the temperature at 300 K with a time constant of 0.1 ps. Non-bonded interactions were included up to 16 Å, with the interactions beyond 13 Å being updated every tenth step; no long-range corrections were applied. Only the C-H bond lengths were constrained. The box was first equilibrated at a constant volume corresponding to the experimental density.¹⁶ Then a manostat¹⁵ was turned on to keep the pressure at 1 atmosphere, using a typical time constant $\tau_p = 0.5$ ps and the experimental value of the isothermal compressibility,¹⁶ $\beta = 9.7 \cdot 10^{-10}$ Pa⁻¹. Immediately the volume of the box decreased by about 15%. At this new value the volume oscillated with a period of 10 ps. By increasing τ_p to 5.0 ps, in which case our β to τ_p ratio equalled the one used by Müller-Plathe,¹⁴ the box regained its proper density. We conjecture that the manostat failed because of the shape and corresponding potential of the benzene molecule.

After equilibrating the benzene box at 1 atmosphere, the calix[4]arene and the solvent were combined into a single box, a truncated octahedron of about 52 nm³ containing 343 benzene molecules. This box was thoroughly equilibrated, at constant volume first and at constant pressure next, before the actual production run began. The normal mode based umbrella, that performed so well *in vacuo*, was used as the umbrella of the solvated molecule. The resulting probability distribution, sampled in 0.75 ns of simulation time, is shown in Fig. 5.4. Comparison of this distribution with the one from the simulation in vacuum beautifully reveals the solvent effect: the probability at $\xi \approx -0.4$ increases drastically, while the *paco* conformation is depleted. In order to get better statistics, two additional simulations were run in which the reaction coordinate was limited to sample the two wells only. The three distributions were combined and transformed into a free energy by means of Eq. (5.9). As a check, this potential was added to the existing umbrella, which was then used to sample the final distribution, which indeed was satisfactorily flat. The free energy difference between the *paco* and the cone was calculated to be 8.4 kcal/mol, the difference between the saddle plane and the cone is 12.5 kcal/mol, from which finally followed $k_f^{TST} = 471$ s⁻¹.

As a comparison, in Fig. 5.4 we have also plotted the probability distribution of a calix[4]arene in chloroform. This distribution was calculated previously using the same techniques described here, but with a different umbrella.⁷ We converted this distribution into the distribution that we would have obtained in chloroform with the current vacuum umbrella. From the plot it follows that both solvents destabilise the *paco* conformation. The region around the saddle point is stabilised by both solvents, but appreciably more so by benzene than by chloroform. The main difference between the two solvents occurs in the cone region, which is strongly promoted in chloroform but hardly in benzene. The resulting free energy difference between the saddle plane and the cone well in chloroform therefore is larger than in benzene; correspondingly $k_f^{TST} = 84$ s⁻¹ is smaller than in benzene.

5.3.2 Transmission coefficient

In order to calculate the transmission coefficient, Eq. (5.5), conformations needed to be sampled in the transition plane. One thousand conformations were created by means of an MD simulation of a solvated calix[4]arene during which the value of the reaction coordinate was constrained to zero; atomic coordinates and velocities were saved every picosecond. Each of these configurations was used as the starting point of a 2 ps relaxation run. At the start of every relaxation run the velocity of the reaction coordinate, which was zero during the constrained run, was replaced by a new velocity drawn from a velocity-weighted Maxwell-Boltzmann distribution.⁶ The transmission coefficient as a function of time is shown in Fig. 5.5. The dotted line shows the contribution to the transmission coefficient from those molecules which cross the transition state at time zero with a positive velocity and finally settle in the product well, or to put differently, the fraction of the product bound flux through the transition state that ends up in the product well. Likewise, the dashed line gives the contribution to the transmission coefficient from those molecules which cross the transition state at time zero with a negative velocity and end up in the product state; these molecules must therefore have crossed the transition state at least once. Both curves live up to their expectation: they start at respectively one and zero, at short times they decrease because of molecules recrossing the transition state, and at longer times they settle at a stable level. The solid line, the transmission function, is obtained by summing these two contributions. After 2 ps a plateau of 0.56 is reached. In combination with the previously calculated k_f^{IST} , the true reaction rate is then found to be $k_f^{RF} = 264 \text{ s}^{-1}$.

Similar simulations of calix[4]arene in chloroform yielded $\kappa = 0.43$, which together with

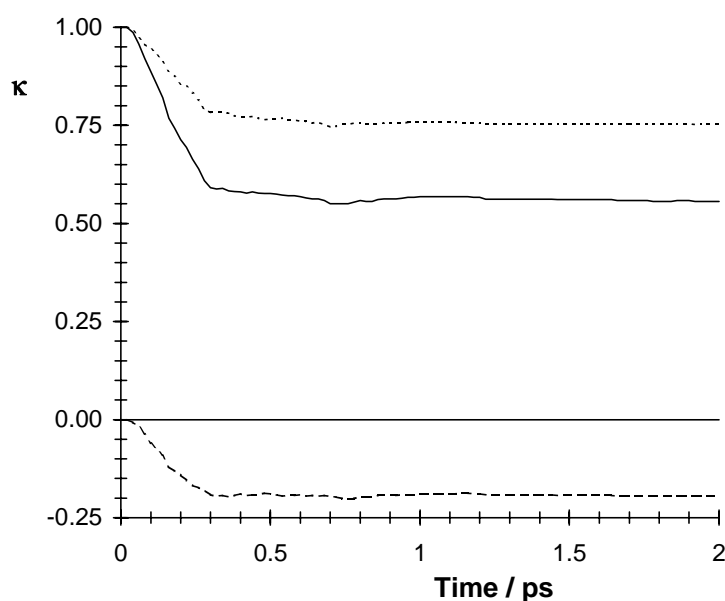


Figure 5.5. Transmission coefficient (solid) of a calix[4]arene in benzene. The dotted (dashed) line gives the contribution of molecules that settle in the paco conformation after crossing the transition state with a positive (negative) transient velocity.

Table 5.1. Computed and experimental rates for the cone to paco conversion.

Solvent and method	k^{TST} / s^{-1}	κ	k^{RF} / s^{-1}	k^{exp} / s^{-1}
Vacuum normal mode analysis	174			
Vacuum umbrella sampling, $t = 0.6$ ps	241	0.92	222	
Vacuum umbrella sampling, $t = 2.0$ ps	241	0.82	198	
Chloroform umbrella sampling	84	0.43	36	$30^{\text{a}}, 8^{\text{b}}$
Benzene umbrella sampling	471	0.56	264	202^{a}

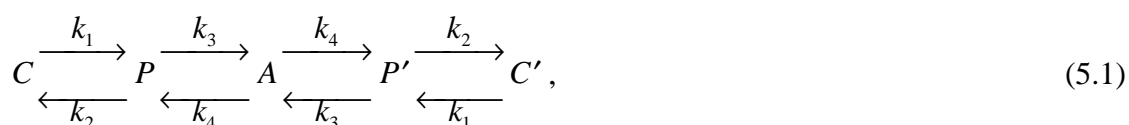
^a Data by Gutsche and Bauer,¹⁷ converted to 300 K.

^b Data by Araki *et al.*¹⁸

the transition state value $k_f^{\text{TST}} = 84 \text{ s}^{-1}$ yielded $k_f^{\text{RF}} = 36 \text{ s}^{-1}$. The influence of the solvent is seen to be more prominent in the free energy differences than on the transmission coefficients.

All results so far have been collected in Table 5.1, together with a few more results from vacuum simulations. Simulations⁶ *in vacuo* with the same transition state produced a transmission coefficient which arrived at a plateau of 0.92 after 0.6 ps, indicating that in this case the TST rate is an excellent approximation of the real rate. After about 0.8 ps the transmission function started to decrease again, and eventually settled at a second plateau of 0.82. This decrease was caused by molecules which left the paco well after having made one full oscillation in this well; this would not have occurred if the paco well had acted as a perfect sink.

The isomerisation rates of calix[4]arenes in solvents have been measured using ¹H-NMR.^{17,18} It was found that for the particular molecule studied here, the paco is too short-lived to be detectable. The measured rate constants correspond to the cone to inverted cone reaction, i.e. a process in which all four phenol rings rotate. This reaction consists of four steps, with one phenol ring rotating in each step.⁹ If we assume these steps to be independent, the reaction scheme becomes



where C , P and A denote respectively cone, paco and alternate, and where primes indicate conformations in which the majority of the phenols is pointing downwards. In reasonable approximation the overall cone to inverted cone rate constant is found to be related to the calculated cone to paco rate by⁷ $k_{CC'} \approx 3k_f^{\text{RF}}$.

Gutsche and Bauer¹⁷ measured the coalescence temperature with temperature dependent ¹H-NMR, and derived the isomerisation rate at this temperature from the chemical shift. They converted the rate into a free energy by

$$\Delta A^\ddagger = RT_{\text{coalescence}} \ln \left(\frac{6.62 \cdot 10^{12}}{k_{\text{coalescence}}} \right). \quad (5.2)$$

For calix[4]arene in benzene they found $\Delta A^\ddagger = 13.8$ kcal/mol and $T_{\text{coalescence}} = 15$ °C. With these data we have calculated the isomerisation rate at the coalescence temperature. By using Eq. (5.11), and assuming that the free energy is independent of the temperature, we then found a rate of 607 s^{-1} at 300 K for the cone to inverted cone reaction, hence a rate of 202 s^{-1} for the cone to paco reaction. The data for a calix[4]arene in chloroform were converted likewise, and yielded a rate of 30 s^{-1} . Araki *et al.*¹⁸ measured the reaction rate and the free energy of a calix[4]arene in chloroform as a function of temperature, resulting in a rate of 8 s^{-1} at 300 K. From their data it followed that the entropic contribution to the free energy is of minor importance in the above extrapolations, at most equal to about 0.1 kcal/mol, which is comparable with the uncertainty of the ΔA^\ddagger . All data are summarised in Table 5.1. The computed reaction rates compare very well with the measured rates, the former being slightly higher.

5.4 Conclusions

The isomerisation rate of a calix[4]arene in benzene and in chloroform has been studied with molecular dynamics simulations. The free energy as a function of the reaction coordinate was calculated by means of umbrella sampling. The rate constants obtained with the reactive flux method were in good agreement with the experimental values. In chloroform the cone conformation was found to be stabilised by the solvent, appreciably reducing the reaction rate with respect to the vacuum value. The reaction coordinate defined as the displacement along the unstable normal mode at the saddle point of the potential energy surface was shown to be very convenient in these calculations. An excellent first guess at the umbrella potential was obtained by a straightforward normal mode analysis. The same reaction coordinate can, in principle, be applied to numerous reactions.

5.5 References

- ¹ C. D. Gutsche, *Calixarenes* (Royal Society of Chemistry, Cambridge, U. K. 1989); *Calixarenes. A Versatile Class of Compounds*, edited by J. D. Vicens and V. Böhmer (Kluwer Academic Publishers, Dordrecht, The Netherlands, 1991).
- ² P. Hänggi, P. Talkner and M. Borkovec, *Rev. Mod. Phys.* **62**, 251 (1990).
- ³ P. W. Atkins, *Physical Chemistry* (Oxford University Press: Oxford, U. K., 1990).
- ⁴ D. Chandler, *J. Chem. Phys.* **68**, 2959 (1978).
- ⁵ W. H. Miller, *Acc. Chem. Res.* **9**, 306 (1976).
- ⁶ W. K. den Otter and W. J. Briels, *J. Chem. Phys.* **106**, 5494 (1997) (Chapter 3).
- ⁷ W. K. den Otter and W. J. Briels, *J. Chem. Phys.* **107**, 4968 (1997) (Chapter 4).

-
- ⁸ D. Frenkel and B. Smit, *Understanding Molecular Simulation* (Academic Press, San Diego, CA, 1996).
- ⁹ S. Fischer, P. D. J. Grootenhuis, L. C. Groenen, W. P. van Hoorn, F. C. J. M. van Veggel, D. N. Reinhoudt and M. Karplus, *J. Am. Chem. Soc.* **117**, 1611 (1995).
- ¹⁰ S. Fischer and M. Karplus, *Chem. Phys. Lett.* **194**, 252 (1992).
- ¹¹ B. R. Brooks, R. E. Bruccoleri, B. D. Olafson, D. J. States, S. Swaminathan and M. Karplus, *J. Comp. Chem.* **4**, 187 (1983).
- ¹² H. J. C. Berendsen and W. F. van Gunsteren, *GROMOS Reference Manual* (University of Groningen, Groningen, The Netherlands, 1987).
- ¹³ W. L. Jorgensen and D. L. Severance, *J. Am. Chem. Soc.* **112**, 4768 (1990).
- ¹⁴ F. Müller-Plathe, *Macromolecules* **29**, 4782 (1996).
- ¹⁵ H. J. C. Berendsen, J. P. M. Postma, W. F. van Gunsteren, A. DiNola and J. R. Haak, *J. Chem. Phys.* **81**, 3684 (1984).
- ¹⁶ *Handbook of Chemistry and Physics*, 50th ed., edited by R. C. Weast (The Chemical Rubber Co., Cleveland, OH, 1969).
- ¹⁷ C. D. Gutsche and L. J. Bauer, *J. Am. Chem. Soc.* **107**, 6052 (1985).
- ¹⁸ K. Araki, S. Shinkai and T. Matsuda, *Chem. Lett.* **1989**, 581 (1989).

Chapter 6

The calculation of free energy differences by constrained molecular dynamics simulations*

Abstract

The use of constraints in molecular dynamics simulations is known to affect the sampled phase space distribution. We derive the corrections needed to calculate the free energy of an unconstrained system from an MD simulation with constraints, for the thermodynamic integration and the thermodynamic perturbation methods. Both the dependence of the free energy on a coupling parameter and on a reaction coordinate are discussed. The correct relation between the constraint force and the derivative of the free energy with respect to an internal coordinate is derived. Two applications are presented. Several other methods with a similar objective are discussed and proven incorrect.

6.1 Introduction

It is common practice in molecular dynamics (MD) simulations to constrain the ‘hard’ coordinates of a molecule, often the bond lengths.¹ The elimination of these high frequency vibrations allows for a larger time step in the simulation, which is often desirable. Constraints may also be used to restrict the dynamics of a system to a specific part of configuration space in order to calculate conditional averages. For instance, in the calculation of the transmission coefficient of the reactive flux method a constraint can be used to sample configurations in the transition state of the reacting molecule.²

Obviously, the constrained molecule samples only a hyperplane of the full phase space. But, in addition, the probability distribution on this hyperplane is different for the constrained and the unconstrained molecule.^{3,4} Both distributions are derived in section 6.2. The difference between the two distributions is relatively easily corrected for, so the

* W. K. den Otter and W. J. Briels, submitted to J. Chem. Phys.

unconstrained averages needed in the calculation of the free energy can be calculated by means of a constrained MD simulation, as is described in section 6.3.

In rate theory one is interested in the free energy of a reacting system as a function of an internal coordinate of the system, the reaction coordinate $\xi(\{\mathbf{x}_i\})$. From this free energy function follow the equilibrium constant of the reaction and the transition state theory estimate of the reaction rate. In section 6.4 it will be shown that the derivative of the free energy with respect to ξ is closely related to the constraint force needed to keep the system at the hyperplane $\xi(\{\mathbf{x}_i\}) = \bar{\xi}$. This relation is illustrated in section 6.5 with the simulations of two prototypical molecules. In the literature there have appeared a number of methods to calculate the free energy as a function of a reaction coordinate. Several of these methods, and their shortcomings, are discussed in section 6.6. The GASP method, which in a sense is very similar to these methods, will also be discussed. We end with a short remark on how the theory presented here for molecular dynamics simulations ought to be used in Monte Carlo simulations.

6.2 Constraints and probability distributions

In this section we introduce the probability distributions resulting from unconstrained and constrained molecular dynamics simulations, and describe them. Their relation is derived in section 6.2.1 in terms of generalised coordinates. Some aspects of the implementation of constraints in Cartesian coordinates are discussed in section 6.2.2.

6.2.1 Generalised coordinates

Consider a molecule consisting of N atoms. The configuration of this molecule is described by $3N$ Cartesian coordinates, $\mathbf{X} = \{\mathbf{x}_i\}$, or by an equal number of generalised coordinates, $(\mathbf{q}, \boldsymbol{\sigma})$. We have split the generalised coordinates into two groups, namely the L coordinates $\boldsymbol{\sigma}$ that are going to be constrained in the MD run and the remaining $3N - L$ unconstrained coordinates.

First we consider the case in which none of the coordinates, including $\boldsymbol{\sigma}$, is constrained. The Lagrangian of this system reads as

$$L^u(\mathbf{q}, \boldsymbol{\sigma}, \mathbf{v}_{q\sigma}) = \frac{1}{2} \mathbf{v}_{q\sigma}^T \mathbf{A}_{q\sigma} \mathbf{v}_{q\sigma} - \Phi(\mathbf{q}, \boldsymbol{\sigma}), \quad (6.1)$$

where $\mathbf{v}_{q\sigma}^T = (\dot{\mathbf{q}}^T, \dot{\boldsymbol{\sigma}}^T)$ is the row vector of all generalised velocities and Φ is the potential energy. The conjugate momenta are given by

$$\mathbf{p}_{q\sigma} = \mathbf{A}_{q\sigma} \mathbf{v}_{q\sigma}, \quad (6.2)$$

with $\mathbf{p}_{q\sigma}^T = (\mathbf{p}_q^T, \mathbf{p}_\sigma^T)$, and the Hamiltonian reads

$$H^u(\mathbf{q}, \boldsymbol{\sigma}, \mathbf{p}_{q\sigma}) = \frac{1}{2} \mathbf{p}_{q\sigma}^T \mathbf{A}_{q\sigma}^{-1} \mathbf{p}_{q\sigma} + \Phi(\mathbf{q}, \boldsymbol{\sigma}). \quad (6.3)$$

The probability distribution of the unconstrained system with these coordinates is

$$P^u(\mathbf{q}, \boldsymbol{\sigma}, \mathbf{p}_{q\sigma}) \propto \exp[-\beta H^u(\mathbf{q}, \boldsymbol{\sigma}, \mathbf{p}_{q\sigma})], \quad (6.4)$$

where $\beta = 1/k_B T$, k_B is Boltzmann's constant and T is the absolute temperature.

For future convenience we will write the $3N \times 3N$ dimensional mass-metric matrix $\mathbf{A}_{q\sigma}$ in block form as

$$\mathbf{A}_{q\sigma} = \begin{pmatrix} \mathbf{A}_q & \mathbf{B}_\sigma \\ \mathbf{B}_\sigma^T & \mathbf{C}_\sigma \end{pmatrix}, \quad (6.5)$$

$$\mathbf{A}_{q\sigma}^{-1} = \begin{pmatrix} \mathbf{X}_q & \mathbf{Y}_\sigma \\ \mathbf{Y}_\sigma^T & \mathbf{Z}_\sigma \end{pmatrix}, \quad (6.6)$$

where \mathbf{A}_q is the $(3N - L) \times (3N - L)$ upper left block of $\mathbf{A}_{q\sigma}$, etc. The mass-metric matrix can easily be obtained by transforming the kinetic energy of the unconstrained system from Cartesian coordinates to generalised coordinates:

$$\mathbf{A}_{q\sigma} = \mathbf{J}^T \mathbf{M} \mathbf{J}, \quad (6.7)$$

where \mathbf{M} is a $3N \times 3N$ matrix containing all atomic masses down the diagonal, and

$$\mathbf{J} = \begin{pmatrix} \frac{\partial \mathbf{X}}{\partial \mathbf{q}} & \frac{\partial \mathbf{X}}{\partial \boldsymbol{\sigma}} \end{pmatrix} \quad (6.8)$$

is the Jacobi matrix of the transformation. The inverse matrix $\mathbf{A}_{q\sigma}^{-1}$ is readily obtained from Eqs. (6.7) and (6.8). In what follows we will use the matrices \mathbf{Z}_σ and \mathbf{Y}_σ , whose components are then found to be

$$(\mathbf{Z}_\sigma)_{ij} = \sum_{k=1}^N \frac{1}{m_k} \frac{\partial \sigma_i}{\partial \mathbf{x}_k} \cdot \frac{\partial \sigma_j}{\partial \mathbf{x}_k}, \quad (6.9)$$

$$(\mathbf{Y}_\sigma)_{ij} = \sum_{k=1}^N \frac{1}{m_k} \frac{\partial q_i}{\partial \mathbf{x}_k} \cdot \frac{\partial \sigma_j}{\partial \mathbf{x}_k}. \quad (6.10)$$

A second important relation is³

$$|\mathbf{A}_q| = |\mathbf{A}_{q\sigma}| |\mathbf{Z}_\sigma|, \quad (6.11)$$

which follows from

$$\begin{pmatrix} \mathbf{A}_q & \mathbf{0} \\ \mathbf{B}_\sigma^T & \mathbf{1} \end{pmatrix} = \mathbf{A}_{q\sigma} \mathbf{A}_{q\sigma}^{-1} \begin{pmatrix} \mathbf{A}_q & \mathbf{0} \\ \mathbf{B}_\sigma^T & \mathbf{1} \end{pmatrix} = \mathbf{A}_{q\sigma} \begin{pmatrix} \mathbf{1} & \mathbf{Y}_\sigma \\ \mathbf{0} & \mathbf{Z}_\sigma \end{pmatrix} \quad (6.12)$$

by using Eqs. (6.5) and (6.6), and taking the determinant on both sides.

The Hamiltonian of the $\boldsymbol{\sigma}$ -constrained system must be derived from the Lagrangian of the constrained system, which in turn is obtained from the Lagrangian of the unconstrained system by imposing the constraints $\boldsymbol{\sigma} = \bar{\boldsymbol{\sigma}}$ and $\dot{\boldsymbol{\sigma}} = \mathbf{0}$. The usual operations yield

$$H_\sigma^c(\mathbf{q}, \mathbf{p}_q) = \frac{1}{2} \mathbf{p}_q^T \mathbf{A}_q^{-1} \mathbf{p}_q + \Phi(\mathbf{q}, \bar{\boldsymbol{\sigma}}), \quad (6.13)$$

with $\mathbf{p}_q = \mathbf{A}_q \dot{\mathbf{q}}$. The corresponding probability distribution reads as

$$P_\sigma^c(\mathbf{q}, \mathbf{p}_q) \propto \exp[-\beta H_\sigma^c(\mathbf{q}, \mathbf{p}_q)]. \quad (6.14)$$

This is the distribution which is sampled with a constrained MD run. It differs from the unconstrained distribution not only by $\boldsymbol{\sigma}$ being equal to $\bar{\boldsymbol{\sigma}}$, but also by the absence of the impulses \mathbf{p}_σ , so care must be taken if one is to calculate unconstrained conditional averages, with $\boldsymbol{\sigma} = \bar{\boldsymbol{\sigma}}$ being the conditions, by means of a constrained dynamics simulation.

We will denote by

$$\langle F \rangle_\sigma = \frac{\int d\mathbf{q} \int d\mathbf{p}_q F P_\sigma^c(\mathbf{q}, \mathbf{p}_q)}{\int d\mathbf{q} \int d\mathbf{p}_q P_\sigma^c(\mathbf{q}, \mathbf{p}_q)} \quad (6.15)$$

the average of some function F over a constrained Hamiltonian, and by

$$\langle F \rangle_u = \frac{\int d\mathbf{X} \int d\mathbf{p}_x F P^u(\mathbf{X}, \mathbf{p}_x)}{\int d\mathbf{X} \int d\mathbf{p}_x P^u(\mathbf{X}, \mathbf{p}_x)} \quad (6.16)$$

the corresponding unconstrained average. We will now express the unconstrained average of the function F in terms of a constrained average, for those cases when the usual assumption for ‘hard’ variables can be made, i.e. when a factor of $\delta(\boldsymbol{\sigma} - \bar{\boldsymbol{\sigma}})$ can be introduced in the integral. More precisely, we write the potential energy as⁵

$$\Phi(\mathbf{q}, \boldsymbol{\sigma}) \approx \Phi(\mathbf{q}, \bar{\boldsymbol{\sigma}}) + \frac{1}{2} [\boldsymbol{\sigma} - \bar{\boldsymbol{\sigma}}]^T \mathbf{F} [\boldsymbol{\sigma} - \bar{\boldsymbol{\sigma}}], \quad (6.17)$$

where \mathbf{F} is assumed to be independent of \mathbf{q} , and integrate over the $\boldsymbol{\sigma}$ to obtain for the numerator of Eq. (6.16):

$$N \propto |\mathbf{F}|^{-1/2} \int d\mathbf{q} d\boldsymbol{\sigma} \int d\mathbf{p}_{q\sigma} F \exp[-\beta \{ \frac{1}{2} \mathbf{p}_{q\sigma}^T \mathbf{A}_{q\sigma}^{-1} \mathbf{p}_{q\sigma} + \Phi(\mathbf{q}, \boldsymbol{\sigma}) \}] \delta[\boldsymbol{\sigma} - \bar{\boldsymbol{\sigma}}]. \quad (6.18)$$

Making the same approximation in the denominator, Q , we arrive at the conditional average referred to above. Even though the variations in $\boldsymbol{\sigma}$ are so small that they can be replaced by a Dirac-delta in the integral, the variations in the associated momenta are not small and must be taken into account explicitly. Writing

$$\mathbf{p}_{q\sigma}^T \mathbf{A}_{q\sigma}^{-1} \mathbf{p}_{q\sigma} = \mathbf{p}_q^T \mathbf{A}_q^{-1} \mathbf{p}_q + (\mathbf{p}_\sigma - \mathbf{Z}_\sigma^{-1} \mathbf{Y}_\sigma^T \mathbf{p}_q)^T \mathbf{Z}_\sigma (\mathbf{p}_\sigma - \mathbf{Z}_\sigma^{-1} \mathbf{Y}_\sigma^T \mathbf{p}_q) \quad (6.19)$$

and integrating over the momenta \mathbf{p}_σ , we find

$$N \propto \int d\mathbf{q} \int d\mathbf{p}_q F \exp[-\beta \{ \frac{1}{2} \mathbf{p}_q^T \mathbf{A}_q^{-1} \mathbf{p}_q + \Phi(\mathbf{q}, \bar{\boldsymbol{\sigma}}) \}] |\mathbf{Z}_\sigma|^{-1/2}. \quad (6.20)$$

The exponential is proportional to the probability distribution of the constrained system, Eq. (6.14). The factor $|\mathbf{Z}_\sigma|^{-1/2}$ is seen to convert the integral over the constrained ensemble into the corresponding integral over the unconstrained ensemble; this factor is to be

interpreted as the ratio of the momentum spaces of the constrained and the unconstrained systems at $(\mathbf{q}, \bar{\boldsymbol{\sigma}})$. By applying the above transformation rule, the expectation value of F in an unconstrained ensemble can be calculated from a constrained ensemble by

$$\langle F \rangle_u = \frac{\langle F |\mathbf{Z}_\sigma|^{-1/2} \rangle_\sigma}{\langle |\mathbf{Z}_\sigma|^{-1/2} \rangle_\sigma}. \quad (6.21)$$

Almost all expressions in this article will be of this form. It is clear that F may not depend on $\boldsymbol{\sigma}$, nor on $\dot{\boldsymbol{\sigma}} = \mathbf{Z}_\sigma (\mathbf{p}_\sigma - \mathbf{Z}_\sigma^{-1} \mathbf{Y}_\sigma^T \mathbf{p}_q)$, for this expression to hold. Notice that the expression is valid even if F depends on the momenta \mathbf{p}_q , a fact overlooked by Ruiz-Montero *et al.*,⁶ but not if F depends on the velocities $\dot{\mathbf{q}}$.

6.2.2 Simulation in Cartesian coordinates

The generalised coordinates of the previous section are very useful for the theoretical understanding of the problem. However, in computer simulations the generalised coordinates are rather awkward to use, and Cartesian coordinates are being used instead. The Cartesian equations of motion for a constrained system follow from the Lagrangian

$$L^*(\mathbf{X}, \dot{\mathbf{X}}, t) = L^u(\mathbf{X}, \dot{\mathbf{X}}, t) + \sum_{l=1}^L \lambda_l \cdot (\sigma_l(\mathbf{X}) - \bar{\sigma}_l), \quad (6.22)$$

where the Lagrange multipliers, λ_l , are determined by demanding that the constraints are fulfilled at all times. From the equations of motion it follows that each atom feels a constraint force given by

$$\mathbf{F}_i^c = \sum_{l=1}^L \lambda_l \nabla_i \sigma_l. \quad (6.23)$$

If initially $\sigma_l(\mathbf{X}) = \bar{\sigma}_l$ and $\dot{\sigma}_l = 0$, the constraints can be fulfilled by demanding $\ddot{\sigma}_l = 0$; together with the equations of motion and Eq. (6.9) this leads to^{1,7}

$$\lambda_l = \sum_{k=1}^L (\mathbf{Z}_\sigma^{-1})_{lk} \left(\sum_{i=1}^N m_i^{-1} \nabla_i \sigma_k \cdot \nabla_i \Phi - \sum_{i,j=1}^N \dot{\mathbf{x}}_j \cdot \nabla_i \nabla_j \sigma_k \cdot \dot{\mathbf{x}}_i \right). \quad (6.24)$$

Simulations in which these analytical expressions for the Lagrange multipliers are actually being used, as a consequence of numerical inaccuracies due to the use of a finite time step, gradually drift away from the constraint hyperplane, $\boldsymbol{\sigma}(\mathbf{X}) = \bar{\boldsymbol{\sigma}}$. They therefore need to be reset to the hyperplane once every while.⁸

In the SHAKE⁹ algorithm the constraints are rigorously met every simulation step. First, in a regular MD step without constraints the atomic positions are advanced from $\mathbf{x}_i(t)$ to $\mathbf{x}'_i(t + \Delta t)$, resulting in a violation of the constraints. In the second step a force of the form of Eq. (6.23) is used in the Verlet algorithm to move the atoms to

$$\mathbf{x}_i(t + \Delta t) = \mathbf{x}'_i(t + \Delta t) + \frac{(\Delta t)^2}{m_i} \sum_{l=1}^L \lambda_l \nabla_i \sigma_l, \quad (6.25)$$

again accompanied by a change of the constraints. The Lagrange multipliers are chosen such that the constraints are restored to their initial values. To this end a Taylor expansion of σ is made to first order in $\mathbf{x}_i(t + \Delta) - \mathbf{x}'_i(t + \Delta)$, assuming that the gradients of σ_l hardly change during the unconstrained MD step,

$$\sigma_l(t + \Delta t) = \sigma'_l(t + \Delta t) + (\Delta t)^2 \sum_{k=1}^L \lambda_k \sum_{i=1}^N \frac{1}{m_i} \nabla_i \sigma_l(t) \cdot \nabla_i \sigma_k(t). \quad (6.26)$$

With $\sigma_l(t + \Delta t)$ equal to $\bar{\sigma}_l$, this is a set of equations which may be solved for the λ_k . The second step must be repeated until all constraints are met to within acceptable accuracy. The Lagrange multipliers obtained in this way are comparable with the ones calculated analytically, so in section 6.4 we shall assume them to be identical.

One particular system worth mentioning is a molecule in which only the distance between atoms 1 and 2 is constrained, $\sigma = |\mathbf{r}_{12}|$, where $\mathbf{r}_{12} = \mathbf{r}_2 - \mathbf{r}_1$. Equation (6.24) then yields

$$\lambda = \mu \left(\frac{\mathbf{F}_1}{m_1} - \frac{\mathbf{F}_2}{m_2} \right) \cdot \frac{\mathbf{r}_{12}}{r_{12}} + \mu \frac{\dot{\mathbf{r}}_{12} \cdot \dot{\mathbf{r}}_{12}}{r_{12}}, \quad (6.27)$$

the familiar result from the Gauss' principle of least constraint.⁸

As a final remark we note that the constraint force resulting from constraining an internal coordinate of a molecule does not effect the total momentum nor the total angular momentum of this molecule. Therefore, there is no need to explicitly use this conservation property when calculating the constraint force, as was done by Tobias and Brooks.¹⁰

6.3 Thermodynamic integration and perturbation

Suppose one is interested to know the free energy of a system as a function of some parameter. This parameter could be an internal coordinate of some molecule, for example a reaction coordinate. Or it could be a parameter occurring in the potential energy of the molecule, a so-called coupling parameter. There are two common ways of calculating free energy differences in these cases, namely thermodynamic integration and thermodynamic perturbation. All four possible combinations will be briefly addressed in this section.

6.3.1 Reaction coordinate ξ

In this subsection we will calculate the probability distribution of a given molecule along some internal coordinate ξ . Our main interest is when ξ is a reaction coordinate, since the probability of finding the molecule at the transition state, i.e. when $\xi = \xi^\ddagger$, is directly related to the rate of the reaction. The calculation of this distribution by means of a standard MD run usually is an impossible task, since the high energy barriers prohibit sampling all values of ξ . With umbrella sampling the probability of crossing existing energy barriers is enhanced by

deliberately lowering the barriers by means of an extra potential. In the subsequent analysis of the run appropriate corrections are made for this extra potential. In this section we will discuss an alternative method, using constrained MD simulations, in which the system is forced to sample only regions of phase space where ξ has some prescribed value. In addition to this constraint on the reaction coordinate ξ , L hard variables σ will also be constrained. The atomic masses and $\bar{\sigma}$, the values to which the σ variables will be constrained, are assumed independent of ξ .

Our notation requires some minor changes to accommodate the extra constrained coordinate. The $3N \times 3N$ mass-metric matrix will henceforth be written as

$$\mathbf{A}_{q\xi\sigma} = \begin{pmatrix} \mathbf{A}_q & \mathbf{B}_{\xi\sigma} \\ \mathbf{B}_{\xi\sigma}^T & \mathbf{C}_{\xi\sigma} \end{pmatrix} = \begin{pmatrix} \mathbf{A}_{q\xi} & \mathbf{B}_\sigma \\ \mathbf{B}_\sigma^T & \mathbf{C}_\sigma \end{pmatrix}, \quad (6.28)$$

$$\mathbf{A}_{q\xi\sigma}^{-1} = \begin{pmatrix} \mathbf{X}_q & \mathbf{Y}_{\xi\sigma} \\ \mathbf{Y}_{\xi\sigma}^T & \mathbf{Z}_{\xi\sigma} \end{pmatrix} = \begin{pmatrix} \mathbf{X}_{q\xi} & \mathbf{Y}_\sigma \\ \mathbf{Y}_\sigma^T & \mathbf{Z}_\sigma \end{pmatrix}, \quad (6.29)$$

where \mathbf{A}_q and \mathbf{X}_q are $(3N - L - 1) \times (3N - L - 1)$ dimensional matrices, $\mathbf{A}_{q\xi}$ and $\mathbf{X}_{q\xi}$ are $(3N - L) \times (3N - L)$ dimensional, etc. The results of section 6.2.1 can now easily be generalised, for example Eq. (6.11) now reads as

$$|\mathbf{A}_{q\xi\sigma}| = |\mathbf{A}_{q\xi}| |\mathbf{Z}_\sigma|^{-1} = |\mathbf{A}_q| |\mathbf{Z}_{\xi\sigma}|^{-1}. \quad (6.30)$$

The probability distribution of the (ξ, σ) -constrained ensemble can be shown to be

$$P_{\xi\sigma}^c(\mathbf{q}, \mathbf{p}_q) \propto \exp\left[-\beta\left\{\frac{1}{2}\mathbf{p}_q^T \mathbf{A}_q^{-1} \mathbf{p}_q + \Phi(\mathbf{q}, \xi, \sigma)\right\}\right], \quad (6.31)$$

where \mathbf{q} and \mathbf{p}_q have $(3N - L - 1)$ elements. Equation (6.15) generalises to

$$\langle F \rangle_{\xi\sigma} = \frac{\int d\mathbf{q} \int d\mathbf{p}_q FP_{\xi\sigma}^c(\mathbf{q}, \mathbf{p}_q)}{\int d\mathbf{q} \int d\mathbf{p}_q P_{\xi\sigma}^c(\mathbf{q}, \mathbf{p}_q)}. \quad (6.32)$$

The probability distribution along the reaction coordinate reads

$$p(\xi) = \frac{Q(\xi)}{Q} = \frac{1}{Q} \int d\mathbf{X} \int d\mathbf{p}_x \exp[-\beta H^u(\mathbf{X}, \mathbf{p}_x)] \delta[\xi(\mathbf{X}) - \xi], \quad (6.33)$$

where Q is a normalisation factor. This distribution is often expressed as a free energy by

$$A(\xi) = -k_B T \ln Q(\xi). \quad (6.34)$$

The direct evaluation of the partition function $Q(\xi)$ is virtually impossible, but its derivative is relatively simple to calculate. This fact is used in the thermodynamic integration method, which allows $A(\xi)$ to be calculated up to some constant:

$$A(\xi) = A(0) + \int_0^\xi \frac{dA(\xi')}{d\xi'} d\xi', \quad (6.35)$$

with

$$\frac{dA(\xi)}{d\xi} = -\frac{k_B T}{Q(\xi)} \frac{dQ(\xi)}{d\xi}. \quad (6.36)$$

There are several ways to differentiate the partition function with respect to the reaction coordinate, all leading to the same final result of course. The obvious way to go at this point, given what has been said in the previous sections, is to write

$$Q(\xi) \propto \int d\mathbf{q} \int d\mathbf{p}_q \exp[-\beta H^c] |\mathbf{Z}_{\xi\sigma}|^{-1/2}, \quad (6.37)$$

and to differentiate with respect to ξ , obtaining

$$\begin{aligned} \frac{dQ(\xi)}{d\xi} &\propto \int d\mathbf{q} \int d\mathbf{p}_q \exp[-\beta H^c] |\mathbf{Z}_{\xi\sigma}|^{-1/2} \\ &\times \left\{ -\frac{1}{2} \beta \mathbf{p}_q^T \frac{\partial \mathbf{A}_q^{-1}}{\partial \xi} \mathbf{p}_q - \beta \frac{\partial \Phi}{\partial \xi} - \frac{1}{2} |\mathbf{Z}_{\xi\sigma}|^{-1} \frac{\partial |\mathbf{Z}_{\xi\sigma}|}{\partial \xi} \right\}. \end{aligned} \quad (6.38)$$

Using

$$\begin{aligned} &\int d\mathbf{p}_q \exp\left[-\frac{1}{2} \beta \mathbf{p}_q^T \mathbf{A}_q^{-1} \mathbf{p}_q\right] \mathbf{p}_q^T \frac{\partial \mathbf{A}_q^{-1}}{\partial \xi} \mathbf{p}_q \\ &= k_B T \text{Tr} \left(\mathbf{A}_q \frac{\partial \mathbf{A}_q^{-1}}{\partial \xi} \right) \int d\mathbf{p}_q \exp\left[-\frac{1}{2} \beta \mathbf{p}_q^T \mathbf{A}_q^{-1} \mathbf{p}_q\right] \\ &= -k_B T |\mathbf{A}_q|^{-1} \frac{\partial |\mathbf{A}_q|}{\partial \xi} \int d\mathbf{p}_q \exp\left[-\frac{1}{2} \beta \mathbf{p}_q^T \mathbf{A}_q^{-1} \mathbf{p}_q\right] \end{aligned} \quad (6.39)$$

and Eq. (6.30) we arrive at

$$\frac{dA(\xi)}{d\xi} = \frac{1}{\langle |\mathbf{Z}_{\xi\sigma}|^{-1/2} \rangle_{\xi\sigma}} \left[\left\langle \frac{\partial \Phi}{\partial \xi} |\mathbf{Z}_{\xi\sigma}|^{-1/2} \right\rangle_{\xi\sigma} - \frac{1}{2} k_B T \left\langle \frac{\partial |\mathbf{A}_{q\xi\sigma}|}{\partial \xi} |\mathbf{A}_{q\xi\sigma}|^{-1} |\mathbf{Z}_{\xi\sigma}|^{-1/2} \right\rangle_{\xi\sigma} \right]. \quad (6.40)$$

In Eq. (6.39) Tr denotes the trace; in the first step of this equation we have used the symmetry of \mathbf{A}_q , and in the second step we have used $\text{Tr}(\mathbf{A}_q \partial \mathbf{A}_q^{-1} / \partial \xi) = \partial / \partial \xi \text{Tr} \ln \mathbf{A}_q^{-1} = \partial / \partial \xi \ln |\mathbf{A}_q^{-1}| = -\partial / \partial \xi \ln |\mathbf{A}_q|$. If finally we would use Eq. (6.7) in the form $|\mathbf{A}_{q\xi\sigma}| = |\mathbf{M}||\mathbf{J}|^2$, we would arrive at a result similar to Eq. (6.40), with $|\mathbf{A}_{q\xi\sigma}|$ in the last term replaced by $|\mathbf{J}|$, and the factor $1/2$ replaced by unity.⁷ The two terms between the large square brackets are readily recognised by their temperature dependence as being the energetic and the entropic contributions to the free energy difference.

A different technique for calculating free energy differences is the thermodynamic perturbation method. The free energy difference is then calculated directly by

$$\begin{aligned}
A(\xi_2) - A(\xi_1) &= -k_B T \ln \frac{\iint d\mathbf{X} d\mathbf{p}_x \exp[-\beta H^u(\mathbf{X}, \mathbf{p}_x)] \delta[\xi - \xi_2]}{\iint d\mathbf{X} d\mathbf{p}_x \exp[-\beta H^u(\mathbf{X}, \mathbf{p}_x)] \delta[\xi - \xi_1]} \\
&= -k_B T \ln \frac{\iint d\mathbf{q} d\mathbf{p}_q \exp[-\beta H_2^c] \left| \mathbf{Z}_{\xi_2 \sigma} \right|^{-1/2}}{\iint d\mathbf{q} d\mathbf{p}_q \exp[-\beta H_1^c] \left| \mathbf{Z}_{\xi_1 \sigma} \right|^{-1/2}}, \tag{6.41}
\end{aligned}$$

where H_i^c is the constrained Hamiltonian with ξ constrained to the value ξ_i . We now want to refer the numerator to an average over the probability distribution used in the denominator. To this end we use

$$\int d\mathbf{p}_q \exp\left[-\frac{1}{2} \beta \mathbf{p}_q^T \mathbf{A}_q^{-1}(\xi_2) \mathbf{p}_q\right] = \frac{\left| \mathbf{A}_q(\xi_2) \right|^{1/2}}{\left| \mathbf{A}_q(\xi_1) \right|^{1/2}} \int d\mathbf{p}_q \exp\left[-\frac{1}{2} \beta \mathbf{p}_q^T \mathbf{A}_q^{-1}(\xi_1) \mathbf{p}_q\right] \tag{6.42}$$

and $\left| \mathbf{A}_q \right| \left| \mathbf{Z}_{\xi \sigma} \right|^{-1} = \left| \mathbf{A}_{q\xi\sigma} \right| = \left| \mathbf{M} \right| \left| \mathbf{J} \right|^2$, obtaining

$$A(\xi_2) - A(\xi_1) = -k_B T \ln \frac{\left\langle \exp[-\beta \Delta \Phi_{12}] \left| \mathbf{J}(\xi_1) \right|^{-1} \left| \mathbf{J}(\xi_2) \right| \left| \mathbf{Z}_{\xi_1 \sigma} \right|^{-1/2} \right\rangle_{\xi_1 \sigma}}{\left\langle \left| \mathbf{Z}_{\xi_1 \sigma} \right|^{-1/2} \right\rangle_{\xi_1 \sigma}}, \tag{6.43}$$

where $\Delta \Phi_{12} = \Phi(\mathbf{q}, \xi_2, \boldsymbol{\sigma}) - \Phi(\mathbf{q}, \xi_1, \boldsymbol{\sigma})$ and $\left| \mathbf{J}(\xi_i) \right|$ is the Jacobian with ξ put equal to ξ_i . Dividing Eq. (6.43) by $\xi_2 - \xi_1$ and taking the limit of this difference going to zero we again obtain Eq. (6.40).

6.3.2 Coupling parameter λ

A coupling parameter λ is used to transform the force field representative of molecule A into the force field representative of molecule B via a series of intermediate, non-physical, molecules. For a linear transformation the intermediate force fields read as $\Phi_\lambda = (1 - \lambda) \cdot \Phi_A + \lambda \cdot \Phi_B$. Non-linear transformations were found to be useful in cases where the number of atoms in molecules A and B differ. Examples where the method has been used include the calculation of the difference of the free energy of hydration of ethanol and the free energy of hydration of ethane¹¹, the difference of the free energies of complexation of 18-crown-6 with sodium or potassium ions,¹² and the solvability of methane versus neopentane in water.¹³

The partition function of an unconstrained molecule with a λ -dependent Hamiltonian is given by

$$\begin{aligned}
Q(\lambda) &\propto \int d\mathbf{X} \int d\mathbf{p}_x \exp[-\beta H^u(\mathbf{X}, \mathbf{p}_x; \lambda)] \\
&\propto \left| \mathbf{F}(\lambda) \right|^{-1/2} \int d\mathbf{q} d\boldsymbol{\sigma} \int d\mathbf{p}_{q\sigma} \exp\left[-\beta \left\{ \frac{1}{2} \mathbf{p}_{q\sigma}^T \mathbf{A}_{q\sigma}^{-1}(\mathbf{q}, \boldsymbol{\sigma}; \lambda) \mathbf{p}_{q\sigma} + \Phi(\mathbf{q}, \boldsymbol{\sigma}; \lambda) \right\}\right] \delta[\boldsymbol{\sigma} - \bar{\boldsymbol{\sigma}}(\lambda)], \tag{6.44}
\end{aligned}$$

where in the second line we have made the usual assumptions for the hard variables. In trying to be as general as possible, we allow for a coupling parameter dependence of the force field, the atomic masses and the value of the constrained coordinates. In the present case we shall explicitly assume that the force constant matrix \mathbf{F} associated with the constraints depends on λ , like for example when a constrained C-H bond is turned into a constrained O-H bond.

The derivation of the expressions for thermodynamic integration is analogous to that of the previous section, and the final result reads

$$\begin{aligned} \frac{dA(\lambda)}{d\lambda} = \frac{1}{\langle |\mathbf{Z}_\sigma|^{-1/2} \rangle_{\sigma;\lambda}} & \left[\left\langle \frac{d\Phi}{d\lambda} \middle| \mathbf{Z}_\sigma \right|^{-1/2} \right\rangle_{\sigma;\lambda} - \frac{1}{2} k_B T \left\langle \frac{d|\mathbf{A}_{q\sigma}|}{d\lambda} \middle| \mathbf{A}_{q\sigma} \right|^{-1} \middle| \mathbf{Z}_\sigma \right|^{-1/2} \right]_{\sigma;\lambda} \\ & + \frac{1}{2} k_B T |\mathbf{F}|^{-1} \frac{d|\mathbf{F}|}{d\lambda}. \end{aligned} \quad (6.45)$$

There are a few differences between this result and Eq. (6.40). First, the potential energy function may depend on the coupling parameter explicitly, but also implicitly via the constrained coordinates,

$$\frac{d\Phi(\mathbf{q}, \bar{\sigma}(\lambda); \lambda)}{d\lambda} = \frac{\partial\Phi(\mathbf{q}, \bar{\sigma}(\lambda); \lambda)}{\partial\lambda} + \sum_{i=1}^L \frac{d\bar{\sigma}_i(\lambda)}{d\lambda} \frac{\partial\Phi(\mathbf{q}, \bar{\sigma}(\lambda); \lambda)}{\partial\bar{\sigma}_i}. \quad (6.46)$$

Second, since the atomic masses may depend on λ , use of Eq. (6.7) yields

$$\frac{1}{|\mathbf{A}_{q\sigma}|} \frac{\partial|\mathbf{A}_{q\sigma}|}{\partial\lambda} = \frac{2}{|\mathbf{J}|} \sum_{i=1}^L \frac{\partial|\mathbf{J}|}{\partial\bar{\sigma}_i} \frac{d\bar{\sigma}_i(\lambda)}{d\lambda} + \frac{1}{|\mathbf{M}|} \frac{\partial|\mathbf{M}|}{\partial\lambda}. \quad (6.47)$$

The first term on the right hand side is the usual term. The second term on the right hand side, after having been used in Eq. (6.45), and after a subsequent integration with respect to λ yields the obvious contribution to ΔA . In all meaningful applications this contribution will be irrelevant. Finally, there is an extra term in Eq. (6.45), stemming from the constrained variables, which in many applications, but not all, will be irrelevant.

The expression for thermodynamic perturbation is readily found to be

$$\Delta A = -k_B T \ln \frac{\left\langle \exp[-\beta\Delta\Phi_{12}] |\mathbf{M}(\lambda_1)|^{-1/2} |\mathbf{M}(\lambda_2)|^{1/2} |\mathbf{J}(\lambda_1)|^{-1} |\mathbf{J}(\lambda_2)| \middle| \mathbf{Z}_\sigma \right|^{-1/2} \right\rangle_{\sigma;\lambda_1}}{\left\langle \middle| \mathbf{Z}_\sigma \right|^{-1/2} \right\rangle_{\sigma;\lambda_1}}, \quad (6.48)$$

where $\Delta\Phi_{12} = \Phi(\mathbf{q}, \bar{\sigma}(\lambda_2); \lambda_2) - \Phi(\mathbf{q}, \bar{\sigma}(\lambda_1); \lambda_1)$, as follows by reasoning along the lines that lead to Eq. (6.43).

6.4 Relation between the thermodynamic force and the constraint force

We now return to Eq. (6.40), restricting ourselves to the case where no additional constraints σ are being applied. Using $|\mathbf{A}_{q\xi}| = |\mathbf{M}||\mathbf{J}|^2$, we may write

$$\frac{dA(\xi)}{d\xi} = \frac{1}{\langle Z_\xi^{-1/2} \rangle_\xi} \left\langle \frac{\partial}{\partial \xi} (\Phi - k_B T \ln |\mathbf{J}|) Z_\xi^{-1/2} \right\rangle_\xi. \quad (6.49)$$

Calculation of the right hand side of this equation is rather cumbersome, because the evaluation of $|\mathbf{J}|$ and $\partial/\partial\xi$ require the introduction of a full set of generalised coordinates.

The combination $\Phi - k_B T \ln |\mathbf{J}|$ may be interpreted as a potential, whose negative derivative with respect to ξ is a force. Equation (6.49) then says that the average of this force is equal to the thermodynamic force $-dA(\xi)/d\xi$. On similar intuitive grounds van Gunsteren¹⁴ suggested that all that the constraint forces do during a constrained MD simulation is to counterbalance the thermodynamic force, and that therefore $dA(\xi)/d\xi$ should be equal to the constraint force. Later, Mülders *et al.*¹⁵ provided an almost correct justification for this method. Based on their methods we shall now derive the correct relationship between $dA(\xi)/d\xi$ and the average constraint force.

Since we shall need it further on in this section, we shall first derive the explicit expression of the Lagrange multiplier λ_ξ in terms of the quantities occurring in the Lagrangian. From the Lagrangian L^* , Eq. (6.22), expressed in generalised coordinates, we obtain the equation of motion of the constrained coordinate,

$$\frac{d}{dt} (\mathbf{B}_\xi^T \dot{\mathbf{q}} + C_\xi \dot{\xi}) = \frac{1}{2} \mathbf{v}_{q\xi}^T \frac{\partial \mathbf{A}_{q\xi}}{\partial \xi} \mathbf{v}_{q\xi} - \frac{\partial \Phi}{\partial \xi} + \lambda_\xi. \quad (6.50)$$

Upon substitution of $\ddot{\xi} = 0$, we solve for the Lagrange multiplier by demanding $\ddot{\xi} = 0$, obtaining

$$\begin{aligned} \lambda_\xi &= -\frac{1}{2} \dot{\mathbf{q}}^T \frac{\partial \mathbf{A}_q}{\partial \xi} \dot{\mathbf{q}} + \frac{\partial \Phi}{\partial \xi} + \frac{d}{dt} (\mathbf{B}_\xi^T \dot{\mathbf{q}}) \\ &= \frac{1}{2} \mathbf{p}_q^T \frac{\partial \mathbf{A}_q^{-1}}{\partial \xi} \mathbf{p}_q + \frac{\partial \Phi}{\partial \xi} + \frac{d}{dt} (\mathbf{B}_\xi^T \dot{\mathbf{q}}), \end{aligned} \quad (6.51)$$

where we have used $\dot{\mathbf{q}} = \mathbf{A}_q^{-1} \mathbf{p}_q$ in the second line.

We now start the main derivation of this section. In the present case, Eq. (6.38) reads

$$\frac{dQ(\xi)}{d\xi} \propto \int d\mathbf{q} \int d\mathbf{p}_q \exp[-\beta H^c] Z_\xi^{-1/2} \left\{ -\frac{1}{2} \beta \mathbf{p}_q^T \frac{\partial \mathbf{A}_q^{-1}}{\partial \xi} \mathbf{p}_q - \beta \frac{\partial \Phi}{\partial \xi} - \frac{1}{2} Z_\xi^{-1} \frac{\partial Z_\xi}{\partial \xi} \right\}. \quad (6.52)$$

Combining this equation with Eq. (6.51) we find

$$\begin{aligned} \frac{dQ(\xi)}{d\xi} &\propto \int d\mathbf{q} \int d\mathbf{p}_q \exp[-\beta H^c] Z_\xi^{-1/2} \left\{ -\beta\lambda_\xi + \frac{1}{2} \beta \mathbf{B}_\xi^T \dot{\mathbf{q}} Z_\xi^{-1} \frac{dZ_\xi}{dt} - \frac{1}{2} Z_\xi^{-1} \frac{\partial Z_\xi}{\partial \xi} \right\} \\ &+ \int d\mathbf{q} \int d\mathbf{p}_q \exp[-\beta H^c] \beta \frac{d}{dt} \left(Z_\xi^{-1/2} \mathbf{B}_\xi^T \dot{\mathbf{q}} \right). \end{aligned} \quad (6.53)$$

The last term, being the average of a time derivative, vanishes when ergodicity is assumed and the ensemble average may be replaced by a time average. We next make use of

$$\begin{aligned} \int d\mathbf{p}_q \exp[-\beta H^c] \dot{\mathbf{q}} \frac{dZ_\xi}{dt} &= \int d\mathbf{p}_q \exp[-\beta H^c] \dot{\mathbf{q}} \dot{\mathbf{q}}^T \frac{\partial Z_\xi}{\partial \mathbf{q}} \\ &= k_B T \mathbf{A}_q^{-1} \frac{\partial Z_\xi}{\partial \mathbf{q}} \int d\mathbf{p}_q \exp[-\beta H^c], \end{aligned} \quad (6.54)$$

where $\partial Z_\xi / \partial \mathbf{q}$ denotes the column vector of derivatives of Z_ξ with respect to the generalised coordinates except ξ . Introducing Eq. (6.54) into Eq. (6.53), and replacing $\mathbf{B}_\xi^T \mathbf{A}_q^{-1}$ by $-Z_\xi^{-1} \mathbf{Y}_\xi^T$, as follows from $\mathbf{A}_{q\xi}^{-1} \mathbf{A}_{q\xi} = \mathbf{1}$, we obtain

$$\frac{dQ(\xi)}{d\xi} \propto \int d\mathbf{q} \int d\mathbf{p}_q \exp[-\beta H^c] Z_\xi^{-1/2} \left\{ -\beta\lambda_\xi - \frac{1}{2} Z_\xi^{-2} \left(\mathbf{Y}_\xi^T \frac{\partial Z_\xi}{\partial \mathbf{q}} + Z_\xi \frac{\partial Z_\xi}{\partial \xi} \right) \right\}. \quad (6.55)$$

We finally introduce the analogues of Eqs. (6.9) and (6.10) to obtain

$$\frac{dA(\xi)}{d\xi} = \frac{\left\langle \lambda_\xi Z_\xi^{-1/2} \right\rangle_\xi + \frac{1}{2} k_B T \left\langle \left\{ \sum_{i=1}^N m_i^{-1} \nabla_i \xi \cdot \nabla_i Z_\xi \right\} Z_\xi^{-5/2} \right\rangle_\xi}{\left\langle Z_\xi^{-1/2} \right\rangle_\xi}. \quad (6.56)$$

The importance of this expression is that it can be evaluated without explicitly introducing the complementary generalised coordinates \mathbf{q} ; all that is needed is the readily available expression for ξ in terms of the Cartesian coordinates. A second important property of Eq. (6.56) is that it is manifestly independent of the coordinates \mathbf{q} , as is obvious from Eq. (6.33), but which is not evident at all from Eq. (6.40).

6.5 Numerical examples

To illustrate Eq. (6.56) with concrete applications, we have calculated the free energies along the reaction coordinate for two simple systems. As our first example serves a molecule consisting of three atoms, with the bending angle in the role of the reaction coordinate. The Jacobian determinant of the transformation from Cartesian coordinates to a set of coordinates containing the bond lengths l_{12} and l_{23} and the bending angle ξ , is $|\mathbf{J}| = l_{12}^2 l_{23}^2 \sin \xi \sin \psi_2$, where ψ_2 is one of the Euler angles needed to describe the orientation of the molecule. We shall assume that the potential energy can be written as a sum of terms, with only one term depending on the reaction coordinate, $\Phi = V(\xi) + V_{rest}(l_{12}, l_{23})$. The partition function is then readily evaluated, and the free energy reads

$$A(\xi) = -k_B T \ln(\sin \xi) + V(\xi) + A_{rest}, \quad (6.57)$$

where A_{rest} is independent of ξ . Differentiation with respect to ξ gives

$$\frac{dA(\xi)}{d\xi} = -k_B T \cot \xi + \frac{\partial V(\xi)}{\partial \xi}, \quad (6.58)$$

which is to be compared with the results from the simulation runs.

In our simulation the bending potential was put equal to zero, $V(\xi) = 0$, in order to enhance the effect of the other contributions to the free energy. All atoms had a mass of 12 a.m.u. The two potentials for bond stretching were quadratic with a spring constant of $600 \text{ kcal mol}^{-1} \text{ \AA}^{-2}$ and an equilibrium length of 1.5 \AA . The integration time step was 0.2 fs. Brownian dynamics with a friction constant of 25 ps^{-1} was used to maintain an average temperature of 300 K. The maximum allowed deviation in the bending angle when applying the shake algorithm was 10^{-4} degree. At each value of the reaction coordinate the molecule was first equilibrated for 0.1 ns, followed by a production run of 1 ns. Figure 6.1 shows the averaged constraint force, once as the uncorrected average of the Lagrange multiplier and once as the corrected average of the Lagrange multiplier, with

$$Z_\xi = \frac{1}{m_1 l_{12}^2} + \frac{l_{12}^2 + l_{23}^2 - 2l_{12}l_{23} \cos \xi}{m_2 l_{12}^2 l_{23}^2} + \frac{1}{m_3 l_{23}^2}. \quad (6.59)$$

The difference between the two results is surprisingly large, and neither of the two is in agreement with Eq. (6.58). The most probable value of the reaction coordinate is too large by

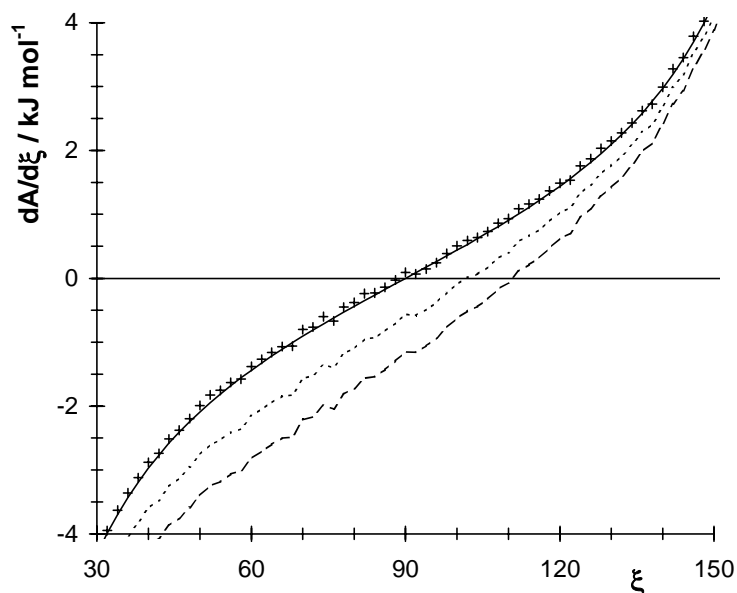


Figure 6.1. Derivative of the free energy along the bending angle of a three atom molecule. The averaged constraint force is shown as a dotted line, the same quantity averaged according to Eq. (6.21) is shown as a dashed line, the crosses are obtained with Eq. (6.56) and the solid line is the theoretical result.

10 to 20 degrees. The crosses in Fig. 6.1 represent the results obtained with Eq. (6.56), with

$$\sum_{i=1}^3 \frac{1}{m_i} \nabla_i \xi \cdot \nabla_i Z_\xi = \frac{4 \sin \xi}{m_2 l_{12} l_{23}} Z_\xi. \quad (6.60)$$

The agreement with the theoretically predicted results is perfect; the differences between the calculated points and the predicted values are of the order of 0.05 kJ mol^{-1} , with the calculated values being predominantly too high. With similar simulations of molecules consisting of three atoms of unequal masses and non-zero bending potentials Eq. (6.56) was found to be in good agreement with the theoretical predictions.

As a second example we have calculated the free energy of a four atom molecule as a function of the dihedral angle. This particular example was chosen because there are numerous reactions in which a rotation around a dihedral can serve as the reaction coordinate. As internal coordinates we use the bond lengths l_{12} , l_{23} and l_{34} , the bending angles ϕ_2 and ϕ_3 and the dihedral angle ξ . The transformation from Cartesian coordinates to the internal coordinates yields the Jacobian⁵ determinant $|\mathbf{J}| = l_{12}^2 l_{23}^2 l_{34}^2 \sin \phi_2 \sin \phi_3 \sin \psi_2$, which is independent of ξ ; ψ_2 again is one of the Euler angles needed to specify the orientation of the molecule. Assuming again that the potential energy can be split into parts of which only one term depends on ξ , the free energy is equal to this particular term, $A(\xi) = V(\xi)$.

The derivation of Z_ξ is considerably more complicated in this case. Using the expressions for $\nabla_i \xi$ given by Wilson *et al.*,¹⁶ which were recently rederived by Bekker *et al.*,¹⁷ we found

$$\begin{aligned} Z_\xi = & \frac{1}{m_1} \left(\frac{1}{l_{12} \sin \phi_2} \right)^2 + \frac{1}{m_4} \left(\frac{1}{l_{34} \sin \phi_3} \right)^2 \\ & + \frac{1}{m_2} (A_2^2 + B_3^2 - 2 \cos \xi A_2 B_3) + \frac{1}{m_3} (A_3^2 + B_2^2 - 2 \cos \xi A_3 B_2) \end{aligned} \quad (6.61)$$

with

$$A_2 = \frac{l_{23} - l_{12} \cos \phi_2}{l_{12} l_{23} \sin \phi_2}, \quad (6.62)$$

$$A_3 = \frac{l_{23} - l_{34} \cos \phi_3}{l_{34} l_{23} \sin \phi_3}, \quad (6.63)$$

$$B_2 = \frac{\cos \phi_2}{l_{23} \sin \phi_2}, \quad (6.64)$$

$$B_3 = \frac{\cos \phi_3}{l_{23} \sin \phi_3}, \quad (6.65)$$

in agreement with the result of Depaepe *et al.*¹⁸ Next, after some laborious mathematics we arrived at

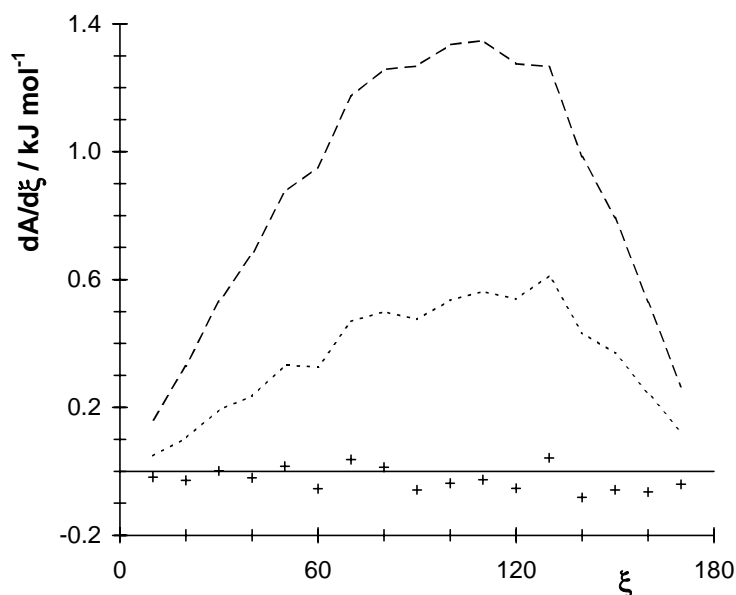


Figure 6.2. Derivative of the free energy along the dihedral angle of a four atom molecule. The meaning of the lines is the same as in Fig. 6.1.

$$\begin{aligned}
& \sum_{i=1}^4 \frac{1}{m_i} \nabla_i Z_\xi \cdot \nabla_i \xi = 4Z_\xi \sin \xi \left(\frac{A_2 B_3}{m_2} - \frac{A_3 B_2}{m_3} \right) \\
& + 2 \frac{\sin \xi}{l_{23}^2 m_2^2} \left[2A_2 B_3 - \cos \xi (A_2^2 + B_3^2) \right] + 2 \frac{\sin \xi}{l_{23}^2 m_3^2} \left[2A_3 B_2 - \cos \xi (A_3^2 + B_2^2) \right] \\
& - \frac{2 \sin \xi}{m_2 m_3} \left[(A_2^2 + B_3^2 - 2 \cos \xi A_2 B_3) A_3 B_2 + (A_3^2 + B_2^2 - 2 \cos \xi A_3 B_2) A_2 B_3 \right] \quad (6.66) \\
& - \frac{2 \sin \xi}{m_2 m_3} \frac{l_{12} - l_{23} \cos \phi_2}{l_{12} l_{23}^2 \sin^2 \phi_2} \left[A_3 (A_2 - \cos \xi B_3) + B_3 (B_2 - \cos \xi A_3) \right] \\
& - \frac{2 \sin \xi}{m_2 m_3} \frac{l_{34} - l_{23} \cos \phi_3}{l_{34} l_{23}^2 \sin^2 \phi_3} \left[A_2 (A_3 - \cos \xi B_2) + B_2 (B_3 - \cos \xi A_2) \right].
\end{aligned}$$

The simulations with the four atom molecule were done under the same conditions as those with the three atomic molecule; the bending potential was quadratic with a spring constant of $50 \text{ kcal mol}^{-1} \text{ rad}^{-2}$ and an equilibrium value of 120° . In particular, $V(\xi) = 0$, so we expect $dA(\xi)/d\xi = 0$. The results of the calculations are presented in Fig. 6.2. Again, the average constraint force gives an incorrect distribution, even more so after correcting the average by means of Eq. (6.21). From the area under the curves it follows that the free energy difference between the cis and the trans conformation is off by -1.1 and -2.6 kcal/mol . The values obtained with Eq. (6.56) are in good agreement with the theoretical predictions.

6.6 Comments on the literature

The topics covered in the previous sections have been the subject of various articles in the literature. In this section we will comment on several of these articles.

6.6.1 Use and misuse of Z_ξ , $|\mathbf{Z}_\sigma|$ and $|\mathbf{Z}_{\xi\sigma}|$

If only bond lengths are constrained, $|\mathbf{Z}_\sigma|$ in Eq. (6.21) is a function of the atomic masses of the atoms involved in the constrained bonds, and of the bending angles between the constrained bonds. The latter dependence only arises if there are atoms that are involved in more than one constraint. For instance, in the case of the three atom molecule of section 6.5 with two bond length constraints one finds

$$|\mathbf{Z}_\sigma| = \left(\frac{1}{m_1} + \frac{1}{m_2} \right) \left(\frac{1}{m_3} + \frac{1}{m_2} \right) - \frac{\cos^2 \xi}{m_2^2}. \quad (6.67)$$

If atom 2 is much heavier than the other two atoms, or if the variation of the bending angle is strongly limited by a bending potential, then the factor $|\mathbf{Z}_\sigma|$ may be assumed constant and can be neglected in the averages. For other constraints than the one considered here, or in the case the atoms are of comparable masses, omission of $|\mathbf{Z}_\sigma|$ should be considered with the outmost care.

Many authors are aware of the difference between constrained and unconstrained averages, yet all too often they calculate the partition function of constrained rather than unconstrained systems.^{14,15,19-22} When dealing with a coupling parameter they consequently have no factor $|\mathbf{Z}_\sigma|^{-1/2}$ in the partition function. All terms in the derivative of the partition function then lack a factor $|\mathbf{Z}_\sigma|^{-1/2}$, and moreover a term $-\frac{1}{2} \langle |\mathbf{Z}_\sigma|^{-1/2} d \ln |\mathbf{Z}_\sigma| / d\lambda \rangle_{\sigma;\lambda}$ is missing. In the equivalent of Eq. (6.45) again all terms lack the factor $|\mathbf{Z}_\sigma|^{-1/2}$, and in the second term on the right hand side $|\mathbf{A}_{q\sigma}|$ is replaced by $|\mathbf{A}_q|$. Since in the coupling parameter method often only bond lengths are constrained, the effect of neglecting $|\mathbf{Z}_\sigma|^{-1/2}$ turns out to be of minor importance according to the considerations following Eq. (6.67).

When dealing with a reaction coordinate, however, the often complicated nature of this coordinate makes $Z_\xi^{-1/2}$ an essential, non-negligible, ingredient of the partition function. Omission of the factor $Z_\xi^{-1/2}$, like it has been done by van Gunsteren *et al.*¹⁹ for the system described in section 6.4 produces the partition function of a ξ -constrained molecule, i. e. a molecule with a prescribed value for ξ and with $\dot{\xi} = 0$. However, one would like to know the partition function of a molecule with a prescribed value of ξ , regardless of the velocity $\dot{\xi}$; the contribution of this velocity to the partition function is lost when $Z_\xi^{-1/2}$ is omitted. If section 6.4 had been based on this partition function, the result would have been¹⁵ $dA/d\xi = \langle \lambda_\xi \rangle$. As a second example, consider a molecule with one reaction coordinate, ξ , and with L constraints on the σ . Ciccotti, Kapral and co-workers^{21,22} have used the partition function

$$\begin{aligned}
Q'(\bar{\xi}) &\propto \int d\mathbf{X} \exp[-\beta\Phi(\mathbf{X})] \delta[\xi(\mathbf{X}) - \bar{\xi}] \delta[\boldsymbol{\sigma}(\mathbf{X}) - \bar{\boldsymbol{\sigma}}] |\mathbf{Z}_\sigma(\mathbf{X})|^{1/2} \\
&\propto \iint d\mathbf{q} d\xi d\mathbf{p}_{q\xi} \exp\left[-\beta\left\{\frac{1}{2}\mathbf{p}_{q\xi}^T \mathbf{A}_{q\xi}^{-1} \mathbf{p}_{q\xi} + \Phi(\mathbf{q}, \xi, \bar{\boldsymbol{\sigma}})\right\}\right] \delta[\xi - \bar{\xi}].
\end{aligned} \tag{6.68}$$

for this case. From the second line this function is seen to be proportional to the probability distribution along ξ of a $\boldsymbol{\sigma}$ -constrained system, i.e. with $\boldsymbol{\sigma}$ equal to the prescribed value $\bar{\boldsymbol{\sigma}}$, and with $\dot{\boldsymbol{\sigma}} = \mathbf{0}$. Note that $\dot{\xi}$ is treated correctly, and in this respect the procedure is superior to the one of van Gunsteren *et al.*,¹⁹ but contributions to the partition function resulting from motion along $\boldsymbol{\sigma}$ are still lost. The correct application of this partition function to the calculation of the transmission coefficient in the reactive flux method has been discussed elsewhere.²

As was said above, van Gunsteren *et al.*^{14,19} in their discussion of the coupling parameter approach ignore the factor $|\mathbf{Z}_\sigma|^{-1/2}$. They then go on by ascribing the properties of $|\mathbf{Z}_\sigma|$ discussed above to $|\mathbf{A}_q|$, i.e. that in common cases the latter is nearly independent of \mathbf{q} and can therefore be ignored. Effectively then, by ignoring $|\mathbf{Z}_\sigma|$ and $|\mathbf{A}_q|$ they have performed a coordinate transformation from Cartesian coordinates to generalised coordinates without introducing the appropriate Jacobian determinant.

6.6.2 Equivalence of thermodynamic force and constraint force

The possibility of a relationship between the thermodynamic force, Eq. (6.49), and the constraint force was first suggested by van Gunsteren.¹⁴ His motivation is rather poor, since it is based on the work done by the constraint forces, which according to textbooks²³ on classical mechanics vanishes. The algorithm proposed to calculate the thermodynamic force has, to the best of our knowledge, never been used.

In the hands of Straatsma *et al.*¹¹ the relationship underwent a drastic change. They suggested that in those cases where constraints can profitably be used, the constrained coordinates and the unconstrained coordinates are completely decoupled, i.e. that the Hamiltonian can be split into two parts of which one depends on the unconstrained coordinates and one on the constrained coordinates. In the case of a coupling parameter and one constraint, for example,

$$H^u(\mathbf{q}, \boldsymbol{\sigma}; \lambda) = H^c(\mathbf{q}; \lambda) + \mathcal{H}(\boldsymbol{\sigma}(\lambda); \lambda). \tag{6.69}$$

Neglecting the factor $Z_\sigma^{-1/2}$ in the partition function, they then conclude that the derivative of the free energy with respect to λ is proportional to

$$\left\langle \frac{dH^u}{d\lambda} \right\rangle = \left\langle \frac{\partial \Phi}{\partial \lambda} \right\rangle_{\sigma, \lambda} + \langle \lambda_\sigma \rangle_{\sigma, \lambda} \frac{\partial \sigma}{\partial \lambda}. \tag{6.70}$$

Obviously, the complete decoupling of the Hamiltonian needed for this derivation is a gross oversimplification. Incidentally, notice that λ_σ would be constant in this case. Continuing to

neglect $Z_\sigma^{-1/2}$, Mülders *et al.*¹⁵ have given a convincing derivation of Eq. (6.70). Using the methods of sections 6.3 and 6.4 one easily obtains the correct expression:

$$\begin{aligned} \frac{dA(\lambda)}{d\lambda} = & \frac{\left\langle \frac{\partial \Phi}{\partial \lambda} Z_\sigma^{-1/2} \right\rangle_\sigma}{\left\langle Z_\sigma^{-1/2} \right\rangle_\sigma} + \frac{1}{2} k_B T |\mathbf{F}|^{-1} \frac{d|\mathbf{F}|}{d\lambda} - \frac{1}{2} k_B T |\mathbf{M}|^{-1} \frac{d|\mathbf{M}|}{d\lambda} \\ & + \frac{\left\langle \lambda_\sigma Z_\sigma^{-1/2} \right\rangle_\sigma + \frac{1}{2} k_B T \left\langle \left\{ \sum_{i=1}^N m_i^{-1} \nabla_i \sigma \cdot \nabla_i Z_\sigma \right\} Z_\sigma^{-5/2} \right\rangle_\sigma}{\left\langle Z_\sigma^{-1/2} \right\rangle_\sigma} \frac{d\bar{\sigma}}{d\lambda}. \end{aligned} \quad (6.71)$$

From the results of Straatsma *et al.*¹¹ it can be seen that the constraint force makes a major contribution to the free energy if a constrained bond length changes. This effect arises from the velocity term in the Lagrange multiplier, Eq. (6.24). Over the years several physical interpretations have been given to this term, ranging from momenta of inertia correction,¹¹ dynamic stretch force resulting from the centrifugal force²⁴ to the Jacobian.²⁰ From the intricate nature of Eq. (6.56) it follows that all these interpretations are incorrect, and that a physically intuitive explanation most likely does not exist.

6.6.3 Potential force method

Pearlman²⁵ discussed a non-circular molecule with a constraint on the length of the bond between the atoms *A* and *B*, $\xi = r_{AB}$. He used

$$\left\langle \frac{\partial H}{\partial \xi} \right\rangle = - \left\langle \sum_{i=1}^N \frac{\partial \mathbf{x}_i}{\partial \xi} \cdot \mathbf{F}_i \right\rangle_\xi, \quad (6.72)$$

$$\frac{\partial \mathbf{x}_i}{\partial \xi} = \varepsilon_i \frac{\mathbf{r}_{AB}}{2r_{AB}}, \quad (6.73)$$

where $\varepsilon_i = +1$ for all atoms that are connected to atom *A*, and $\varepsilon_i = -1$ for all atoms that are connected to atom *B*. It is clear that during the displacements $d\mathbf{x}_i = (\partial \mathbf{x}_i / \partial \xi) d\xi$ internal coordinates other than ξ do not change, but in general the external coordinates will be affected. Obviously, in Eq. (6.72) the Jacobian term is missing, see Eq. (6.49).

As a test case, Pearlman transformed an ethane molecule with dummy atoms bonded to a hydrogen atom at a distance r_A into an ethane molecule with dummy atoms bonded to a different hydrogen atom at a distance r_B , expecting a zero free energy difference. In the simulations *in vacuo* he indeed found no free energy difference between the two final molecules. However, direct evaluation of the partition function shows that the free energy difference is^{20,26} $6k_B T \ln r_A / r_B$, which we verified numerically by normal mode analysis. For $r_A \neq r_B$ the free energy difference should therefore be non-zero. This incorrect ‘zero sum’ test case has also been used by others.^{13,27} Only when performing two legs of a

thermodynamic cycle, i.e. performing the same change *in vacuo* and in a solvent, will both runs yield the same result regardless of r_A and r_B .

6.6.4 Mean force independent of complementary coordinates

Recently, Ruiz-Montero *et al.*⁶ exploited the freedom of choice of the \mathbf{q} in Eq. (6.49) to simplify the resulting expressions. They chose to complement the coordinate ξ , which is dictated by the physics of the problem under investigation, by a set of coordinates obeying

$$\sum_{i=1}^N \nabla_i q_j \cdot \nabla_i q_k = \delta_{jk}, \quad (6.74)$$

$$\sum_{i=1}^N \nabla_i \xi \cdot \nabla_i q_k = 0. \quad (6.75)$$

The Jacobian and the partial derivatives needed in Eq. (6.49) then take a particularly simple form, and the derivative of the free energy reads

$$\frac{dA(\xi)}{d\xi} = \frac{1}{\langle Z_\xi^{-1/2} \rangle_\xi} \left\{ \left\langle \frac{\sum_{i=1}^N \nabla_i \Phi \cdot \nabla_i \xi}{|\nabla \xi|^2} Z_\xi^{-1/2} \right\rangle_\xi + k_B T \left\langle \frac{\sum_{i=1}^N (\nabla_i |\nabla \xi|) \cdot \nabla_i \xi}{|\nabla \xi|^3} Z_\xi^{-1/2} \right\rangle_\xi \right\}, \quad (6.76)$$

where $|\nabla \xi|^2 = \sum_{i=1}^N \nabla_i \xi \cdot \nabla_i \xi$.

Generalised coordinates with the above properties do in general not exist, however, and the validity of Eq. (6.76) consequently must be doubted. As an example, consider a two dimensional plane in which an atom is constrained to a circle with radius ξ , centred at the origin. Obviously,

$$\nabla \xi = \frac{1}{\sqrt{x^2 + y^2}} \begin{pmatrix} x \\ y \end{pmatrix}, \quad (6.77)$$

and the only possible solution of Eqs. (6.74) and (6.75), up to a minus sign, is

$$\nabla q = \frac{1}{\sqrt{x^2 + y^2}} \begin{pmatrix} -y \\ x \end{pmatrix}. \quad (6.78)$$

The second derivatives of the alleged function q then are

$$\frac{\partial}{\partial y} \left(\frac{\partial q}{\partial x} \right) = \frac{-x^2}{(x^2 + y^2)^{3/2}}, \quad (6.79)$$

$$\frac{\partial}{\partial x} \left(\frac{\partial q}{\partial y} \right) = \frac{y^2}{(x^2 + y^2)^{3/2}}, \quad (6.80)$$

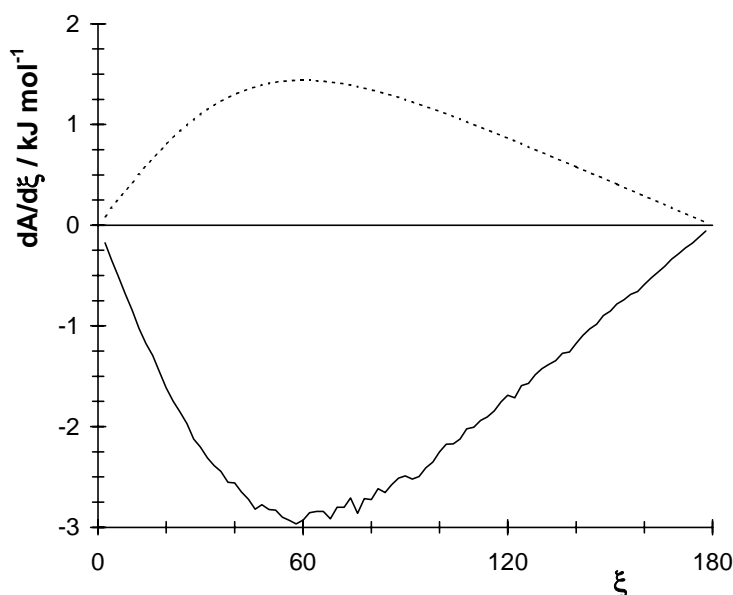


Figure 6.3. The right hand sides of Eqs. (6.76) (solid line) for the three atom molecule. The dotted line is the second term on the right hand side of Eq. (6.76), which under the current conditions is identical to the second term on the right hand side of Eq. (6.56).

from which it follows that the coordinate q with the requested properties does not exist. Coordinates of the form of Eqs. (6.74) and (6.75) are reminiscent of the non-coordinate bases of differential geometry.²⁸

To test the validity of Eq. (6.76) we have applied it to the three atom molecule of section 6.5. The results shown in Fig. 6.3 prove that Eq. (6.76) must be wrong.

Incidentally, if the masses of all atoms whose Cartesian coordinates occur in the definition of the reaction coordinate are equal,

$$\left\langle \frac{\sum_{i=1}^N (\nabla_i |\nabla \xi|) \cdot \nabla_i \xi}{|\nabla \xi|^3} Z_\xi^{-1/2} \right\rangle_\xi = \frac{1}{2} \left\langle Z_\xi^{-5/2} \sum_{i=1}^N \frac{1}{m} \nabla_i Z_\xi \cdot \nabla_i \xi \right\rangle_\xi, \quad (6.81)$$

and the first term between the curly brackets on the right hand side of Eq. (6.76) reduces to the contribution of the potential to $\langle \lambda_\xi Z_\xi^{-1/2} \rangle_\xi$, see Eq. (6.24). Therefore, under the equal mass condition the expression by Ruiz-Montero *et al.* differs from our result only by the velocity contribution to the Lagrange multiplier.

6.6.5 Generalised Alteration of Structure and Parameters (GASP)

An inherent problem of the free energy perturbation technique is that configurations of the ' λ_1 ensemble' are used to sample the ' λ_2 ensemble', see Eq. (6.48). Only if these two ensembles are rather similar, i.e. if their minimum energy conformations are alike, will the average in the numerator of Eq. (6.48) converge rapidly. This often means that the step size

$\lambda_2 - \lambda_1$ should be fairly small. Especially potentials with a quadratic contribution whose minimum depends on the coupling parameter,

$$\varphi(q; \lambda) = \frac{1}{2} C(\lambda) [q - q_0(\lambda)]^2, \quad (6.82)$$

are prone to problems.¹³ An interesting way of avoiding these problems is by using the generalised alteration of structure and parameters method (GASP) of Severance *et al.*²⁷ They suggested to transform to new coordinates $r_i = q_i - \Delta q_i$ in the λ_2 ensemble, and $r_i = q_i$ in the λ_1 ensemble. Here $\Delta q_i = 0$, except for the coordinate q of Eq. (6.82), in which case it is Δq . The potential energy difference then reads

$$\Delta\varphi_{12} = \frac{1}{2} C(\lambda_2) [r + \Delta q - q_0(\lambda_2)]^2 - \frac{1}{2} C(\lambda_1) [r - q_0(\lambda_1)]^2. \quad (6.83)$$

Obviously, if Δq is of the order $q_0(\lambda_2) - q_0(\lambda_1)$, $\exp(-\beta\Delta\Phi_{12})$ will fluctuate much less than before. Notice that $\Delta\Phi_{12}$ not only contains $\Delta\varphi_{12}$, but also contributions resulting from a change of the Cartesian coordinates of all atoms in the molecule caused by the change of q . In the case of an ideal gas of two atom molecules, with q chosen to be the length of the bond, and if $C(\lambda_2) = C(\lambda_1)$ and $\Delta q = q_0(\lambda_2) - q_0(\lambda_1)$, then this exponent will even be constantly equal to one. This should make us suspicious. Indeed, what has not yet been discussed is the Jacobian determinant. To appreciate this factor, which is not present in the equations of Severance *et al.*, we write the partition function as

$$\begin{aligned} Q(\lambda_2) &\propto \int d\mathbf{q} |\mathbf{A}(\mathbf{q}; \lambda_2)|^{1/2} \exp[-\beta\Phi(\mathbf{q}; \lambda_2)] \\ &= \int d\mathbf{r} |\mathbf{A}(\mathbf{r} + \Delta\mathbf{q}; \lambda_2)|^{1/2} \exp[-\beta\Phi(\mathbf{r} + \Delta\mathbf{q}; \lambda_2)]. \end{aligned} \quad (6.84)$$

Following the usual procedure we obtain

$$\begin{aligned} A(\lambda_2) - A(\lambda_1) &= \\ &= -k_B T \ln \frac{\left\langle \exp[-\beta\Delta\Phi_{12}(\mathbf{X})] \frac{|\mathbf{J}(\mathbf{r}(\mathbf{X}) + \Delta\mathbf{q}; \lambda_2)|}{|\mathbf{J}(\mathbf{r}(\mathbf{X}); \lambda_1)|} \frac{|\mathbf{M}(\lambda_2)|^{1/2}}{|\mathbf{M}(\lambda_1)|^{1/2}} |\mathbf{Z}_\sigma(\mathbf{X}; \lambda_1)|^{-1/2} \right\rangle_{\sigma; \lambda_1}}{\left\langle |\mathbf{Z}_\sigma|^{-1/2} \right\rangle_{\sigma; \lambda_1}}, \end{aligned} \quad (6.85)$$

where we have added the possibility that constraints are applied to the σ variables. We could have anticipated this result from Eq. (6.48). Let us finally notice that in the derivation we have tacitly assumed that the coordinates \mathbf{r} in both ensembles are defined on the same intervals.

6.6.6 Monte Carlo

So far we have concentrated on the calculation of free energies by molecular dynamics simulations. We will now briefly consider doing the same thing with Monte Carlo simulations, restricting ourselves to the example of section 6.3.1. Starting with the partition

function $Q(\xi)$ of Eq. (6.33), we integrate over all Cartesian momenta, transform to the generalised coordinates $(\mathbf{q}, \xi, \boldsymbol{\sigma})$, integrate over $\boldsymbol{\sigma}$ using Eq. (6.17) and integrate over ξ to arrive at

$$Q(\xi) \propto |\mathbf{F}|^{-1/2} \int d\mathbf{q} |\mathbf{J}(\mathbf{q}, \xi, \boldsymbol{\sigma})| \exp[-\beta\Phi(\mathbf{q}, \xi, \boldsymbol{\sigma})]. \quad (6.86)$$

Differentiation with respect to ξ yields

$$\frac{dA(\xi)}{d\xi} = \frac{\int d\mathbf{q} |\mathbf{J}| \exp[-\beta\Phi] \left\{ \frac{\partial\Phi}{\partial\xi} - k_B T |\mathbf{J}|^{-1} \frac{\partial|\mathbf{J}|}{\partial\xi} \right\}}{\int d\mathbf{q} |\mathbf{J}| \exp[-\beta\Phi]}. \quad (6.87)$$

From this example we see that the sampling of phase space with constrained Monte Carlo requires the rather cumbersome evaluation of the Jacobian to get the correct sampling of configuration space. Secondly, the expressions for the derivative of the free energy are the same as those for the molecular dynamics simulations, apart from the factors $|\mathbf{Z}_{\xi\sigma}|^{-1/2}$.

6.7 Conclusions

We have derived the correct relation between the constraint force needed to constrain an internal coordinate in a molecular dynamics simulation and the derivative of the free energy with respect to this internal coordinate. Previously published methods with a similar objective are critically discussed. We show that in most of these methods a term arising from integration over the momenta, i.e. a Jacobian, is included only partly, or not included at all. Two prototypical numerical examples are included to support our views. Of particular importance is the discussion on the calculation of the free energy as a function of a dihedral angle, as the dihedral angle is often used as the reaction coordinate in reaction rate calculations.

6.8 References

- ¹ G. Ciccotti and J. P. Ryckaert, *Comp. Phys. Rep.* **4**, 347 (1986).
- ² W. K. den Otter and W. J. Briels, *J. Chem. Phys.* **106**, 5494 (1997) (Chapter 3).
- ³ M. Fixman, *Proc. Nat. Acad. Sci. USA* **71**, 3050 (1974).
- ⁴ E. Helfand, *J. Chem. Phys.* **71**, 5000 (1979).
- ⁵ N. Gō and H. A. Scheraga, *Macromolecules* **9**, 535 (1976).
- ⁶ M. J. Ruiz-Montero, D. Frenkel and J. J. Brey, *Mol. Phys.* **90**, 925 (1997).
- ⁷ D. Frenkel and B. Smit, *Understanding Molecular Simulation* (Academic Press, San Diego, CA, 1996).
- ⁸ R. Edberg, D. J. Evans and G. P. Morris, *J. Chem. Phys.* **84**, 6933 (1986).
- ⁹ J.-P. Ryckaert, G. Ciccotti and H. J. C. Berendsen, *J. Comp. Phys.* **23**, 327 (1977).
- ¹⁰ D. J. Tobias and C. L. Brooks III, *J. Chem. Phys.* **89**, 5115 (1988).

- ¹¹ T. P. Straatsma, M. Zacharias and J. A. McCammon, *Chem. Phys. Lett.* **196**, 297 (1992).
- ¹² M. H. Mazor, J. A. McCammon and T. P. Lybrand, *J. Am. Chem. Soc.* **111**, 55 (1989); **112**, 4411 (1990).
- ¹³ D. A. Pearlman and P. A. Kollman, *J. Chem. Phys.* **94**, 4532 (1991).
- ¹⁴ W. F. van Gunsteren in *Computer Simulations of Biomolecular Systems: Theoretical and Experimental Applications*, edited by W. F. van Gunsteren and P. K. Weiner, (ESCOM, Leiden, The Netherlands, 1989), Vol. 1, pp. 27.
- ¹⁵ T. Mülders, P. Krüger, W. Swegat and J. Schlitter, *J. Chem. Phys.* **104**, 4869 (1996).
- ¹⁶ E. B. Wilson Jr., J. C. Decius and P. C. Cross, *Molecular vibrations: the theory of infrared and Raman vibrational spectra* (McGraw-Hill, New York, NY, 1955).
- ¹⁷ H. Bekker, H. J. C. Berendsen and W. F. van Gunsteren, *J. Comp. Chem.* **16**, 527 (1995).
- ¹⁸ J.-M. Depaepe, J.-P. Ryckaert, E. Paci and G. Ciccotti, *Mol. Phys.* **79**, 515 (1993).
- ¹⁹ W. F. van Gunsteren, T. C. Beutler, F. Fraternali, P. M. King, A. E. Mark and P. E. Smith in *Computer Simulation of Biomolecular Systems: Theoretical and Experimental Applications*, edited by W. F. van Gunsteren, P. K. Weiner and A. J. Wilkinson, (ESCOM, Leiden, The Netherlands, 1993), Vol. 2, pp. 315.
- ²⁰ S. Boresch and M. Karplus, *J. Chem. Phys.* **105**, 5145 (1996).
- ²¹ E. A. Carter, G. Ciccotti, J. T. Hynes and R. Kapral, *Chem. Phys. Lett.* **156**, 472 (1989).
- ²² E. Paci, G. Ciccotti, M. Ferrario and R. Kapral, *Chem. Phys. Lett.* **176**, 581 (1991).
- ²³ H. Goldstein, *Classical Mechanics* (Addison-Wesley, Reading, MA, 1980).
- ²⁴ L. Wang and J. Hermans, *J. Chem. Phys.* **100**, 9129 (1994).
- ²⁵ D. A. Pearlman, *J. Chem. Phys.* **98**, 8946 (1993).
- ²⁶ D. R. Herschbach, H. S. Johnston and D. Rapp, *J. Chem. Phys.* **31**, 1652 (1959).
- ²⁷ D. L. Severance, J. W. Essex and W. L. Jorgensen, *J. Comp. Chem.* **16**, 311 (1995).
- ²⁸ B. F. Schutz, *A First Course in General Relativity* (Cambridge University Press, Cambridge, U. K., 1984).

Chapter 7

Summary and outlook

7.1 Summary

The isomerisation rates of a calix[4]arene *in vacuo* and in two solvents have been computed by means of molecular dynamics simulations (MD). In MD the equations of classical mechanics are used to calculate the motion of the reacting molecule and the surrounding solvent molecules. Thus, the intricate influence of the solvent on the reacting molecule is realistically accounted for. Unfortunately, MD simulations are computationally very demanding because of the large number of non-bonded interactions between the molecules, and the rapid internal motions of the molecules which make it necessary to calculate the interactions at femtosecond intervals.

During an isomerisation reaction a molecule goes from one energetically favourable conformation to another energetically favourable conformation without breaking or forming covalent bonds. Such events are rare on the time scale of the normal dynamics of the molecule, i. e. the motion within a low energy region, since during the reaction the molecule has to pass through an energetically unfavourable region. In MD simulations of the isomerisation of a calix[4]arene in a solvent, with an experimental rate constant of about 100 s^{-1} , a reaction event occurs roughly once every 100,000 CPU-years.

With the appropriate statistical mechanical methods, as explained in chapter 2, the required CPU time can be reduced to the order of a month. Before these methods can be applied to a particular reaction, one has to introduce a reaction coordinate, a method of telling reactants and products apart. This coordinate also defines a dividing-plane between the reactants and the products. In transition state theory (TST) the forward rate constant of a reaction is expressed in terms of the instantaneous product bound flux through this plane and the average number of molecules on the reactant side of the plane. The calculation of the TST rate only requires knowing the free energy of the molecule as a function of the reaction coordinate. In the reactive flux method (RF) the exact rate is obtained by multiplying the TST rate by a transmission coefficient, κ , which takes into account that only a fraction of the product bound flux through the dividing plane will actually reach the product well.

In chapter 3 we propose a systematic definition of the reaction coordinate, based on the unstable normal mode at the saddle point of the potential energy surface. This coordinate has

several features which make it a very useful coordinate in rate calculations. Although the coordinate can not be expressed as a simple analytic function of the Cartesian coordinates of the reacting molecule, it can be computed swiftly by means of the rapidly converging Newton-Raphson method. The gradient of the reaction coordinate, which is needed in constrained runs and in umbrella sampling runs, is then obtained analytically. With this coordinate the transmission coefficient will be fairly high, thus reducing the CPU-time spent in the calculation of the rate constant. An excellent approximation of the free energy of the molecule *in vacuo* is obtained by performing a normal mode analysis at fixed values of the reaction coordinate.

These topics are discussed in detail in chapters 3 through 5, where the proposed reaction coordinate is employed to calculate the TST and RF isomerisation rates of a calix[4]arene *in vacuo*, in chloroform and in benzene. We find that both solvents destabilise the paco conformation and stabilise the transition state configuration with respect to the situation in vacuum. Chloroform stabilises the cone conformation, thus reducing the rate constant to below the value in vacuum, while in benzene the reaction is faster than in vacuum. The calculated rates are in good agreement with the experimental data. Although we have concentrated on the isomerisation of a calix[4]arene, the introduced reaction coordinate can in principle be applied to any reaction with a high energy barrier between the reactants and the products. The isomerisation of *n*-butane is briefly discussed in chapter 3.

In chapter 6 we explore the connection between the derivative of the free energy as a function of a coordinate, and the force needed to constrain this coordinate to a fixed value in an MD simulation. The relation between the two is found to be more complicated than was previously assumed by other authors. The correct formula is applied to calculate the free energy of a butane-like molecule as a function of the dihedral angle, as in many isomerisation reactions a dihedral angle serves as the reaction coordinate. Several methods for calculating free energy differences that have appeared in the literature are commented upon.

7.2 Outlook

The erratic motion of the reaction coordinate, as calculated in the above discussed MD simulations, is reminiscent of the motion of a Brownian particle. In some reaction rate theories, therefore, the rate of escape from the reactant well is modelled by the statistical tools developed in the study of Brownian dynamics. The idealised motion of the reaction coordinate, ξ , with an effective mass, m , in a bath of non-reactive motions is given by the Langevin equation,

$$m\ddot{\xi} = -\frac{dU(\xi)}{d\xi} - \zeta\dot{\xi} + R(t). \quad (7.1)$$

The potential is often approximated by a parabola near the transition state, $U = E_{act} - \frac{1}{2}m\omega_b^2\xi^2$. The motion of the reaction coordinate is opposed by the friction, ζ , of

the bath. The stochastic force, R , with zero mean, models the unpredictable aspects of the interactions with the bath. In a consistent model the friction and the random force are related by the second fluctuation-dissipation theorem,

$$\langle R(t)R(0) \rangle = 2\zeta k_B T \delta(t). \quad (7.2)$$

Kramers¹ in 1940 derived an expression for the transmission coefficient of the system described in Eq. (7.1), yielding the curve of Fig. 7.1. At high friction the transmission coefficient becomes inversely proportional to the friction coefficient. Due to the strong interactions with the bath, the velocity $\dot{\xi}$ often changes direction, while ξ hardly changes. Thus any correlation between the direction in which the molecule crossed the transition state and the well where the molecule ends up some time later is lost. At low friction the reaction coordinate keeps swinging back and forth through the reactant well and the product well before losing enough energy to settle in either of the two wells. The transmission coefficient then is proportional to the friction coefficient. This regime is commonly referred to as the energy-diffusion regime, as the energy of the molecule performs a Brownian motion. In chapter 3 we saw that the isomerisations of *n*-butane and of calix[4]arene *in vacuo* tend to the low friction regime. The isomerisation of a dissolved calix[4]arene lies in the high friction regime. By increasing the friction, for instance by replacing the hydrogens at the upper rim by a more bulky group such as a tert-butyl, we expect the transmission function to decrease.

In chapter 6 we derived two expressions for the derivative of the free energy with respect to the reaction coordinate, see Eqs. (6.49) and (6.56). Both these equations can be combined with the reaction coordinate introduced in chapter 3. The Jacobian in Eq. (6.49) is already given in Eq. (4.45), and the partial derivatives follow from $\partial F / \partial \xi = \sum_{i=1}^N \nabla_i F \cdot \mathbf{a} \mathbf{q}_i^r$. The gradient of Z_ξ , as required in Eq. (6.56), is readily evaluated with the methods described in

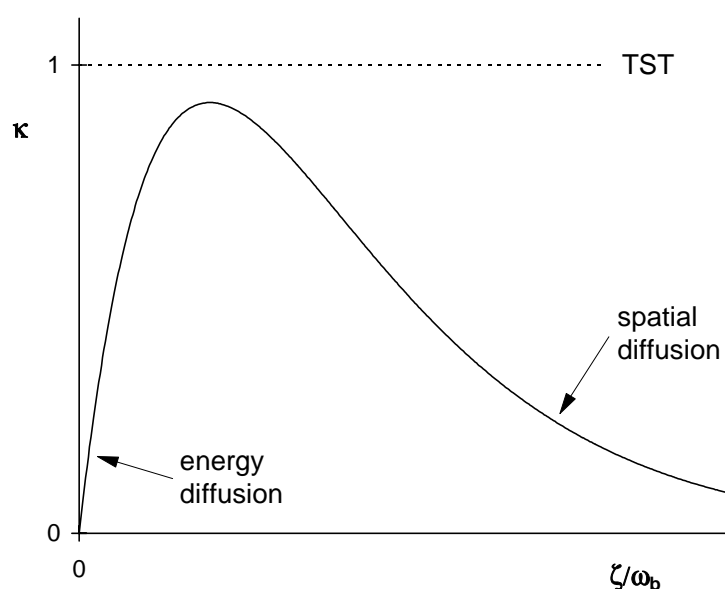


Figure 7.1. Sketch of transmission coefficient as a function of the friction.

section 3.3.1. Both methods can be applied to a set of ξ -constrained simulations to verify the free energy distributions of chapters 4 and 5. With these simulations one may also calculate the autocorrelation of the stochastic force. If this force is delta-correlated, as in Eq. (7.2), the transmission coefficient follows directly from Kramers expression, and can then be compared with the results of chapters 3 and 5. Probably, the stochastic force will not be delta-correlated, in which case the equation of motion for the reaction coordinate, Eq. (7.1), must be expanded to contain a friction coefficient with memory. Even for this situation the transmission coefficient can be calculated analytically.^{2,3}

7.3 References

- ¹ H. A. Kramers, *Physica (Utrecht)* **7**, 284 (1940).
- ² R. F. Grote and J. T. Hynes, *J. Chem. Phys.* **73**, 2715 (1980).
- ³ E. Pollak, *Chem. Phys. Lett.* **127**, 178 (1986); *J. Chem. Phys.* **85**, 865 (1986).

Samenvatting

De isomerisatiesnelheden van een calix[4]areen in vacuüm en in twee oplosmiddelen zijn berekend gebruik makend van moleculaire dynamica simulaties (MD). In MD worden de bewegingsvergelijkingen van de klassieke mechanica gebruikt om de bewegingen van het reagerende molecuul en van de omringende oplosmiddelmoleculen te bepalen. Zodoende wordt de gecompliceerde invloed van het oplosmiddel op de reactie realistisch in rekening gebracht. Helaas zijn MD simulaties erg rekenintensief vanwege het grote aantal wisselwerkingen tussen de moleculen, en door de snelle bewegingen van die moleculen waardoor de interacties om de femtoseconde (10^{-15} s) opnieuw bepaald dienen te worden.

Tijdens een isomerisatiereactie gaat een molecuul van de ene energetisch gunstige conformatie naar een andere energetisch gunstige conformatie, zonder dat daarbij covalente bindingen worden gevormd of verbroken. Deze overgangen zijn uiterst zeldzaam op de tijdschaal van de normale bewegingen van de moleculen, omdat een reagerend molecuul door een energetisch ongunstige overgangstoestand heen moet. In MD simulaties van de isomerisatie van een calix[4]areen in een oplosmiddel, waarvan de experimentele reactiesnelheid ongeveer 100 s^{-1} is, vindt er gemiddeld één reactie plaats per 100.000 jaar rekentijd.

Met de geschikte statistisch mechanische methoden, zoals beschreven in hoofdstuk 2, kan de benodigde rekentijd worden teruggebracht tot de orde van grootte van een maand. Voordat deze methoden op een willekeurige reactie kunnen worden toegepast moet er een reactiecoördinaat worden geïntroduceerd, een coördinaat om reactanten en producten te kunnen onderscheiden. Deze coördinaat definieert tevens een scheidingsvlak tussen de reactanten en de producten. In de overgangstoestand-theorie (transition state theory, TST) wordt de snelheid van de voorwaartse reactie uitgedrukt in termen van de instantane product-gerichte flux door dit scheidingsvlak en het gemiddelde aantal moleculen aan de reactant zijde van het scheidingsvlak. De berekening van de TST reactiesnelheid vereist alleen kennis van de vrije energie van het molecuul als een functie van de reactiecoördinaat. In de reactieve flux methode (RF) wordt de reactiesnelheid verkregen door de TST snelheid te vermenigvuldigen met een transmissiecoëfficiënt, die verdisconteert dat slechts een deel van de product-gerichte flux door het scheidingsvlak ook daadwerkelijk aankomt aan de productzijde.

In hoofdstuk 3 stellen we een systematische definitie van de reactiecoördinaat voor, gebaseerd op de instabiele normal mode van het zadelpunt van het potentiële-energie-oppevlak van de reactie. Deze coördinaat heeft verscheidene kenmerken die hem uitermate geschikt maken voor gebruik in reactiesnelheidsberekeningen. Alhoewel de coördinaat niet geschreven kan worden als een analytische uitdrukking in termen van de Carthesische

coördinaten van het molecuul, kan hij toch snel worden uitgerekend met de vlug convergerende Newton-Raphson methode. De gradiënt van de reactiecoördinaat, die we nodig hebben in geconstraineerde simulaties en bij umbrella sampling, kan dan analytisch worden bepaald. Met deze reactiecoördinaat zal de transmissiecoëfficiënt vrij hoog zijn, waardoor de benodigde hoeveelheid rekentijd binnen de perken blijft. Een uitstekende benadering van de vrije energie van een molecuul in vacuüm wordt verkregen door een aantal normal mode analyses uit te voeren bij constante waarden van de reactiecoördinaat.

Deze onderwerpen worden verder toegelicht in de hoofdstukken 3 tot en met 5, waar de voorgestelde reactiecoördinaat gebruikt wordt om de TST en RF reactiesnelheden te bepalen van een calix[4]areen in vacuüm, in chloroform en in benzeen. We vinden dat beide oplosmiddelen de paco conformatie destabiliseren en de overgangstoestand stabiliseren ten opzichte van de situatie in vacuüm. Chloroform stabiliseert de cone conformatie, waardoor de reactiesnelheid lager wordt dan in vacuüm, terwijl in benzeen de reactie sneller verloopt dan in vacuüm. De berekende snelheden zijn in goede overeenstemming met de experimentele gegevens. Alhoewel we ons onderzoek geconcentreerd hebben op de isomerisatie van een calix[4]areen, kan de beschreven reactiecoördinaat in principe voor elke reactie met een hoge energiebarrière tussen de reactanten en de producten gebruikt worden. Zo wordt in hoofdstuk 3 de isomerisatie van *n*-butaan kort bekeken.

In hoofdstuk 6 onderzoeken we het verband tussen de afgeleide van de vrije energie als functie van een coördinaat en de kracht die nodig is om deze coördinaat in een MD simulatie op een constante waarde te houden. Het verband blijkt veel gecompliceerder te zijn dan tot nu toe in de literatuur wordt aangenomen. De gecorrigeerde formule wordt gebruikt om de vrije energie van een butaan-achtig molecuul uit te rekenen als een functie van de dihedrale coördinaat, daar in veel isomerisatiereacties de dihedrale coördinaat als reactiecoördinaat wordt gebruikt. Verscheidene in de literatuur beschreven methoden om vrije energie verschillen uit te rekenen zijn kritisch bekeken.

Dankwoord

Met dit hoofdstuk wil ik iedereen die heeft bijgedragen aan de totstandkoming van het voor u liggende proefschrift hartelijk bedanken. Enkelen wil ik met naam en toenaam vermelden, zonder daarbij een ieder die niet vermeld wordt te kort te willen doen.

In de eerste plaats gaat mijn dank uit naar Wim Briels, die nooit om een leuk idee verlegen zat en mij voortdurend gemotiveerd heeft om op de ingeslagen weg door te gaan. De promotor Dick Feil wil ik er voor bedanken dat hij mij in de gelegenheid heeft gesteld om dit onderzoek uit te voeren. Verder bedank ik Frank Leuwerink die howling mad otterw in de wondere wereld van GROMOS heeft ingeleid, Roelof de Vries die als kamergenoot enkele jaren lang mijn verbale uitingen bij het programmeren heeft moeten aanhoren, Maarten Nollen en Santiago Diaz Fernandez die ik mocht begeleiden bij hun eerste schreden op simulatie gebied, Willem Paul van Hoorn die de zadelpunten heeft uitgerekend, de overige collega-AIO-s en studenten die de afgelopen jaren tot een leerzame en aangename periode hebben gemaakt, en, last but not least, mijn ouders.

Curriculum Vitae

De schrijver van dit proefschrift werd op 20 mei 1969 geboren te Eindhoven. Van 1981 tot 1987 doorliep hij atheneum B op het 'Serviam' in Sittard. Daarna begon hij aan de studie technische natuurkunde aan de Technische Universiteit Eindhoven. In april 1993 studeerde hij af bij Prof. dr. H. H. Brongersma, vakgroep fysica van oppervlakken en grenslagen, en Dr. H. Feil, Philips Natlab, op de numerieke simulatie van lage energie ionen verstrooiing aan een gedragen rhodium katalysator. Vanaf juli 1993 heeft hij als AIO gewerkt in de vakgroep chemische fysica, faculteit chemische technologie, van de Universiteit Twente. Hij werd door Dr. W. J. Briels begeleid bij het onderzoek dat in dit proefschrift beschreven is.